6-3-2019

Decadal Changes in Salt Marsh Succession and Assessing Salt Marsh Vulnerability using High-Resolution Hyperspectral Imagery

Sarah Goldsmith
sbg4917@rit.edu

Decadal Changes in Salt Marsh Succession and Assessing Salt Marsh Vulnerability using High-Resolution Hyperspectral Imagery

By: Sarah Goldsmith

Thesis Submitted in Partial Fulfillment of the Requirements for the Degree of

Master of Science in Environmental Science

Gosnell School of Life Sciences

College of Science

Environmental Science Program

Rochester Institute of Technology

Rochester, NY

June 3, 2019

Committee Approval:

Anna Christina Tyler, PhD — Date
Chair of Committee, Thesis Advisor

Charles Bachmann, PhD — Date
Committee Member

David Osgood, PhD — Date
Committee Member

Table of Contents

List of Tables and Figures

Acknowledgements

My deepest thanks goes towards my advisor, Dr. Christy Tyler, who supported me throughout it all and always pushed me academically, from my very first environmental science class through to the end of my thesis. I never would have made it this far without her help and guidance, and reassurances that everything would, in fact, be alright, even if I did inadvertently melt some of my samples that one time.

I also extend my thanks to my committee members, for their valuable feedback and guidance on this project. To Dr. Chip Bachmann, who provided a wealth of knowledge and expertise on the remote sensing front, and Dr. David Osgood, for his thoughtful comments, excellent music taste, and for all the drives up to Rochester to be there in person. Additionally, I would like to thank Dr. John Walsh for his willingness to share his data.

I would also like to thank the biophysical field crew, who endured those unnecessarily hot Virginia days sampling out in the marsh and still made it through with good humor and cheer— Patrick Minnig, Ryan Brett, Sarah Ponte-Cabral, and Sydney VanWinkle. Furthermore, I would like to thank Rehman Eon, Chris Lapszynski, and Greg Badura for their invaluable assistance with the remote sensing analysis.

Thank you to my friends and family for always being there for me— to my brother, Adam, who tolerated my beginner's programming questions, and to my parents, for instilling a love of nature and encouraging my curiosity from a young age, for always being there for me when things were hard, and making sure I stuck with it until the end. And last but not least, thank you to my cat, Shiro, for all the times you sat on my laptop and deleted pages of my thesis and replaced it with your wisdom (mostly consisting of "aaaaaaaaaahjk;nlkkkkkkkk"). I couldn't have done it without all of you.

ABSTRACT

Change in the coastal zone is accelerating with external forcing by sea-level rise, nutrient loading, drought and over-harvest is impacting salt marshes. Understanding marsh resilience, including recovery from coastal storms and detection of stress, is essential for conservation and prediction of ecosystem services. The 'chronosequence approach' of predicting future state change by examining ecosystem structure and function in existing ecosystems of different ages is a powerful tool, but assumes that the past mimics the future, and time is the dominant driver of change. This approach was evaluated by replicating a 1995 salt marsh chronosequence study in back-barrier marshes ranging from 4 to >170 yr old on Hog Island, Virginia. Physico-chemical properties, such as porewater redox potential and sediment organic matter and nutrients, followed predictable age-related patterns. However, invertebrate abundance, plant biomass, and sediment grain size instead seemed to respond to sea level rise and stochastic die-off and sand deposition. Thus, while time drives the intrinsic evolution of some physico-chemical components, extrinsic drivers exert a strong influence on key biotic-abiotic feedbacks. Exacerbation of external forcing may push the trajectory of marsh succession away from a predictable trajectory, limiting ecosystem services. This rapid evolution of marsh state makes the ability to detect stressors prior to marsh collapse important. Hyperspectral imagery of plants was collected in marshes of varying age/stressor characteristics, including salinity, sediment redox potential and nitrogen availability, and in the greenhouse, where environmental conditions were manipulated. Models developed to stressors based on plant spectral response were useful for salinity and nitrogen within the greenhouse or within the field, but were not transferable from lab to field. This study is an important step towards development of a remote sensing tool for tracking of ecosystem development, marsh health, and future ecosystem services.

Chapter 1 : Introduction

1.1 Salt Marshes

Salt marshes are a category of coastal wetlands that form in intertidal zones where physical wave energy is low enough that vegetation can establish. As such, these ecosystems are frequently located in gently sloping estuaries and lagoons as well as on barrier islands (Friedrichs & Perry, 2001). Along the Atlantic coast of North America, the vegetation in the low zone of salt marshes is typically dominated by the perennial grass *Spartina alterniflora* (smooth cordgrass). *S. alterniflora* grows in monospecific stands that vary in morphology and productivity across the intertidal zone. Marsh grasses typically establish between the mean tide level and the spring high tide, where there is an absence of the chemical stresses associated with frequent inundation on the seaward side and competition with more terrestrial plants on the landward side (Friedrichs & Perry, 2001). As a result, the vegetation in salt marshes is highly zoned into monospecific bands that run parallel to the coastline and are highly dependent on elevation (Silliman, 2014). Tall-form plants tend to be found along creek banks and the shoreline, where there is higher porewater drainage and increased sediment oxidation; height decreases with distance from creeks and the shore (Howes et al., 1986). Short-form plants grow towards the interior of the marsh, where there is greater soil hypoxia and increased sulfide and salinity, which interfere with the uptake of ammonium (Mendelssohn & Morris, 2002)

Coastal wetlands provide the greatest number of ecological services of any coastal environment, including support for coastal fisheries, important habitat, protection from storm surges, and reduction of nutrient loading to coastal waters (Boesch & Turner, 1984; Barbier et al., 2008; Koch et al., 2009; Morgan et al., 2009). Additionally, salt marshes sequester carbon at rates that are potentially an order of magnitude greater than that of terrestrial forests (Chmura, 2013). As such, there has recently been much attention on 'Blue Carbon,' the stock of carbon in

seagrasses and coastal wetlands, including salt marshes, and the potential for salt marshes to offset human greenhouse gas emissions (e.g. Chmura et al., 2003; Mcleod et al., 2011; Hopkinson et al., 2012). However, carbon storage in marshes is extremely variable on very small spatial scales, in part due to the aforementioned plant zonation, and there is still great uncertainty in salt marsh carbon sequestration and other ecosystem services due to this heterogeneity.

Modern salt marshes are vulnerable to a variety of anthropomorphic influences including human manipulation, land conversion, invasive species, water-borne pollution, and the effects of global climate change, especially increased temperatures and sea level rise. However, there is substantial uncertainty regarding how these factors will affect salt marshes and the ecosystem services they provide (e.g. Gedan et al., 2009; Gedan & Bertness, 2010; Kirwan & Mudd, 2012; Chmura, 2013). The long-term persistence of salt marshes (and other intertidal ecosystems) relies on vertical accretion through accumulation of organic matter and sediment deposition to avoid inundation from rising sea level (Friedrichs & Perry, 2001; Morris et al., 2002). Increased sea level can augment production of *S. alterniflora* to a point, and increase the opportunity for sediment deposition; however, if the tidal submergence is too great, it results in decreased productivity and marsh submergence (Reed, 1995; Friedrichs & Perry, 2001; Chmura, 2013).

Increased flooding associated with rapid sea level rise is also likely a driver of landward expansion of low marsh into high marsh and upland zones (Donnelly & Bertness, 2001). Additionally, salt marshes are susceptible to lateral edge erosion (Kastler & Wiberg, 1996; Priestas et al., 2015) and in recent decades there has been increased observation of acute marsh die-off, which is likely related to changes in trophic structure and precipitation (Silliman & Bertness, 2002a; Alber et al., 2008; Bertness & Silliman, 2008).

1.2 Salt marsh succession

Salt marshes often form on the landward side of barrier islands, which are long islands composed of unconsolidated sediment that run parallel to coastlines. The seaward side of the island is typically composed of beach and dune elements, while the middle is composed of an upland region. The landward side consists of marsh and, in lower elevations, tidal flats (Davis, 2012). Barrier islands off the eastern coast of North America are subjected to overwash events during which intense waves from storms wash over the island, removing large quantities of sand from the beach face and creating overwash fans that are gradually recolonized by marsh plants (Fahrig et al., 1993). Recurring overwash events result in marshes of differing ages, providing a unique opportunity to predict ecosystem trajectories over time as well as examine the effect of stressors and die-off events as they relate to marsh age. Prior work conducted on salt marsh chronosequences (e.g. Tyler & Zieman, 1999; Walsh, 1998) generated theories about salt marsh succession; however, chronosequence sites that are used to generate theories of succession are are rarely revisited to determine if predictions prove true or not.

Understanding the processes that occur in marshes of differing ages can be important for predicting various stressors that act on the marsh and may ultimately lead to marsh collapse. Several stressors in salt marshes, including hypoxia and nitrogen availability, vary with marsh age, and others, such as salinity, vary naturally over the chronosequence. Changes in external factors and stressors may be important drivers of marsh trajectories, and it is important to detect these stressors prior to marsh collapse.

1.3 Remote Sensing

Field-based methods in salt marshes can be disruptive, labor intensive, and impractical due to high heterogeneity and varied spatial distribution. Remote sensing techniques such as satellite or flyover imagery and light detection and ranging (LIDAR) are increasingly important in determining the sustainability and permanence of salt marshes and may be used to ascertain the future of essential ecosystem services such as Blue Carbon storage (Chmura, 2013). Hyperspectral imagery produces contiguous, high spectral resolution data and can be used to link subtle spectral differences to biophysical properties (Artigas & Yang, 2006). However, marsh vegetation can be very heterogeneous along small spatial scales and traditional remote sensing techniques such as flyover or satellite-based imagery may not have sufficient spatial resolution to determine plant characteristics. High-resolution (sub-centimeter scale) hyperspectral imagery can provide unprecedented levels of detail that matches the scale of heterogeneity within the marsh and has the potential to predict important factors that influence *S. alterniflora* production.

1.3 Overview of study

The objectives of this study were to:

1. Evaluate the relative roles of marsh age and multiple external stressors on ecosystem development using a chronosequence approach for storm-derived salt marshes.

    H1. Ecosystem development is primarily driven by marsh age.

2. Evaluate the physiological response and hyperspectral signature of *S. alterniflora*, the dominant plant in salt marshes, subjected to relevant stressors.

    H2.a. Stress response in *S. alterniflora* will be evident in changes in biomass, plant allometrics, foliar chlorophyll *a*, and tissue total C, N, and P.

H2.b. Stress response in *S. alterniflora* will be detectable as a spectral shift in vegetation indices and reflectance due to the changes in factors listed in H2.a.

3. Develop models of stressors from hyperspectral imagery that allow prediction of marsh states in the field.

H3. Spectral data will enable prediction of marsh states in the field.

The focus of Chapter 2 is to validate predictions of salt marsh succession that were generated in the 1990s based on a back-barrier island chronosequence. In Chapter 3, the use of high-resolution hyperspectral imagery to detect stressors in both a greenhouse and field setting are discussed.

Chapter 2 : Decadal Changes in Salt Marsh Succession

2.1 Introduction

Coastal salt marshes provide numerous ecosystem services, including coastal protection through wave dissipation, erosion control, water purification, fishery maintenance, tourism, recreation, and education (Barbier et al., 2011). Marshes also play an important role in the global carbon cycle, potentially sequestering more carbon per unit area than any terrestrial ecosystem (Nellemann, 2009; Mcleod et al., 2011; Chmura, 2013). At the same time, coastal marshes are also increasingly threatened by a variety of stressors, including sea level rise, and other climate forcing, shifts in trophic structure, and nutrient pollution (Morris et al., 2002; Bertness & Silliman, 2008; Gedan et al., 2009; Deegan et al., 2012). These drivers may alter resilience and the ability of marshes to recover from episodic threats such as coastal storms. Understanding how marshes change over time thus has implications for predicting resilience and maintenance of coastal zone ecosystem services.

Classic models of ecological succession (Cowles, 1899; Clements, 1916) propose that succession is linear, directional and driven by autogenic processes to a distinct endpoint in a final equilibrium. This paradigm was originally challenged by Tansley (1935) and drove development of the ecosystem concept, wherein the climax community is driven by spatially explicit biotic and abiotic factors. While these foundational theories of succession were largely driven by predictions for plant community composition, many salt marshes remain dominated by a single plant along the continuum of age. As such, studies of marsh development have focused on geomorphological or whole ecosystem approaches in to order to define successional seres.

Early geomorphological descriptions of salt marsh succession suggest two developmental trajectories: the ‘Mudge-Davis’ marsh, transgressing upland as a result of rising sea level and peat accumulation, and the ‘Shaler’ marsh, where unvegetated mudflat is colonized seaward by

S. alterniflora (Davis, 1910). Later descriptions focused on defining the suite of physicochemical and biological variables that define successional seres (Walsh, 1998; Tyler & Zieman, 1999; Tyler et al., 2003). However, these models have been challenged by observations that marsh morphology and vertical accretion are highly dynamic and rapidly respond to changes in physical forcing (Friedrichs & Perry, 2001). Present-day marshes are also subjected to rapidly evolving drivers associated with climate change, including sea level rise, drought, high temperatures, species range shifts or depletions, and increasing storm frequency and intensity (Morris et al., 2002; McKee et al., 2004; Gedan et al., 2009; Crosby et al., 2017), that may shift the trajectory of marsh development.

The narrow salt marshes that fringe barrier islands provide a unique test case for the study of marsh development. Barrier islands of the Western Atlantic are subject to episodic "overwash" events, during which intense waves from storms wash over the island, removing sand from the beach face and depositing it over the island interior (Godfrey & Godfrey, 1976; Goodbred & Hine, 1995). The sand accumulation can be several meters deep, burying plants and seeds, and preventing germination (Fahrig et al., 1993). This deposition creates overwash fans that effectively re-set the successional clock and are gradually recolonized by marsh plants. The temporal variation in recolonization of overwash fans creates a chronosequence, where marshes of different ages may exist side by side, providing the opportunity to use the "space-for-time" approach to understand ecosystem development (Pickett, 1989). This approach avoids the need for long-term monitoring at a single site; however, differences between sites are attributed to ecosystem development when they may instead be due to past disturbances or underlying differences in site history (Pickett, 1989; Johnson & Miyanishi, 2008). Much of what is known about marsh succession on barrier islands is the result of work conducted at a chronosequence on

Hog Island, a back-barrier island off the coast of Virginia, USA, which is part of the Virginia Coast Reserve Long Term Ecological Research site (VCR LTER), during the mid-1990s (Osgood & Zieman, 1993; Walsh, 1998; Tyler & Zieman, 1999; Tyler et al., 2003).

Models developed during the 1990s suggested that for marshes where *S. alterniflora* is both the pioneer and climax plant species, succession is marked by predictable changes in biophysical properties and community composition of other organisms. With increasing age, sediment shifted from larger-grained sandy substrate to fine-grained, muddy substrate (Redfield, 1972; Osgood & Zieman, 1993; Walsh, 1998). Microalgae, such as diatoms and cyanobacteria, functioned as important pioneer species during the formation of a marsh and along with vascular plants, contributed organic matter and nitrogen to sediments (Tyler et al., 2003). Soil organic matter accumulated over time, resulting in higher C, N, and P concentrations and lower bulk density. Older marshes also had lower redox potential and higher concentrations of hydrogen sulfide (Osgood et al., 1995). Plants exhibited allometric, phenological and physiological differences: plants in older marshes were taller, heavier, had greater tissue N, and more frequently exhibited sexual reproduction than plants in younger marshes (Tyler & Zieman, 1999). However, areal *S. alterniflora* primary productivity peaked at an intermediate age, where nutrient standing stocks were more developed than at younger stages, but the substrate was presumably less toxic (sulfidic) than that at older ages (Walsh, 1998). Invertebrate density followed *S. alterniflora* biomass, with an overall maximum at an intermediate age. However, individual species densities followed predictable trends: *Ilyanassa obsoleta* was higher in the oldest marshes where finer sediments suit feeding patterns, while *Littoraria irrorata* and *Geukensia demissa* density peaked in intermediate aged marshes where *S. alterniflora* stem

densities were highest (Walsh, 1998). Fiddler-crab species composition shifted predictably from *Uca pugilator* in young, sandy marshes to *U. pugnax* in older, muddy marshes.

From these earlier studies emerged a theory of barrier island salt marsh succession based on the chronosequence technique and the assumption that time was the dominant driver of the observed changes in biophysical and community properties. There are a few studies that have revisited chronosequence sites (e.g., Collins & Adams, 1983; Debussche et al., 1996; Foster & Tilman, 2000), but this is rare, and none have taken place in a system changing as rapidly as coastal ecosystems in the time of accelerating climate change. Thus, there is a significant need to re-evaluate predicted patterns, and determine if modern marshes continue to be pushed along a similar time-driven trajectory, or if rapidly evolving external factors are exerting greater influence and changing the trajectory of ecosystem development. The aim of this study was to replicate studies of salt marsh succession conducted in the 1990s at the same sites (Walsh, 1998; Tyler & Zieman, 1999) to test the hypothesis that barrier island salt marshes follow a predictable developmental trajectory driven by internal feedbacks that are determined by the passing of time.

2.2 Methods

2.2.1 Site description

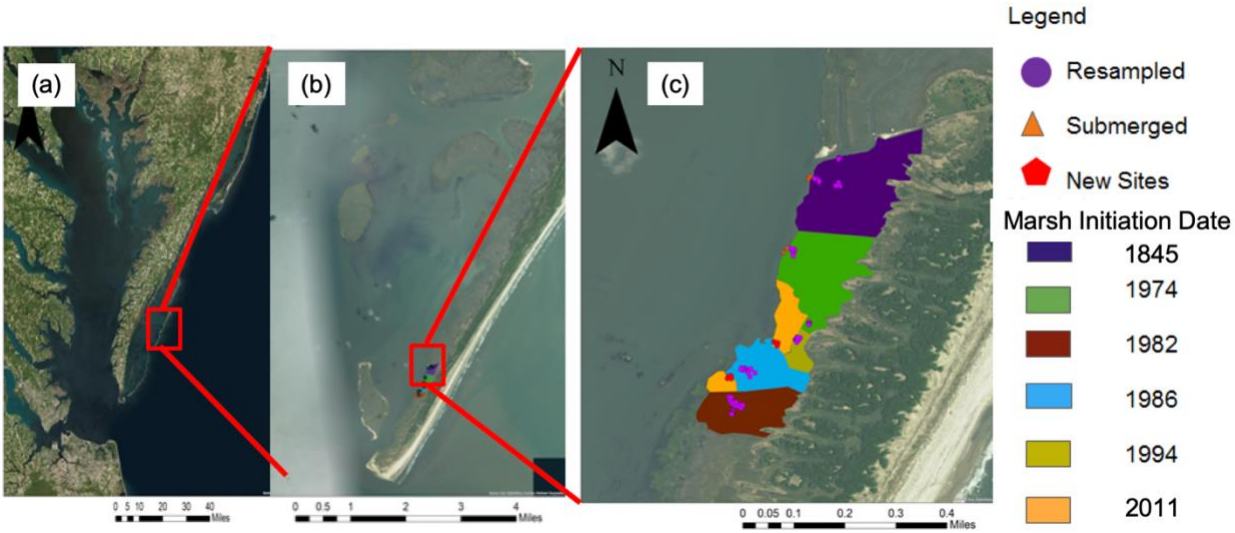

Figure 2.1: *Site map of (a) the Delmarva Peninsula, Va., with Hog Island outlined, (b) Hog island, and (c) the study site indicating the marsh initiation dates, which are defined as the date where S. alterniflora regrowth was documented, and locations of re-established, submerged, and new sites*

This study took place on a low-lying back-barrier island, Hog Island, located 14 km off the coast of Virginia and part of the VCR-LTER (Figure 2.1). The island, 11.3 km long by roughly 0.8 km wide (Day et al., 2001), is a highly dynamic system, with frequent disturbances due to wind, waves, storm surges, and tides (Hayden et al., 1991). The Ash Wednesday storm of 1962 deposited approximately 1 m of sand over the back-barrier marshes at the southern end of the island. The oldest marsh at this site was not affected by the storm and is at least 170 yr old. Since the storm, the fringing marshes have gradually grown back. We define marsh age by the date at which *S. alterniflora* first becomes visible in aerial imagery. Inspection of aerial imagery identified five younger marshes, with establishment dates of 1974, 1982, 1986, 1994 and 2011 (Walsh, 1998; Tyler & Zieman, 1999; Google Earth). The older four of these new marshes were part of previous studies, and the 2011 marsh was added to the chronosequence as part of the present work.

In June 2017, 1 x 1 m^2 plots were re-established in continuous meadows and creekbanks in the five marshes using GPS, following the 1995-1996 work of Walsh (1998) and Tyler & Zieman (1999), respectively. Previously, marsh zones were classified into tall or creekbank, medium, and short based on *S. alterniflora* height and distance from shore. For this analysis, we combined the short and medium height classes into a single "short" class, and the tall and creekbank sites into a "tall" class. These sites were located in five different age groups. Short, medium, and tall meadow plots consisted of three plots per height zone, but this was increased to four plots for more replication. Each of the historic creekbank sites had eight plots located within 3 m of the edge. We were unable to locate some tall zone plots that are presumed to be submerged. Eight new plots were created in areas of marsh expansion that appeared in approximately 2011, bringing the total number of age groups to seven. A summary of the number of plots in each group is available in Table **2.1**. Sampling took place during three field campaigns in June, July, and September 2017 and with minor exceptions, as noted below, was identical to earlier sampling, which took place in June, July, and September of 1995, as described previously. The position of each plot was determined using a Garmin RTK GPS TRM55971.

Table 2.1*: Number of plots in each marsh age group.*

	# of Short Zone Plots		# of Tall Zone Plots	
Marsh Initiation Date	Historic	Contemporary	Historic	Contemporary
1850	6	8	11	8
1974	6	8	3	--
1982	6	8	11	11
1989	6	8	3	4
1991	8	--	3	8
1994	3	4	11	8
2011	--	4	--	4

2.2.2 Porewater Properties

Porewater was extracted from 10 cm depth with a suction lysimeter in 1995 (e.g., Walsh 1998; Tyler & Zieman 1999) and a stainless-steel sampling probe in 2017 (Berg & McGlathery, 2001). We acknowledge potential differences in sampling methodologies, but in both cases, the sample was immediately put into a custom, sealed anaerobic chamber and redox potential and temperature were measured immediately using a Hach MTC-101 ORP probe. Redox potential was corrected to a standard hydrogen electrode by adding 208 at 25 °C and 204 at 30 °C (Hach.com). Salinity was determined using an automatic temperature compensating refractometer.

2.2.3 Sediment characteristics

Two sediment cores (I.D. 5 cm x 10 cm depth) were collected from each plot in June or July using a hammer auger. The first core was analyzed for organic matter using the loss on ignition method at 550 °C (Heiri et al., 2001) and for total phosphate by combustion in the presence of magnesium nitrate, followed by acid extraction and analysis using the ammonium molybdate method with spectrophotometric detection with a Shimadzu 1800 UV-Vis Spectrophotometer (Murphy & Riley, 1962). Historic measurements of total phosphate were from surface sediment (0-3 cm) at the meadow sites. The second core was used for sediment grain size; samples were mixed with 8.25% sodium hypochlorite to remove organic matter and the proportions of sand (diameter > 50 µm), silt (diameter 2 - 50 µm), and clay (diameter < 2 µm) were determined using the hydrometer method (Brower & Zar, 1977). In the historic meadow data, grainsize was measured in the top 0-5 cm. Three additional surface sediment

samples (top 3 cm) were collected with a 5 cc syringe corer and pooled for sediment nitrogen (%N) analysis using a Perkin Elmer 2400 Elemental Analyzer.

Benthic chlorophyll *a* was measured in 1 cm deep cores extracted using a 5 cc syringe corer in both June and July in both datasets (but only in creekbank sites in historic data). Cores were frozen at -80 °C until analysis and then mixed with 90% acetone and sonicated. Following a 24 hr extraction period at -20 °C, the samples were centrifuged and the absorbance of the supernatant at 665 nm and 750 nm measured before and after addition of 1N HCl. Concentrations of chlorophyll *a* and pheopigment were calculated using the Lorenzen (1967) equations.

2.2.4 Aboveground biomass

End of year biomass was determined in September. In all plots, the number of culms within a 0.25 m^2 or 0.065 m^2 sub-plot and height to the tallest leaf of 10 culms located along a diagonal transect were measured. The relationship between stem height and mass was derived by clipping all aboveground biomass in a series of 0.25 m^2 or 0.0625 m^2 quadrats across the chronosequence (n culms = 302), cleaning stems of sediment and removing dead leaves, and measuring the height and dry weight (dried at 60 °C for 24 hr) of each culm. Because allometric characteristics differed across marsh ages, we developed three height-weight regressions: the 1850 marsh, the 2011, 1994 and 1991 marshes, and the 1989 and 1982 marshes (Tables A.4 and A.5). Aboveground biomass in permanent sampling plots was then calculated using these regressions. Three culms were clipped outside but within 0.5 m of each plot and pooled for %C and %N analysis on a Perkin Elmer 2400 Elemental Analyzer, after freeze-drying and homogenization using a Wiley Mill.

2.2.5 Invertebrate Density

Invertebrate density was assessed at each 1 m^2 plot by counting all individuals of *Littorina irrorata, Ilyanassa obsoleta, Crassostrea virginica,* and *Geukensia demissa. Uca* spp. were estimated based on the number of burrows, assuming one crab per burrow (Walsh 1998), and were not identified to species. In the historic data set, invertebrates were measured only in meadow plots.

2.2.6 Data analysis

Tall and short zones were evaluated separately to determine correlation with age and identify differences between sampling periods using a mixed-model ANOVA, with marsh age as a continuous variable and sampling date (historic [1995] vs. contemporary [2017]) as a categorical variable. Normality was tested using the Shapiro-Wilk test and variables that did not meet assumptions of normality were transformed using either square root or logarithmic transformations. Data that could not be transformed to meet assumptions of normality were analyzed by Kruskal-Wallis tests, with both age and sampling date as categorical variables, and Wilcoxon Each Pair was computed as a post-hoc test. To evaluate site-specific changes over the 22-yr period, we conducted a separate comparison between data sets for each site and zone combination (i.e., 1972 marsh tall zone redox potential in historic compared to contemporary) t-test or Wilcoxon test, as dictated by normality of data.

A principal components analysis (PCA) was conducted on variables that were collected across sites in both historic and contemporary datasets, with the tall and short zones combined. Invertebrates and sediment phosphate were not sampled at creek plots in 1995 and benthic chlorophyll was not sampled at meadow plots in 1995, so these variables were excluded from the

PCA. Tall and short zones were evaluated separately using a mixed-model ANOVA as detailed above. All data analysis was conducted in JMP Pro version 14.0.0.

2.3 Results

We observed predictable trends in many of the physico-chemical properties of the marshes that may be attributed to age-related drivers, especially redox potential, sediment organic and nutrient content, and grainsize. However, there were some anomalies in the results that suggest the action of larger drivers of change, especially related to enhanced flooding of short zone marshes and additional deposition of sand at some sites. Biotic community structure also changed somewhat predictably, but there were marked shifts in the invertebrate communities suggesting enhanced resource supply and changes in predation due to increased flooding. Data that were collected, but not included in this analysis are available in Tables A.1 and A.2.

2.3.1 Porewater Properties

In both the tall and short zones, redox potential (Figure 2.2a and 2.2b) was negatively correlated with age ($p < 0.0001$, Table 2.2). While the general negative trend was similar between data sets, the contemporary tall zone overall had lower redox potential between datasets ($p = 0.02$, Table 2.2) and in individual marshes, redox decreased in the 1850 short zone ($p < 0.0001$, Tables 2.3 and A.4), and increased at the 1989 tall zone ($p = 0.04$, Tables 2.3 and A.4) from historic to contemporary datasets. Salinity (Figure 2.2c and 2.2d) was negatively correlated with age in the short zone and lower overall in the contemporary period ($p < 0.0001$ and $p = 0.02$, respectively; Table 2.2). In the 1850 and 1989 short zones, salinity was lower in the

contemporary dataset ($p = 0.002$ and $p = 0.05$ respectively; Tables 2.3 and A.4). There were no significant trends in the tall zone.

2.3.2 Sediment characteristics

Organic matter (Figure 2.2e and 2.2f) was positively correlated with age ($p < 0.0001$, Table 2.2) in both the short and tall zones but overall was higher in the tall zone in the recent series ($p < 0.0001$, Table 2.2). Between the historic and contemporary marsh at a single location, organic matter either remained unchanged or increased (Table 2.3). This trend was particularly noticeable in the 1994 marsh, with a > 5- and 8-fold increase in the short and tall zone respectively ($p = 0.05$, $p < 0.0001$ respectively; Tables 2.3 and A.4). In the 1989 short marsh and 1850 tall marsh, the increase was approximately 1.8 times ($p < 0.0001$, Tables 2.3 and A.4).

Sediment P and N (Figure 2.2g and 1h, and Figure 2.2i and 2.2j, respectively) increased with age in both marsh zones ($p < 0.0001$, Table 2.2). Phosphorus accumulation (slope) was significantly lower in the short zone of the contemporary marsh, as the younger marshes approached the levels of the older marshes (Age x Date interaction, $p = 0.02$, Table 2.2). The greatest change at a single site was an increase of 54% in the 1982 tall zone ($p < 0.0001$, Tables 2.3 and A.4); the only decrease was in the 1994 tall zone, where P was 1.3 times lower ($p = 0.02$, Tables 2.3 and A.4). In the tall zone, the rate of N accumulation was significantly lower in the contemporary marsh but was higher in the new data overall ($p = 0.004$, Table 2.2). Within age groups, sediment N increased at the 1994 short zone and 1991 and 1994 tall zones ($p < 0.005$ for all, Tables 2.3 and A.4).

In both short and tall zones, the overall proportion of clay (Figure 2.3) was lower in the contemporary marsh ($p < 0.0001$, Table 2.2) and negatively correlated with marsh age overall (p

<0.0001, Table 2.2). At individual sites, the proportion of clay decreased at the 1974 and 1982 short zones and 1982 and 1991 tall zones ($p < 0.01$ for all, Tables 2.3 and A.4). Sand was generally higher and clay was generally lower in the younger marshes (Figure 2.3), but because of the lack of normality, this was not evaluated using a mixed model. The only difference between data sets was at the 1974 high marsh (14% increase; $p = 0.004$, Tables 2.3 and A.4). Silt (Figure 2.3) increased slightly (approximately 5%) at the 1850, 1982, and 1994 tall marshes ($p = 0.03$, 0.02, 0.01, respectively; Tables 2.3 and A.4).

Benthic chlorophyll *a* (Figure 2.4a and 2.4b) was negatively correlated with marsh age and was higher in the contemporary dataset in the tall zone ($p < 0.0001$ for interaction, Table 2.2). This increase was consistent at all tall zone sites except at the 1850 marsh ($p <0.01$ for all, Tables 2.3 and A.4). Benthic chlorophyll measurements were not available for the historic short zone, but there was a negative correlation with age in the contemporary values ($p <0.0001$, Table 2.2).

2.3.3 Aboveground Biomass

Overall, *S. alterniflora* density (Figure 2.4c and 2.4d) remained unchanged at the short zone between the historic and contemporary series, with the exception of a small decrease in the 1974 marsh ($p = 0.05$, Tables 2.3 and A.4). However, in the tall zone, density was significantly decreased overall between the historic and contemporary marshes ($p = 0.001$, Table 2.2) and there was a modestly significant interaction between sampling date and marsh age ($p = 0.045$, Table 2.2). The density at the 1982 tall zone decreased by nearly 4-fold between the historic and contemporary marshes, due to patches of total die off ($p = 0.002$, Tables 2.3 and A.4). *S. alterniflora* height (Figure 2.4e and 2.4f) decreased significantly between datasets in both zones

($p < 0.004$ for both, Table 2.2). There was also a significant interaction term between sampling date and marsh age in the tall zone. In the short zone, height at a single site decreased 1.5 - 2.5-fold at all sites except for the 1994 marsh ($p < 0.02$ for all, Tables 2.3 and A.4). In the tall zone, height decreased significantly at the 1850 and 1989 sites ($p = 0.02$, Tables 2.3 and A.4), but increased at the 1991 marsh ($p = 0.02$, Tables 2.3 and A.4).

There was no significant relationship between biomass and marsh age or sampling year in the short zone (Figure 2.4g, Table 2.2), but a nearly twofold decrease in some individual marshes (1982 and 1974; $p < 0.05$ for both, Tables 2.3 and A.4). However, in the tall zone, the parabolic age-biomass relationship observed in the historic dataset was replaced by a negative relationship, driven largely by the very high biomass observed in the youngest marsh and leading to a significant interaction between dataset and age ($p = 0.02$, Table 2.2). Both the contemporary 1850 and 1982 marshes had significantly lower biomass in the tall zone ($p < 0.01$ for both, Tables 2.3 and A.4); however, biomass at the contemporary 1994 marsh increased by more than 1.5 times ($p = 0.05$; Tables 2.3 and A.4).

2.3.4 Invertebrate Density

C. virginica was not present on Hog Island during the sampling of the 1990s. There was notable colonization in ensuing years, and *C. virginica* were present in all short zones except for the 2012 and 1994 (Figure 2.5c); however, populations were not significantly different among age groups. In the tall marsh, *C. virginica* were present in the 2012, 1994, and 1850 age groups (Figure 2.5d), with the greatest numbers in the youngest marsh ($p < 0.0001$, Table 2.4).

Historically, *G. demissa* was absent from the 1994 short marsh, with similar densities in other sites (Wilcoxon each pair, $p = 0.008$, Table 2.4). In the contemporary marsh, populations

increased significantly at the 1850 short zone ($p = 0.05$, Tables 2.3 and A.4, Figure 2.5a and 2.5c). In the historic tall zone, populations were highest in the 1989 and 1982 marshes ($p = 0.002$, Table 2.4). Only the 1994 tall marsh changed significantly between time series, with a significant increase from 0 to 19 individuals m^{-2} ($p = 0.0006$; Tables 2.3 and A.4).

I. obsoleta (Figure 2.5) were historically most abundant in the 1850 short zone and 1974 and 1850 tall zone ($p < 0.0001$, Table 2.4), with populations as high as 311 individuals m^{-2} and virtually absent elsewhere (<1 individual m^{-2}). However, in the contemporary marsh, populations increased significantly at the 1989 and 1982 short zones and 1994 and 1982 tall zones ($p < 0.05$ for all, Tables 2.3 and A.4). There were also significant decreases at both the 1850 short and tall zones, where populations decreased by 50% and 100%, respectively ($p = 0.01$ and $p < 0.001$, respectively, Tables 2.3 and A.4). In the contemporary marsh, density was similar among age groups in the short zone and highest in the intermediate aged (1994 and 1982) tall zones ($p = 0.01$, Table 2.4).

In the short zone historic series, *L. irrorota* population was greatest in the 1974 marsh, and lowest in the 1994 marsh ($p < 0.0001$, Table 2.4). This switched in the contemporary period, when density was highest in the 1994 and 1989 short zones ($p < 0.0001$, Table 2.4). In the historic tall zone, *L. irrorata* was found only in marshes younger than the 1972 marsh during both time series, with similar densities across ages ($p = 0.0007$, Table 2.4). Populations increased significantly at all of the tall zone marshes except the 1850 marsh ($p < 0.02$ for all, Tables 2.3 and A.4), and in the contemporary series, the highest populations were located at the middle-aged marshes, while the lowest populations in the two oldest marshes ($p < 0.0001$, Table 2.4).

Within the short zone, *Uca* spp. was lowest in the youngest and oldest marshes in the historic dataset ($p < 0.0001$, Table 2.4). Populations in the contemporary marsh were 1.5 – 10-

fold lower than historic values, with highest densities in the 1989 and 1982 short zones and lowest in the 1974 and 1850 marshes $p = 0.006$, Table 2.4). *Uca* spp. in the historic tall zone were highest at the 1989 and 1982 marshes and lowest in the 1850 marsh $p = 0.002$, Table 2.4). Between sampling years, populations decreased significantly at all marshes except for the 1850 marsh ($p < 0.02$ for all, Table 2). In the contemporary marsh, the highest populations were found in the three youngest marshes ($p = 0.04$, Table 2.4).

2.3.5 Principal Components Analysis

The first component (PC1) of the principal components analysis explained 46% of the total variance and the second component (PC2) explained 16%. The factor loadings associated with each variable are displayed in Table 2.5. PC1 is primarily composed of sediment properties and redox potential. PC1 is associated with an increase in silt, clay, organic matter, and sediment nitrogen and a decrease in sand and redox potential in the positive direction. PC1 is highly correlated with marsh age in both the contemporary short and tall zones ($R^2 = 0.88$, $p < 0.0001$ and $R^2 = 0.75$, $p < 0.0001$ respectively, Table **2.6**) as well as the historic short and tall zones ($R^2 = 0.82$, $p < 0.0001$ for both). Overall, the factor scores for PC1 in the contemporary short zone are lower than those for the historic marsh ($p = 0.01$, Table 2.2), but were not different in the tall zone.

The contemporary 1974 short zone had a significantly lower factor score than the historic ($p = 0.02$, Tables 2.3 and A.4), but the mean factor score was significantly higher in the contemporary 1994 short zone ($p = 0.02$, Tables 2.3 and A.4) as well as the contemporary 1991 and 1994 tall zones ($p = 0.004$ and $p = 0.04$ respectively, Tables 2.3 and A.4).

The second component (PC2) is associated in the positive direction with increasing salinity and *S. alterniflora* height, and to a lesser extent, *S. alterniflora* density. PC2 was not correlated with marsh age in either the tall or short zones (Table **2.6**). The whole-marsh factor scores were significantly lower in the contemporary marsh for both the short and tall zones ($p < 0.01$ for both, Table 2.2). In the tall zone, scores for an individual site did not change significantly from the historic to contemporary marshes, but in the short zone, all marshes within an age group other than the 1994 marsh were significantly lower in the contemporary marsh ($p <0.004$ for all, Tables 2.3 and A.4).

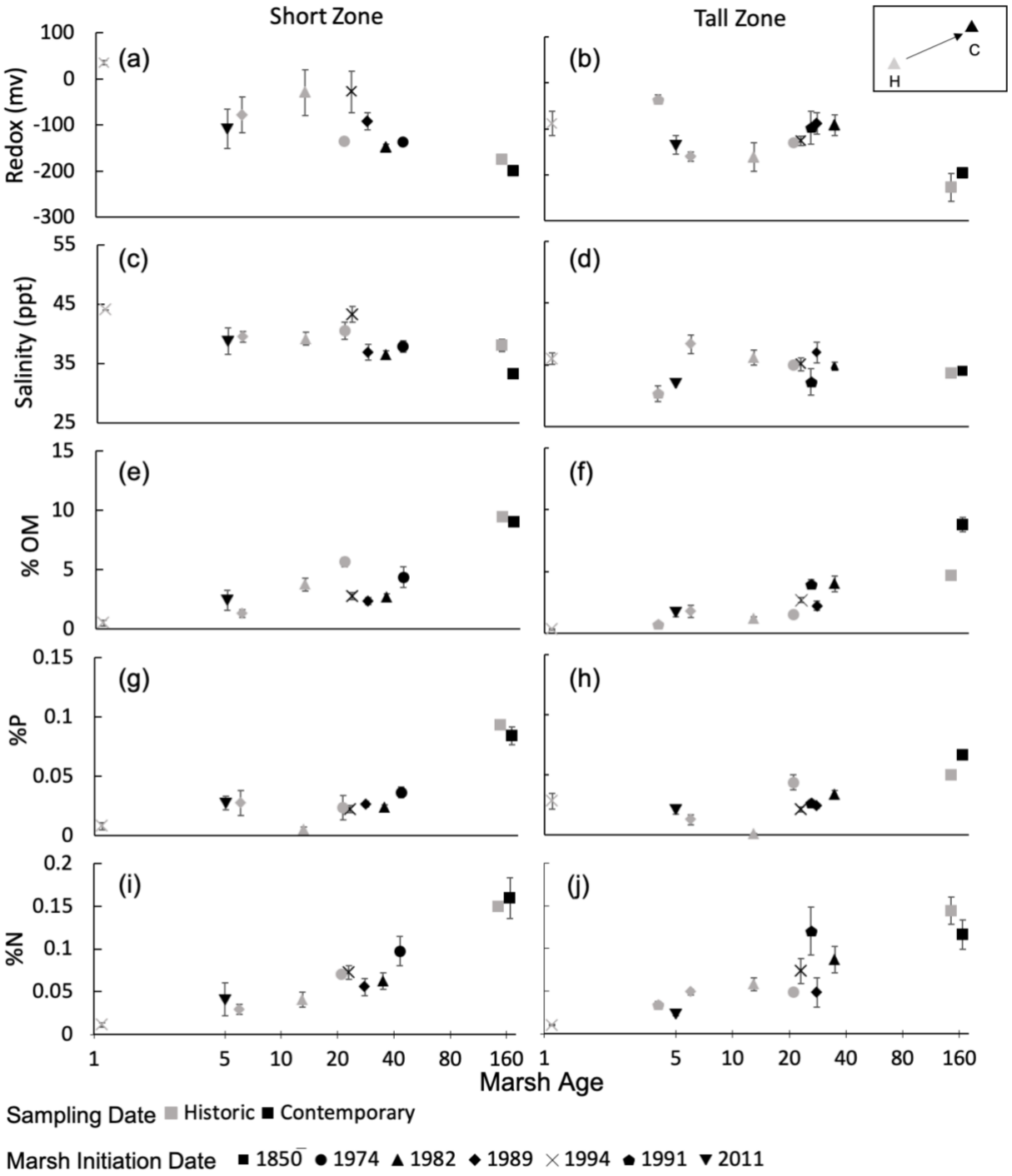

Figure 2.2*: Porewater redox potential (a, b), salinity (c, d), sediment percent organic matter (e, f), phosphorus (g, h), and nitrogen (i, j) in the short zone (left) and tall zone (right). Marsh age (x-axis) represents age of the site at the time of sampling (on a log scale for visibility). Symbol color indicates sampling period, where Historic refers to measurements from 1995-1996 and Contemporary to those from 2017. The symbol shape indicates the date of S. alterniflora appearance on previously unvegetated sand platform (marsh initiation date). Symbols of the same shape indicate the same marsh as it was in 1995/1996 (in black) and 2017 (grey). Error bars are the standard error of the mean.*

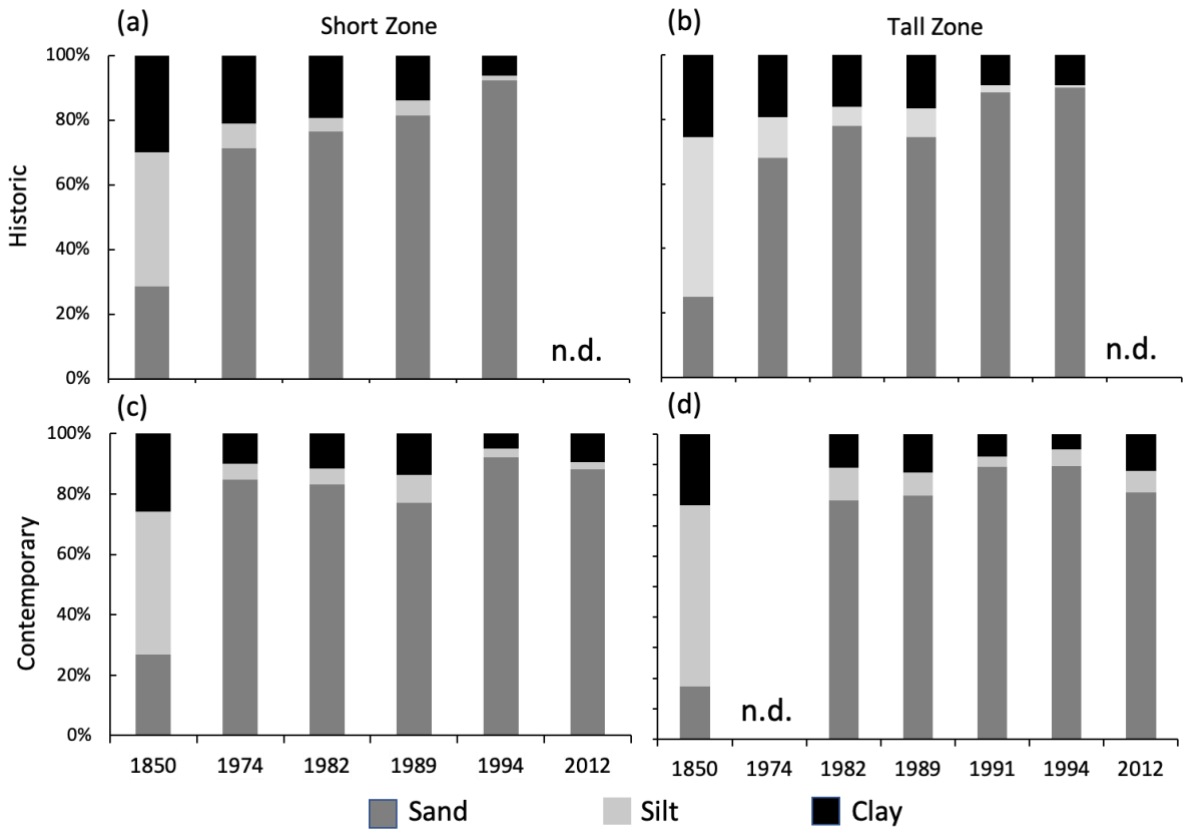

Figure 2.3*: Grain size distribution by marsh initiation date and height zone. (a) historic short zone, (b) historic tall zone, (c) contemporary short zone, (d) contemporary tall zone.*

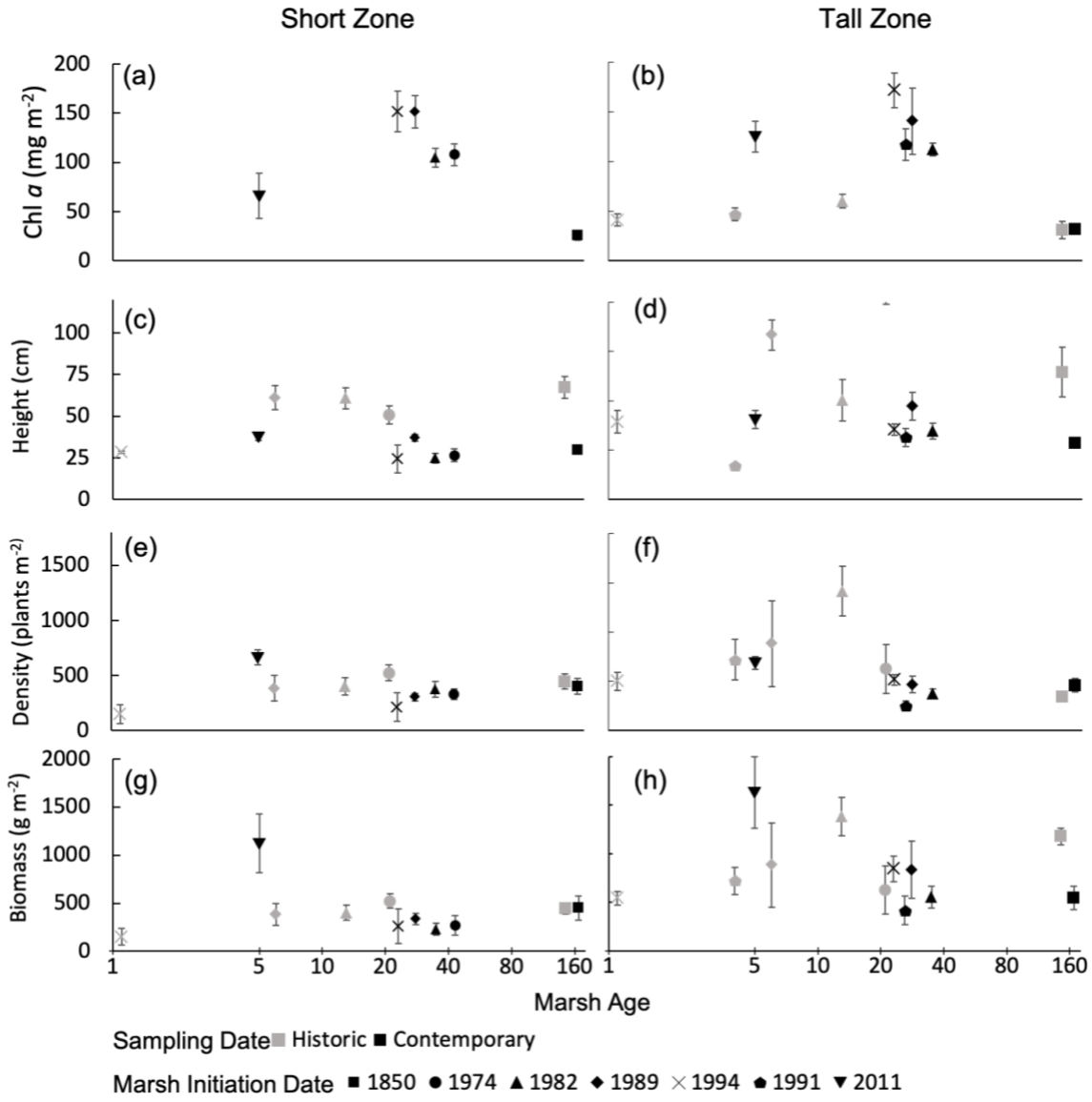

Figure 2.4*: Microalgal benthic chlorophyll a (a, b), S. alterniflora height (c, d), S. alterniflora density (e, f), and S. alterniflora biomass(g, h) in the short zone (left) and tall zone (right). Marsh age (x-axis) represents age of the site at the time of sampling (on a log scale for visibility). Symbol color indicates sampling period, where Historic refers to measurements from 1995-1996 and Contemporary to 2017. The symbol shape is the date of S. alterniflora appearance on previously unvegetated sand platform. Symbols of the same shape indicate the same marsh as it was in 1995/1996 (in black) and 2017 (grey). Error bars are the standard error of the mean.*

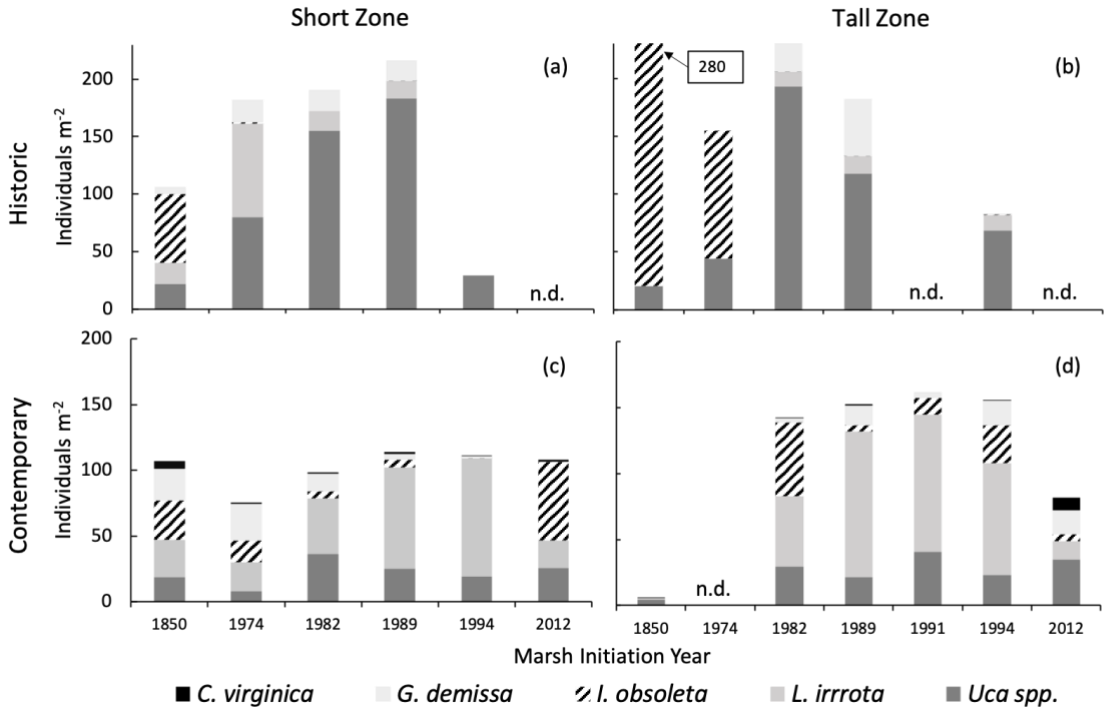

Figure 2.5*: Invertebrate densities (a) historic short zone, (b) historic tall zone, (c) contemporary short zone, (d) contemporary tall zone.*

***Table 2.2**: Results of mixed-model ANOVA on the effects and interactions of sampling date and marsh age at time of sampling. * indicates significance at $p < 0.05$, ** at $p < 0.01$.*

		Short Zone			Tall Zone		
		df	**F**	**P-value**	**df**	**F**	**P-value**
Redox	Date	1,66	2.32	0.13	1,88	5.49	0.02*
	Age	1,66	31.94	<0.0001**	1,88	30.26	<0.0001**
	Date x Age	1,66	0.76	0.67	1,88	3.51	0.06
Salinity	Date	1,64	9.55	0.003**	1,87	0.05	0.82
	Age	1,64	18.30	<0.0001**	1,87	0.32	0.57
	Date x Age	1,64	2.54	0.12	1,87	0.19	0.66
% OM	Date	1,66	2.37	0.13	1,89	90.94	<0.0001**
	Age	1,66	108.53	<0.0001**	1,89	219.48	<0.0001**
	Date x Age	1,66	0.95	0.33	1,89	0.14	0.71
% P	Date	1,65	1.97	0.17	1,74	3.34	0.07
	Age	1,65	102.01	<0.0001**	1,74	40.44	<0.0001**
	Date x Age	1,65	5.93	0.02*	1,74	0.02	0.89
% N	Date	1,66	2.24	0.14	1,88	9.44	0.003**
	Age	1,66	51.83	<0.0001**	1,88	36.97	<0.0001**
	Date x Age	1,66	3.19	0.08	1,88	1.00	0.004*
% Clay	Date	1,65	28.54	<0.0001**	1,88	27.70	<0.0001**
	Age	1,65	67.55	<0.0001**	1,88	64.61	<0.0001**
	Date x Age	1,65	0.23	0.63	1,88	0.04	0.85
Chl *a*	Date	--	--	--	1,107	40.866	<.0001*
	Age	1,39	39.27	<0.0001*	1,107	145.29	<.0001*
	Date x Age	--	--	--	1,107	25.135	0.0001*
Density	Date	1,64	0.4	0.53	1,90	11.55	0.001**
	Age	1,64	0.36	0.55	1,90	3.91	0.051
	Date x Age	1,64	0.33	0.57	1,90	4.12	0.045*
Height	Date	1,64	61.23	<0.0001**	1,90	8.02	0.006**
	Age	1,64	2.5	0.12	1,90	0.96	0.33
	Date x Age	1,64	3.98	0.051	1,90	4.62	0.034*
Biomass	Date	1,64	0.92	0.34	1,90	4.88	0.029*
	Age	1,64	0.42	0.52	1,90	0.41	0.52
	Date x Age	1,64	0.20	0.65	1,90	5.33	0.02*
PC1	Date	1,66	7.44	0.01*	1,90	1.02	0.32
	Age	1,66	352.52	<0.0001**	1,90	321.17	<0.0001**
	Date x Age	1,66	0.06	0.81	1,90	2.22	0.14
PC2	Date	1,66	89.27	<0.0001**	1,90	6.20	0.01*
	Age	1,66	0.41	0.53	1,90	0.52	0.47
	Date x Age	1,66	2.52	0.12	1,90	0.23	0.63

***Table 2.3**: Heat map illustrating the results from a t-test or Kruskal-Wallis(#) comparing contemporary and historic means for each marsh zone and initiation date. Table values are equivalent to p-value where an absent value = $p > 0.05$, 1 = $0.011 < p < 0.05$, 2 = $0.0011 < p < 0.01$, 3 = $0.00011 < p < 0.001$, 4 = $p < 0.00001$. Positive values indicate that the contemporary value is greater than the historic value; negative values indicate that the contemporary value is less than the historic value, and – indicates no data for comparison.5*

	Short					Tall				
	1850	**1974**	**1982**	**1989**	**1994**	**1850**	**1982**	**1989**	**1991**	**1994**
Redox	-4							1		
Salinity	-2		-1	-1						
%OM				1	2	4	3		4	4
Sed. %P			2		1	1	4		--	-2
Sed. %N					2				3	4
%Clay		-4	-1				-2			-1
%Sand #				-2						
%Silt #						1		1		1
Chl *a*	--	--	--	--	--		4	--	3	4
Density		-1					-2			
Height	-2	-2	-2	-1		-1		-1	1	
Biomass		-1	-1			-2	-1			1
G. demissa#	1								--	3
I. obsoleta#	-1		1	1		-3	1		--	1
L. irrorata#		-4		4	2		1	2	--	2
***Uca* spp.#**		-4	-3	-4			-3	-1	--	-2
PC1		-1			1				1	2
PC2	-4	-4	-4	-2						

Legend: -4 -3 -2 -1 1 2 3 4

Table 2.4*: Mean ± standard error for non-normally distributed data. Letters indicate results of Wilcoxon each pair test, where different letters indicate significant differences between means within an age group. * indicates significance at p < 0.05, ** indicates significance at p < 0.001.*

			Marsh Initiation Date									
			1850	1974	1982	1989	1991	1994	2012	df	X^2	p-value
Uca sp.	Short	H	22±4^{c}	80±6^{b}	155±23^{ab}	183±11^{a}	--	29±5^{c}	--	4	39.1	<0.0001**
		C	19±5^{b}	8±1^{b}	37±9^{a}	25±3^{a}	--	19±6^{ab}	26±12^{ab}	5	16.2	0.006**
	Tall	H	21±10^{c}	44±23^{bc}	193±31^{a}	118±30^{a}	0	68±20^{ab}	--	4	17.1	0.002**
		C	4±1^{b}	0	30±9^{ab}	27±11^{ab}	41±6^{a}	23±8^{a}	35±10^{a}	5	11.9	0.036*
L. irrorata	Short	H	18±3^{a}	82±10^{c}	17±4^{a}	16±4^{a}	--	0±0^{b}	--	4	36.1	<0.0001**
		C	28±12^{b}	22±6^{b}	42±9^{b}	77±7^{a}	--	09±17^{a}	21±7^{b}	5	31.6	<0.0001**
	Tall	H	0.2±0.2^{b}	0.2±0.2^{b}	13±4^{a}	15±3^{a}	0±0	14±7^{a}	--	4	19.4	0.0007**
		C	1.1±0.4^{d}	0±0	53±11^{b}	111±25^{a}	104±15^{a}	85±15^{ab}	14±4^{c}	5	33.7	<0.0001
I. obsoleta	Short	H	60±15^{b}	1±1^{a}	0±0^{a}	0.1±0.1^{a}	--	0±0^{a}	--	4	43.2	<0.0001**
		C	30±14	16±7	5±4	6±2	--	0.3±0.3	60±36	5	6.1	0.30
	Tall	H	311±57^{a}	111±27^{b}	0.3±0.2c	0.2±0.2c	0±0	0.8±0.8c	--	4	24.6	<0.0001**
		C	0±0b	0±0	56±21^{a}	4±3^{b}	13±11^{b}	29±12^{a}	5±5^{b}	5	20.0	0.001**
G. demissa	Short	H	7±2^{a}	20±7^{a}	18±6.8^{a}	18±6^{a}	--	0±0^{b}	--	4	13.8	0.008*
		C	24±7^{a}	28±9^{a}	14±5^{a}	4±0.94^{a}	--	1.4±0.9^{b}	0.3±0.3^{b}	5	27.3	<0.0001**
	Tall	H	0±0^{c}	0±0^{c}	31±18^{ab}	49±19^{a}	0±0	0.2±0.2^{bc}	--	4	17.0	0.002*
		C	0±0^{b}	0±0	4±0.84^{c}	15±10^{ab}	4±3^{b}	19±4^{a}	18±8^{a}	5	31.1	<0.0001**
C. virginica	Short	H	--	--	--	--	--	--	--			
		C	0.3±2.4	1±0.5	0.1±0.5	0.4±0.5	--	0±0.3	0±1.7	5	10.2	0.07
	Tall	H	--	--	--	--	--	--	--			
		C	0.1±0.1^{b}	0±0	0±0.1^{b}	0±0.6^{b}	0±0^{b}	0.1±0.9^{b}	4±5^{a}	5	30.3	<0.0001**
% Silt	Short	H	42±3^{a}	8±1^{b}	4±1^{bc}	5±1^{bc}	--	1±0.3^{c}	--	4	19.0	0.0008**
		C	47±4^{a}	5±1^{c}	5±1^{c}	9±1^{b}	--	3±1^{c}	2±1^{c}	5	26.9	<0.0001**
	Tall	H	50±6^{a}	13±9^{b}	6±1	9±4^{b}	2±0.6^{b}	0.9±0.2c	--	5	38.1	<0.0001**
		C	51±6^{a}	0±0	11±2^{b}	8±4^{bc}	3±0.9^{c}	5±2^{c}	7±2^{bc}	5	21.9	0.0006**
% Sand	Short	H	29±3^{c}	71±2^{b}	77±2^{b}	82±3^{b}	--	92±1^{a}	--	4	20.7	0.0004**
		C	27±5^{e}	85±2^{bc}	83±2^{bcd}	77±2^{d}	--	92±1^{ab}	88±3^{ab}	5	27.8	<0.0001**
	Tall	H	25±7^{c}	68±10^{b}	78±1^{b}	72±4^{b}	88±1^{a}	90±0.6^{a}	--	5	39.8	<0.0001**
		C	28±7^{b}	0±0	78±2^{c}	80±5^{abc}	89±2^{a}	90±3^{a}	81±3^{abc}	5	22.8	0.0004**

Table 2.5: *Variables used in the principal components analysis and factor loadings associated with each for components 1 and 2 (PC1 and PC2, respectively)*

	PC1	PC2
% Silt	**0.93**	-0.0003
% Clay	**0.80**	0.34
% OM	**0.79**	-0.03
% N	**0.76**	-0.23
***S. alterniflora* Density**	0.11	0.47
***S. alterniflora* Height**	0.09	**0.80**
Porewater Salinity	-0.30	**0.63**
Redox	**-0.66**	0.06
% Sand	**-0.94**	-0.11

Table 2.6: *Linear regression for PC1 and PC2 versus marsh age at time of sampling. * indicates significance at $p < 0.05$, ** at $p < 0.01$.*

		Short Zone				Tall Zone			
		df	**F**	**P-value**	**R^2**	**df**	**F**	**P-value**	**R^2**
PC1 x age	**H**	1,39	266.05	<0.0001	0.88	1,43	122.79	<0.0001**	0.74
	C	1,26	116.23	<0.0001	0.82	1,46	209.04	<0.0001**	0.82
PC2 x age	**H**	1,39	3.00	0.092	0.05	1,43	0.046	0.83	-0.23
	C	1,26	0.39	0.54	-0.02	1,46	0.57	0.45	-0.01

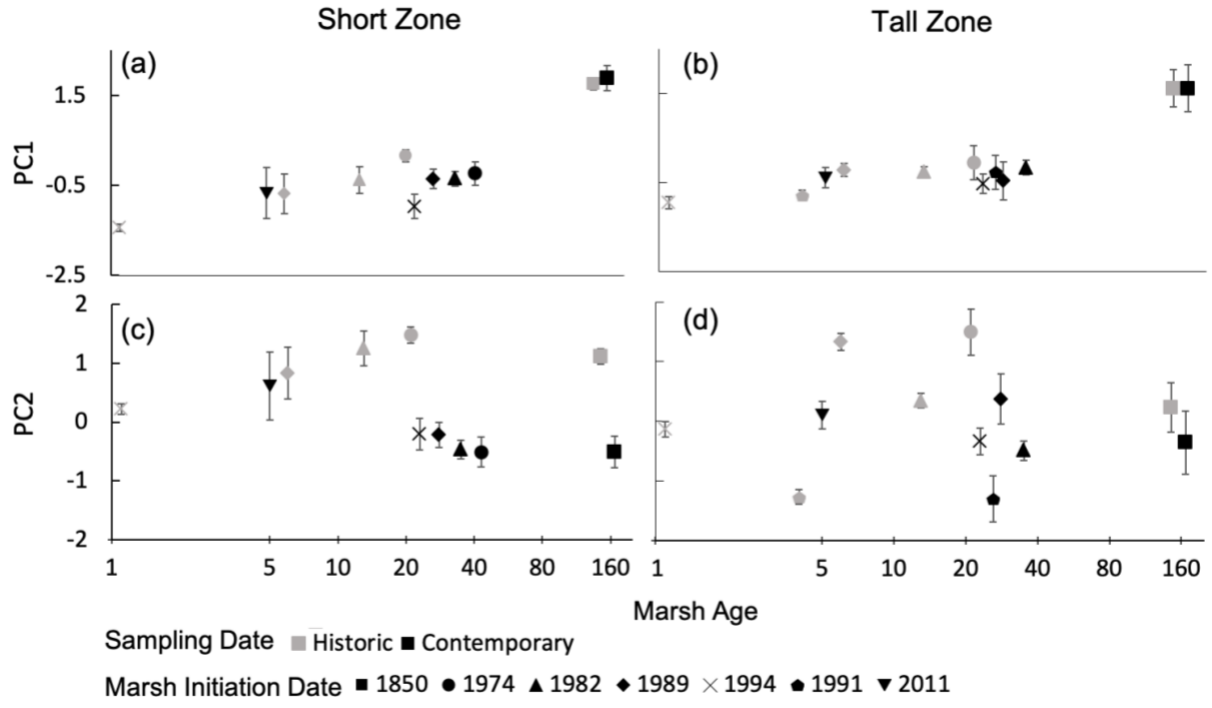

Figure 2.6*: Mean PCA scores (a, b) PC1, (b, c) PC2 in the short zone (left) and tall zone (right). Marsh Age (x-axis) is the age of the site at the time of sampling (on a log scale for visibility). Symbol color indicates sampling period, where Historic refers to measurements from 1995-1996 and Contemporary to 2017. The symbol shape is the date of S. alterniflora appearance on previously unvegetated sand platform. Error bars are the standard error of the mean.*

2.4 Discussion

Hog Island is a rapidly changing environment and was substantially altered since the initial studies were conducted in the 1990s. Sea level rise (SLR) is likely a driver of many of the observed changes. Several plots that were established in the 1990s, including all plots in the 1850 and 1974 tall zones, were cleaved off in the contemporary marsh, with steep scarps indicating edge erosion. SLR can result in both marsh submergence and increased edge erosion, which is a major factor in marsh loss worldwide (Marani et al., 2011). Erosion along marsh edges can lead to substantial land loss, and SLR and climate change-related increases in storm magnitudes and frequencies may influence future rates of erosion (McLoughlin et al., 2015).

Several trends in sediment physico-chemistry were consistent with SLR. However, there were also several regions of marsh expansion, which were estimated from aerial imagery to have established in 2011 and are believed to be the result of additional overwash at that location. Additionally, die-off was prevalent, particularly in the 1850 short zone.

Despite these changes, there were successional patterns that continued to occur in a predictable manner. As the marsh ages, porewater redox potential decreases and sediment organic matter, nitrogen, and phosphorus content increase. Overall, the general trends in these physico-chemical variables remained consistent with the trajectories that were predicted in 1995 and for the most part, the rate at which these variables change relative to marsh age was not significantly different in the historic and contemporary marshes as determined using a space-for-time substitution. However, in some cases, sediment grain size and biological variables tended not to follow the predicted patterns of development, suggesting other drivers of ecosystem change.

The three strongest loadings on PC1, which was correlated with age, were all associated with sediment grain size, such that higher scores (indicating older marshes) are associated with higher silt and clay and lower sand content. Allochthonous sediment is introduced through tidal inundation and vegetation decreases tidal velocities and results in deposition of finer particles such as silts and clays (Friedrichs & Perry, 2001), and may also contribute to sediment carbon (Drexler et al., 2020). Over time, it is predicted that this results in the accumulation of silt and clay in the sediment, and the relative percent of sand decreases (Redfield, 1972; Osgood et al., 1995; Tyler & Zieman, 1999; Walsh, 1998). In this study, the sediment structure demonstrates this predicted pattern with age, such that proportions of clay and silt were higher in older marshes and the percentage of sand lower. Some sites also followed the predicted trajectories

between the historic and contemporary marshes, such as a decrease in % sand at the 1989 short zone and increases in % silt at the 1850, 1989, and 1994 tall zones. However, some individual sites did not follow this trend, with proportions of sand that generally did not change, and clay content decreasing at several sites. Changes in grain size did not always occur along the same trajectory as predicted by the space-for-time substitution, which could indicate that initial or hyper-local conditions such as the amount of overwash, elevation, or geomorphology may be exerting an influence on *S. alterniflora* mediated feedbacks. There may also be trajectory reversals resulting from small overwash events since 1995. Die off and changes in vegetation density could also influence the accumulation of sediment and increase the potential for erosion (Coleman & Kirwan, 2019).

PC1 was highly correlated with marsh age overall, and in the tall zone, the overall whole-marsh scores for PC1 changed predictably in the contemporary 1991 and 1994 marshes, suggesting higher developmental maturity than the historic marsh. The 1850 marsh did not change, suggesting developmental maturity was reached by 1995, and likewise, the 1989 and 1982 tall zone did not change. In the latter two cases, the grainsize distributions suggest a potential reversal of the developmental trajectory driven by external factors such as overwash, edge erosion and SLR in the intervening years.

In the short zone, the 1994 marsh also "aged" as anticipated, but there was no change in overall scores for PC1 between datasets for other marshes, except for the 1974 marsh. The 1974 short marsh was the only marsh age group in which the mean factor score for PC1 was significantly lower between the historic and contemporary marshes, indicating that the developmental trajectory was reversed at this site. The 1974 marsh was substantially different and the original tall zone plots were eroded, leaving the short zone a few meters from the marsh

edge. New overwash may also play a role here, as the proportion of sand was higher, and clay was lower in the contemporary marsh. Likewise, there were significant declines in plant biomass, *Uca* spp., and *L. irrorata*, suggesting an altered state.

Odum (1969) postulated generally for all ecosystems that total organic matter accumulates and nutrient conservation increases with age. This was generally true in this study and the rate of organic matter accumulation was not significantly different between sampling dates. Sediment organic matter and %N also load heavily in the positive direction on PC1. While sediment %P was not included in the PCA as data were not available for the 1995 creek sites, increased %P is likely also a characteristic of developmental maturity. However, the predicted rate of sediment P accumulation was lower in the contemporary short marsh. This may also be related to sea level rise and greater inundation periods, which could result in lower redox and increased phosphate solubility (Rozan et al., 2002).

Sea level rise likely plays a significant role in the lower overall porewater salinity in the contemporary short zone as higher elevations are flooded more frequently and flushing is increased (Morris, 2000). However, marsh elevation on Hog Island demonstrates an age-related decrease and is a confounding factor in this analysis as hydrogeomorphology is a dominant factor driving salt marsh function (Tyler & Zieman, 1999; Walsh, 1998). However, the elevation decrease is likely not directly related to marsh development as overwash events increase the marsh platform and the amount of overwash at any given age zone is unknown (Walsh, 1998). As such, the decline in porewater salinity with age in the short zone is likely influenced by differences in elevation, as lower elevations are flooded and flushed more frequently, and are therefore more susceptible to SLR.

Similarly, porewater ORP decreased with marsh age, corroborating prior studies of salt marsh succession that have found trends of decreasing ORP with marsh age (Osgood & Zieman, 1993; Osgood et al., 1995; Tyler & Zieman, 1999). The higher organic content in older marshes may support greater anaerobic decomposition, which ensues in oxidation-reduction reactions that result in build-up of hydrogen sulfide and contribute to the ORP (Patrick & Delaune, 1977). Additionally, finer-grained sediments have lower porosity and decreased ORP (Argese et al., 1992). Additional overwash events that increased sediment sand content may result in higher ORP, such as at the 1989 tall zone. Elevation and SLR are also contributing factors, as lower elevations are inundated more often. Increased sea level can augment production of *S. alterniflora* to a point; however, if the tidal submergence is too great, it can stress marsh vegetation from increased sediment deposition and waterlogging and decrease productivity (Chmura, 2013). Sulfide concentrations greater than 1 mM can decrease *S. alterniflora* productivity, either through an increase in soil reducing conditions or directly from sulfide toxicity (Mendelssohn & Morris, 2002).

As such, it might be expected that the highest biomass occurs in middle-aged marshes, after nutrient reservoirs have built up, but before the low ORP and build-up of toxic components in the sediment. However, this study indicates that biomass displays only a moderate parabolic relationship with marsh age, and biomass is greater in the youngest marshes, which is consistent with prior studies at this site (Walsh, 1998; Tyler & Zieman, 1999). This is probably due to the variety and spatial heterogeneity of factors that control production. Biomass at the 2012 marsh in both the short and tall zones was quite high relative to other age groups. This is likely due to a combination of biophysical factors at this site that promote production. The sites tended to be at a lower elevation, which may allow for increased flushing. The 2012 marsh may also have

developed over a nutrient-rich mud-flat that was buried during the overwash event, which may provide nutrients to higher depths and support greater plant growth, similar to what was found by (Osgood & Zieman, 1993).

S. alterniflora biomass in the tall zone was significantly lower in the contemporary marsh, which is likely due to substantial edge erosion in the older marshes, combined with generally shorter plants. The 1850 and 1974 tall zone plots were washed away and are now several meters off the current shoreline. The present marsh edge consisted solely of short zone plants, and biomass at the remaining tall zone was lower by more than two times at the 1850 marsh, which may be related to increased inundation time from SLR. *S. alterniflora* height was lower in all the contemporary short zone marshes and biomass was decreased at the 1974 and 1982 short zone marshes as well. The decrease in both biomass and height may be linked to increased flooding durations (Smith & Lee, 2015). The substantial decrease in biomass within the 1850 short marsh may also be related to die off observed in this marsh, which has been linked to changes in tropic structure, precipitation, and edaphic conditions (Silliman & Bertness, 2002a; Alber et al., 2008; Bertness & Silliman, 2008).

2.4.2 Invertebrates

Invertebrate populations tended not to follow the trends predicted in prior studies, and the distribution of invertebrates shifted substantially from what was predicted in 1995. These shifts are likely tied to a variety of factors, but especially to changes in tidal inundation and predation. *L. irrorata, G. demissa* and *Uca* spp. are preyed upon by a variety of fish and crabs, particularly *C. sapidus*, which enters with the incoming tide to forage (Herrnkind, 1968; Seed & Hughes, 1997). However, in the case of *C. virginica*, the rebounding population may be due to external

drivers of population control. *C. virginica* suffered drastic declines in the Chesapeake Bay area during the late 1800s to early 1900s, following widespread habitat destruction and the introduction of mechanized fishing techniques (Rothschild et al., 1994). Fungal disease has also been implicated in their decline (Andrews & Hewatt, 1957). In 1995, no *C. virginica* were present at Hog Island, however, in 2017, they were present in low densities at several marsh ages.

For the most part, *G. demissa* populations within an age group were not significantly different between the contemporary and historic marsh, with the exception of the 1994 tall zone where populations increased. However, in both the historic and contemporary series across initiation dates in the short zone, *G. demissa* populations tended to be higher in the older marshes, while populations in the tall zone tended to be higher in the younger marshes. *G. demissa* is a filter feeder, but populations may be controlled by predation by *C. sapidus* (Seed & Hughes, 1997). As the distribution is linked to elevation, distribution in older short zones and younger tall zones may represent an ideal flooding frequency for feeding with sufficient refuge from predation. The higher populations of *G. demissa* may be linked to the higher biomass seen in the younger tall zone marshes. *G. demissa* is often found attached to *S. alterniflora* stems and roots and may alleviate stressors that limit plant growth by acting as stabilization against physical disturbances and transferring nutrients from the water column to the sediment surface (Bertness, 1984). The presence of mussel mounds has also been linked to increased *S. alterniflora* survival during severe drought periods due to increased water storage and reduced soil salinity (Angelini et al., 2016).

I. obsoleta are often found on exposed mudflats, where they graze on detritus (Cranford, 1988). Previously they were found in high densities at the 1850 and 1974 tall zones, likely due to

the abundance of fine detritus and lower elevation, which suits their feeding habits. However, populations were significantly lower in the contemporary marsh, which is most likely due to the erosion and loss of most of the tall zone in the older marshes, where previously their populations were highest. Decreases in *I. obsoleta* populations could result in accumulation of detritus at sediment surfaces and may be related to the increase in sediment organic matter observed in the 1850 marsh.

In the 1990s, *Uca* spp. populations were highest in intermediate aged marshes; however, there were no differences across sites in 2017. Additionally, *Uca* spp. were significantly less abundant 2017, which is contrary to findings of increased *Uca* spp. burrow density in Rhode Island salt marshes between 1998 and 2016 (Raposa et al., 2018). This could be due to increased predation resulting from a greater tidal range. Changes in *Uca* spp. populations can have implications for *S. alterniflora* growth as they have been implicated as non-trophic facilitators that increase *S. alterniflora* growth through bioturbation (Gittman & Keller, 2013). Thus, the lower plant biomass in the older marshes may be, in part, from a lack of sediment aeration by *Uca* spp.

L. irrorata is one of the most abundant grazers in coastal salt marshes and display low-level, facultative farming mutualism with intertidal marsh fungi, of which they are obligate feeders. This method of grazing can have a negative effect on the host plant and can substantially impact marsh vegetation (Silliman & Newell, 2003). *L. irrorata* can damage *S. alterniflora* foliage while foraging and can destroy the marsh canopy at high densities (Silliman & Bertness, 2002a). *L. irrorata* abundance was much higher in 2017 than in 1995, with increases of 1.5 to over 7-fold in individual marshes. The highest populations were found in areas of marsh die-off (pers. obs.). Grazing by snails may be a response to die-off that was precipitated by other factors,

and runaway grazing has been postulated as a major contributing factor in the spread of marsh die-off (Silliman & Bertness, 2002; Silliman et al., 2005; Bertness & Silliman, 2008).

2.5 Conclusions

This long-term study indicates that there are predictable trends in many of the physico-chemical properties related to marsh age, particularly porewater redox potential, sediment organic matter and nutrients, and grainsize. However, salt marshes are highly dynamic environments with many external drivers of change that may cause reversals in the developmental trajectory. In particular, additional sand deposition associated with coastal storms, and potential drowning from SLR in the short zone appeared to have effects in this marsh. Invertebrate community structure was not predictable based on age alone, but there were indicators of changes in resource supply and/or decreases in predation that drive abundance. Therefore, while time still appears to be a strong driver, other forces are acting on the marsh in tandem, and some properties are more influenced than others. As the effects of climate change and other human pressures are intensified and these external forces are exacerbated, it is likely that the trajectory of change in marsh ecosystem structure will continue to deviate further from the predictions made in the 1990s.

The endpoint of succession may depend more on these external factors and hyper-local forcing, than simply the push of time. While the marshes generally follow the predicted trajectory, there are a few sites where reversals (e.g. additional sand deposition) have taken place or external factors (such as SLR or changing resource availability) may be changing the trajectory of an individual marsh. Instead of converging to a single endmember, these marshes appear to have individual trajectories. However, it is also important to note that this is predicated

on only two sampling dates that are spaced approximately 20 years apart, and further sampling in the future is required to more robustly determine whether the trajectory of a given individual marsh follows the predictions based on the space-for-time substitution or if each marsh has a separate trajectory.

These results may have important implications for ecosystem services such as carbon storage and sequestration. While sediment organic matter had similar rates of accumulation throughout the chronosequence in both the historic and contemporary marsh, aboveground biomass decreased in the contemporary tall zone due to SLR and edge erosion, and some individual marshes in the short zone had much lower aboveground biomass, likely due to SLR and die-off. As stressors increase in the marsh, it is likely that biomass production will also decrease, which in turn will ultimately decrease carbon sequestration capabilities. This may also have implications for habitat and invertebrate population and community composition as resources are depleted and these populations shift as a result.

Understanding the trajectory of marsh development is essential for planning restoration efforts as well as evaluating the success of restoration activities. Developmental trajectories can address management questions and can be used to predict if and when created marsh projects will reach reference levels, develop more effective monitoring protocols, and provide information that is needed to establish mitigation goals (Morgan & Short, 2002). Created wetlands are often measured against natural wetlands of the same type as an indicator of success (Craft, 2016). However, often the age of these reference marshes is not taken into consideration. As evident in this study, young and old marshes have differences in physico-chemical properties and these comparisons between created and reference wetlands may not be appropriate, depending on the age.

Additionally, created wetlands are often evaluated based on factors such as community structure, including vegetation, fauna, and soil properties (Craft, 2016). Vegetation properties (such as density, height, and aboveground biomass) and invertebrate population and community composition, which did not follow clear linear successional trends, may be less predictive of success in created wetlands than sediment properties, which generally did display clear trends. Marsh development may be more clearly indicated by physico-chemcial parameters than biological parameters, which seem to be more influenced by external factors.

Shifts in developmental trajectories similar to those observed here (such as changes in invertebrate densities and aboveground biomass) in created marshes could also indicate changes induced from external factors such as SLR or increasing storm intensity and frequency and may provide opportunities for management practices that could mitigate these effects.

Chapter 3 : Assessing Salt Marsh Vulnerability using High-Resolution Hyperspectral Imagery

3.1 Introduction

Salt marshes are a rapidly changing environment and are vulnerable to a variety of anthropogenic impacts including human manipulation, land conversion, invasive species, water-borne pollution, and global climate change, especially increased temperatures, changing precipitation patterns, and sea level rise (e.g. Morris et al., 2002; McKee et al., 2004; Gedan et al., 2009; Hughes et al., 2012). In recent decades, acute marsh die-off has increased, likely related to climate change-induced stressors such as drought, and changes in trophic structure (Alber et al., 2008; Bertness & Silliman, 2008; McKee et al., 2004). Coastal wetlands provide the greatest number of ecological services of any coastal environment, including support for coastal fisheries, important habitat, protection from storm surges, and reduction of nutrient loading to coastal water (Boesch & Turner, 1984; Barbier et al., 2008; Koch et al., 2009; Morgan et al., 2009). Additionally, salt marshes sequester carbon at high rates and there has recently been much interest in 'Blue Carbon,' the stock of carbon in seagrasses and coastal wetlands, including salt marshes, and the potential for salt marshes to offset human greenhouse gas emissions (Chmura et al., 2003, 2013; Mcleod et al., 2011; Hopkinson et al., 2012). However, marshes are very heterogeneous and there is still great uncertainty in salt marsh carbon sequestration and other ecosystem services due to this heterogeneity (Mcleod et al., 2011).

Sea level rise, changing precipitation patterns, and eutrophication may have substantial influences on salt marsh sustainability. Although salt marsh vegetation self-regulates elevation by accumulating organic matter and trapping sediment, increasing rates of sea level rise may threaten marsh submergence (Morris et al., 2002). If tidal submergence is too great, it can create hypoxic conditions and stress marsh vegetation resulting in decreased productivity, which can further threaten mash persistence (Chmura, 2013). Eutrophication can be a driver of salt marsh

loss as nitrogen-enriched *S. alterniflora* allocates more production to aboveground biomass, resulting in fewer roots that stabilize sediment (Turner et al., 2009). This can result in edge erosion and marsh loss and decreased organic matter accumulation, leading to loss of marsh elevation (Turner et al., 2009; Turner et al., 2004; Deegan et al., 2012). Changes in precipitation events such as drought also have implications for salt marsh health as evapotranspiration occurs during times of reduced rainfall and increases salinity. While *S. alterniflora* is generally salt-tolerant, high salinity can decrease the productivity of marsh plants and is lethal at very high salinities (Hester et al., 1998; Linthurst & Seneca, 1981). Drought conditions also exacerbate the effect of salinity (Brown et al., 2006).

Detecting and understanding how salt marshes react to stressors such as these may assist with conservation and restoration practices as well as improve predictions of present and future ecosystem services. However, field-based methods can be disruptive, labor intensive, and impractical due to inaccessibility, and high heterogeneity. Remote sensing techniques such as satellite or flyover imagery and light detection and ranging (LIDAR) are increasingly important in determining the sustainability and permanence of salt marshes and may be used to ascertain the future of essential ecosystem services, including Blue Carbon storage (Chmura, 2013). High spectral resolution (hyperspectral) data can be used to detect spectral variations which result from biophysical properties (Artigas & Yang, 2006). However, due to the high spatial heterogeneity in salt marshes, traditional remote sensing techniques such as flyover or satellite-based imagery may not have sufficient spatial resolution to determine plant characteristics and stressors. High-resolution (sub-centimeter scale) hyperspectral imagery can provide levels of detail that match the scale of heterogeneity within the marsh, and has been used to predict

properties such as above-ground biomass and leaf area index (Badura et al., 2019; Eon et al., 2019).

Remote sensing has been used to map the extent, land cover, and species composition in coastal wetlands (Bachmann et al., 2002, 2003; Artigas & Yang, 2006; Cheng et al., 2006; Klemas, 2011; Hladik et al., 2013), as well as to detect areas of marsh die off (Ramsey & Rangoonwala, 2005, 2006, 2008; Marsh et al., 2016; Miller et al., 2017). Prior research regarding leaf optical properties in salt marsh die-off zones (e.g. Ramsey & Rangoonwala, 2005; Marsh et al., 2016; Miller et al., 2017) demonstrated that vegetation indices such as the ratio vegetation index (RVI) are capable of detecting the onset and progression of marsh die-off. Ramsey & Rangoonwala (2005) detected leaf optical changes that correlated with distance from dieback sites. The RVI was able to detect late-stage marsh die-off but was not sensitive to the onset of die-off. A ratio of NIR to green detected the initial die-off progression and subsequent recovery. Miller et al (2017) used NDVI to detect change in satellite imagery between years to map the extent of marsh die-off. However, little work has been conducted on detecting specific stressors, particularly edaphic factors, within salt marsh ecosystems using remote sensing techniques.

In agricultural systems and freshwater wetlands, remote sensing has been used to detect various plant properties such as leaf nitrogen content (e.g. LaCapra et al., 1996; Tian et al., 2011; He et al., 2016; O'Connell et al., 2017). Vegetation indices have also been used to detect leaf water content and the effects of porewater salinity and redox potential on plant distribution and growth in a salt marsh dominated by *Salicornia* (Zhang et al., 1997). These efforts provide promise for application of similar techniques in order to determine edaphic factors in salt marshes based on canopy reflectance.

Biomass and productivity are inherently linked to carbon sequestration potential and the ability to predict vulnerability and resilience will aid conservation efforts and carbon assessment. The ability to predict marsh stressors may be an important tool for determining the vulnerability of marshes and could aid in conservation efforts by identifying the most essential locations for conservation and assist in evaluating how stressors impact critical ecosystem services such as Blue Carbon potential.

The objectives of this study were to create predictive models of three stressors (leaf nitrogen, porewater salinity, and porewater oxidation-reduction potential (ORP)) using hyperspectral imagery. In order to isolate the response to specific stressors, the dominant macrophyte in Atlantic salt marshes, *Spartina alterniflora*, was grown in a controlled greenhouse environment and subjected to varying salinity, water level, and nitrogen availability. A similar approach was used across a natural marsh environment with varying salinity, ORP, and nitrogen content. The spectral and biophysical responses from the greenhouse experiment and from field plots were used to create predictive models of stress, which were then applied to a series of marsh chronosequence sites that range in age and degree of stressor impact.

3.2 Methods

3.2.1 Greenhouse Experiment

A greenhouse experiment was conducted to determine spectral responses of *S. alterniflora* to abiotic stressors such as salinity, nutrient availability, and hypoxia in a controlled environment. *S. alterniflora* seedlings were acquired from Pinelands Nursery, Columbus, New Jersey, USA. Three plugs (4-11 culms per pot, between 0.5 and 32 cm in height) were planted in April of 2018 in individual pots containing a 4:1 mixture of sand and Jiffy Mix potting soil

(Naidoo et al., 1992). Pots were placed in a microcosm tidal simulator (MacTavish & Cohen, 2014). Tidal simulation was semidiurnal and consisted of flooding to approximately 2.5 cm above the sediment surface and a 'low tide' with water depths at approximately 2.5 cm. Treatments included variable salinity, nitrogen availability, and varying water level (n = 4). For salinity treatments, artificial seawater (Instant Ocean) was added to tap water to achieve either 20, 30, 40, or 50‰ psu. During the course of the growing period, high salinity due to evaporation (measured with a refractometer) was corrected by adding water. Nitrogen availability consisted of three treatments: 0, 10, and 100 μM, which was added bi-weekly as ammonium chloride to the water column (MacTavish & Cohen, 2017). Flooding conditions were induced by permanently flooding plants to 2.5 cm above the sediment surface. Drought conditions were achieved by inducing high tide only once every other week and maintaining 2.5 cm of standing water otherwise. Water was replaced bi-weekly by emptying buckets and re-filling with the appropriate salinity and ammonium chloride concentrations.

Porewater for determination of salinity, ORP, and ammonium was extracted from 10 cm depth using stainless steel probes (Berg & McGlathery, 2001). Salinity was determined using a refractometer and ORP was determined using a Hach MTC-101 ORP probe. ORP was corrected to a standard hydrogen electrode by adding 208 at 25°C and 204 at 30°C (Hach.com). For porewater ammonium, samples were extracted, filtered, and frozen until analysis using the phenolhypochlorite method as described by (Solórzano, 1969).

Aboveground biomass was clipped, and a subsample was collected using a holepunch of known area for tissue chlorophyll analysis. The remaining biomass was dried at 60°C for 24 hr, weighed to obtain aboveground biomass, assuming the removed portion was of negligible weight and consistent across replicates. Dried plants were ground to homogeneity and analyzed for

carbon and nitrogen on a Perkin Elmer 2400 Elemental Analyzer. Vascular plant chlorophyll samples were frozen at -80°C until analysis to prevent chlorophyll degradation. Samples were ground in a mortar and pestle with liquid nitrogen, then mixed with acetone and ground in a tissue grinder. Following a 24 hr extraction period at -20°C, samples were centrifuged and the absorbance of the supernatant at 663.6 nm and 646. 6 nm (Lichtenhaler & Wellburn, 1983) was measured on a Shimadzu 1800 dual beam spectrophotometer, and chlorophyll concentrations were calculated based on the Lichtenhaler & Wellburn (1983) formulas.

The remaining sediment was washed through a 1 mm sieve and roots extracted to assess belowground biomass. This was dried at 60°C for 24 hr and weighed, then ground and analyzed for carbon and nitrogen on a Perkin Elmer 2400 Elemental Analyzer.

3.2.2 Statistics

A one-way ANOVA was used to analyze biophysical measurements between treatments in the greenhouse experiment and a Tukey HSD was conducted as a post- hoc test. Pearson correlation was used for linear regressions between aboveground biomass and foliar %N, salinity, and ORP.

3.2.3 Imagery

Hyperspectral imagery of all culms within each pot was taken five months following treatment initiation. Imagery was collected using a Headwall VNIR Micro-hyperspec High Efficiency E-series pushbroom system providing spectral measurements from 400 – 1000 nm with 371 spectral bands and 1600 across-track spatial pixels (Bachmann et al., 2019). Images were taken over a two-day period in a laboratory setting with a controlled illumination source

located at 20° zenith. Imagery taken in the laboratory included Spectralon reference panels, which were used as references in the reflectance calculations.

3.2.4 Field Campaign

In July of 2017 and 2018, field campaigns were conducted at a low-lying back-barrier marsh on Hog Island, located in the Virginia Coast Reserve Long Term Ecological Research (VCR LTER) site on the Delmarva Peninsula, one of the most pristine stretches of coastline on the Atlantic seaboard. The island is 11.3 km in length with an average width of 0.8 km (Day et al., 2001) and is a highly dynamic system, with frequent disturbances due to wind, waves, storm surges, and tides (Hayden, 1991). The Ash Wednesday storm of 1962 deposited approximately 1 m of sand over the back-barrier marshes at the southern end of Hog Island. The oldest marsh at this site was not affected by this storm and is at least 170 yrs old. Since the storm, the fringing marshes have gradually grown back, and marsh ages range from 5 to over 170 years old (Walsh, 1998; Tyler & Zieman, 1999). Marshes on Hog Island vary in ecological age and in degree of stressor impact, affording the ideal location to develop scalable estimates of marsh state from hyperspectral imaging. The three marshes used in this study have establishment dates of 1845, 1974, and 1986 (Figure 3.1).

During the field campaigns, spectral measurements were collected using the Headwall hyperspectral camera that is mounted on a telescopic mast. Spectralon reference panels were placed in the field of view and used to convert hyperspectral imagery to reflectance. Ground-truth plots were placed in the field of view and biophysical measurements (as detailed below) were taken contemporaneously at each site. Images were collected from four separate locations

within marshes of three differing ages, and a total of 36 ground truth plots were used for porewater variables and 34 for leaf %N (Figure 3.1).

Porewater was extracted with stainless steel probe inserted into the sediment to a depth of 10 cm (Berg & McGlathery, 2001) and ORP, temperature, and salinity were measured as previously described.

Three culms were clipped within 0.5 m of each plot and pooled for %C and %N analysis after freeze-drying and homogenization on a Wiley Mill or drying at 60°C for at least 24 hr and ground in a coffee grinder. Biomass was determined in September 2017 and 2019. In all plots, the number of culms within a 0.25 m^2 sub-plot and height to the tallest leaf of 10 culms located along a diagonal transect were measured. For plots with very high stem density, the quadrat size was reduced to 0.125 m^2. Aboveground biomass was calculated from pre-determined regressions (see below).

To estimate aboveground biomass, a 0.25 m^2 or 0.0625 m^2 quadrat was thrown randomly outside the plots and all aboveground *S. alterniflora* clipped. Plants were cleaned of sediment and dead leaves were removed and the height to the tallest leaf was measured prior to drying at 60 °C for at least 24 h and weighing to obtain individual dry weights. In 2017, a total of 302 culms were used, and 180 culms for 2018 to create height/weight regression equations, which were calculated by marsh age, with marshes established in 1994 and 1991 combined and 1989 and 1982 combined (Tables A.4 and A.6).

3.3.4 Imagery analysis

Diagrams with the workflow for the laboratory and field imagery appear in Figure 3.2. For the laboratory images, only the reflectance between 475 and 950 nm was used in the analysis

due to excessive noise at other wavelengths. In order to isolate only pure plant pixels, the average reflectance for each plant was calculated by manually selecting approximately 200-300 pixels arbitrarily from each image at the center of the leaf. For field imagery, a Savitzky-Golay smoothing filter was applied using ENVI and the vegetation was isolated by calculating the NDVI for each pixel and masking out all pixels with NDVI < 0.5, in order to remove extraneous soil and water pixels. Approximately 100 pixels were selected around the plots visible in the image and the average reflectance was calculated.

Previously published vegetation indices (Table 3.1) were applied in order to examine their relationship with modeled parameters; however, it was also noted that these may not include wavelengths that could be better predictors. We explored additional wavelengths and 1st and 2nd derivatives that were potentially good predictors by using an elastic net generalized regression (Zou & Hastie, 2005). The elastic net regression method is a shrinkage, or regularization, technique that can be used when the number of predictors is much greater than the number of observations and can be used as a feature selection method. This method constrains the number of predictor variables by adding a penalization term for the number of variables. A model is produced where coefficients that do not explain enough variance are forced to equal zero (and are removed from the regression) and the remaining coefficients are regularized (Zou & Hastie, 2005). Additionally, the continuum-removed reflectance between 475 and 950 nm was calculated in order to compare normalized absorption features between treatments.

To determine the wavelengths that best predict leaf %N, porewater salinity, and redox potential, an elastic net generalized regression was computed for each response variable using the reflectance and first and second derivatives and the best model was selected using Akaike Information Criterion (AICc) validation (Akaike, 1998). A stepwise regression was used for the

vegetation indices and models were selected based on the lowest AICc. These steps were conducted in JMP Pro 14.

The equations generated from the greenhouse imagery were applied to the field plots and the estimated values were compared to measured values using a linear regression analysis. An elastic net regression was also calculated based on the smoothed reflectance and first and second derivatives from the field imagery. For the field imagery, samples were randomly split into training (n = 28) and validation (n = 13), and a linear regression was used to assess models. All models for both the laboratory and field imagery were bootstrapped with 1000 resamples in order to determine 95% confidence intervals for the coefficients. Statistical analyses were conducted in JMP Pro 14.

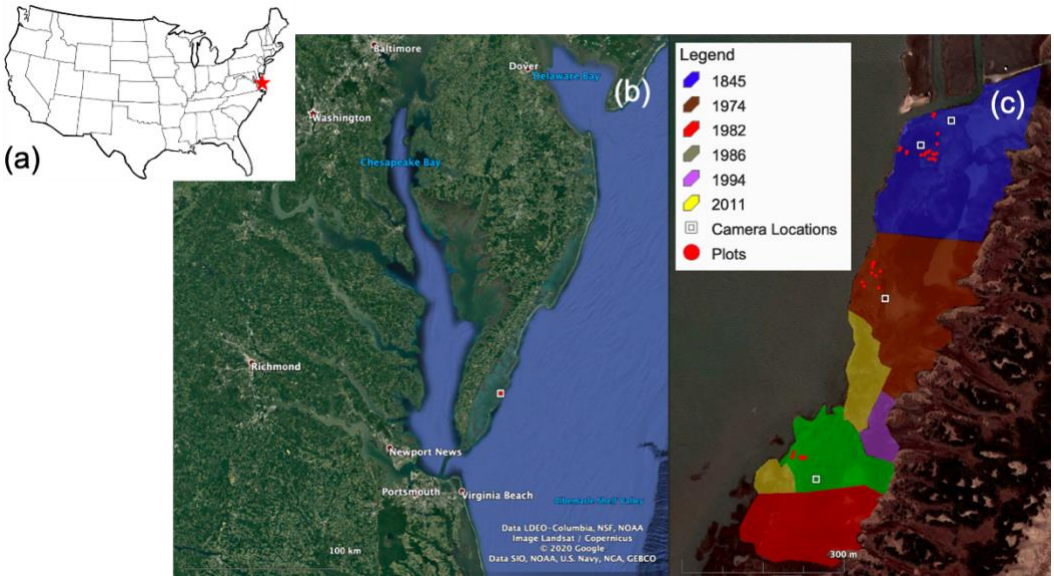

Figure 3.1: *(a) Location of study site in Virginia, USA, (b) location of Hog Island, (c) locations of plots and camera within the Hog Island chronosequence. Color indicates the year initiation year of the marsh.*

Table 3.1: *Vegetation indices applied in this study*

Vegetation Index	Definition	Use	Source
Red edge position linear interpolation (REP)	$700 + \frac{\frac{40 \text{ x } R_{670} + R_{780}}{2} - R_{700}}{R_{740} - R_{700}}$	Chlorophyll concentration	Main et al., 2011
Normalized Difference Vegetation Index (NDVI)	$\frac{R_{800} - R_{680}}{R_{800} + R_{680}}$	Green biomass, chlorophyll concentration	Starr et al., 2018
Water Index (WI)	$\frac{R_{900}}{R_{970}}$	Leaf water content	Starr et al., 2018
Optimized Soil Adjusted Vegetation Index (OSAVI)	$(1 + 0.16)\frac{R_{800} - R_{670}}{R_{800} + R_{670} + 0.16}$	Green biomass	Haboudane et al., 2002
Optimized Soil Adjusted Vegetation Index 2 (OSAVI2)	$(1 + 0.16)\frac{R_{750} - R_{705}}{R_{750} + R_{705} + 0.16}$	Green biomass	Wu et al., 2008
Modified Chlorophyll Absorption Reflectance Index (MCARI)	$\left((R_{700} - R_{670}) - 0.2 \text{ x } (R_{700} - R_{550})\right)\frac{R_{700}}{R_{670}}$	Chlorophyll concentration, leaf area index	Daughtry, 2000
Red Edge Symmetry (RES)	$\frac{R_{718} - R_{675}}{R_{775} - R_{6750}}$	Chlorophyll concentration	Ju et al., 2010
Photochemical Reflectance Index (PRI)	$\frac{R_{531} - R_{570}}{R_{531} + R_{570}}$	Light-use efficiency, plant stress	Naumann et al., 2008
Ratio Vegetation Index (RVI)	$\frac{R_{800}}{R_{680}}$	Green biomass	Jordan, 1969
Green-Red Vegetation Index (GRVI)	$\frac{R_{530} - R_{680}}{R_{530} + R_{680}}$	Green biomass	Motohka et al., 2010
Modified Soil Adjusted Vegetation Index 2 (MSAVI2)	$\frac{2 \text{ x } R_{800} + 1}{2} - \frac{\sqrt{(2 * R_{800} + 1)^2 - 8 * (R_{800} - R_{680})}}{2}$	Green biomass	Haboudane, 2004
Wide Dynamic Range Normalized Difference Vegetation Index (WDR NDVI)	$\frac{0.2\ x\ R_{800} - R_{680}}{0.2\ x\ R_{800} + R_{680}}$	Green biomass	Gitelson, 2004

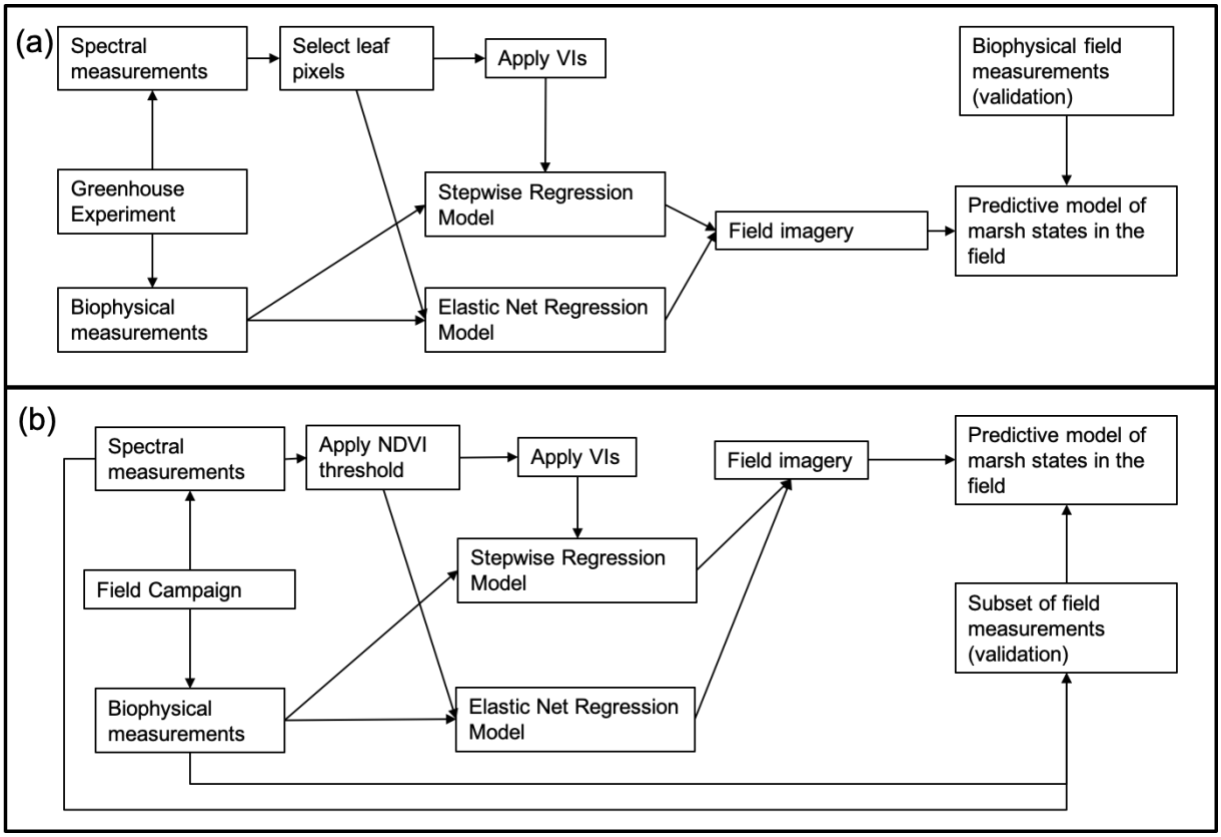

Figure 3.2: *Diagrams showing (a) the workflow for the analysis of the greenhouse experiment and (b) the workflow for the analysis for the field imagery.*

3.3 Results

3.3.1 Greenhouse Experiment

Survival rates for the high and low nutrient, low salinity, and waterlogged treatments was 100% of pots, but was reduced to 75% and 50% of pots in the moderate and high salinity treatments, respectively. In the drought and highest salinity treatments, there was 100% mortality, and these were eliminated from further analysis. Among the 21 pots with surviving plants, porewater salinity ranged from an average of 32 ppt in the low salinity treatment to 56 ppt in the high salinity treatment (Table 3.3). Belowground biomass, leaf chlorophyll *a*, %C, %N, and ORP were not significantly different between treatments. Biomass was highest in the low salinity treatment and was lowest in the high salinity treatment. The ratio of leaf %N to total

chlorophyll was highest in the high nutrient treatment and lowest in the low salinity treatment. Porewater salinity and leaf %N had a significant negative relationship with aboveground biomass (Figure 3.3a and 3.3b, $p = 0.017$, $R_2 = 0.27$ and $p = 0.0006$, $R_2 = 0.47$, respectively). Porewater redox had no correlation with aboveground biomass (Figure 3.3c, $p = 0.76$, $R_2 = 0.005$).

Spectra display the typical vegetation curve (Jensen, 2006), but with pronounced differences between treatments (Figure 3.4a). This is particularly noticeable in the red edge slope (680 - 730 nm) and green peak (520-560 nm) as well as the magnitude of the near infrared (NIR) region, which is reduced in the high salinity treatment relative to the low salinity and low nutrient treatments. These differences are also visible in the continuum-removed spectra (Figure 3.4b), primarily in the green peak region.

A summary of the R_2 values, associated errors, and predictive bands or vegetation indices for the greenhouse experiment appear in Table 3.4. Models developed from the greenhouse experiment ranged in R_2 values from 0.23 to 0.90 for the training data (Table 3.4). Parameter estimates and 95% confidence intervals for all models developed with the greenhouse imagery are available in Tables A.7 and A.8.

3.3.2 Field

Field biomass ranged from 7.8 to 569.9 g m_{-2} across all sites (Table 3.3). Porewater salinity values from field plots ranged from 33-58 ppt. Redox potential ranged from -222 to +162 mV. Leaf N ranged from 0.91 to 2.05% (Table 3.3). When models that were developed using the greenhouse experiment imagery were applied to the field imagery as validation, R_2 values were poor, ranging from <0.1 and 0.39 (Table 3.5). Models trained on a subset of field plots had R_2

values ranging from 0.96 to 0.97 for those developed using the elastic net regression and 0.20 to 0.76 for those developed with the vegetation indices using the stepwise regression (Table 3.5). The leaf N models had the highest R2 value when applied to the validation set. WI, OSAVI, GRVI, and MSAVI2 were the best predictors of salinity, explaining 60% of the variation in the training data and 61% in the validation data. The models for porewater redox potential consistently had the lowest R2 values and highest RMSE. Parameter estimates and 95% confidence intervals for all models developed with the field are available in Tables A.9 and A.10.

Table 3.2: *Mean (SE) aboveground biomass (AG biomass, g), belowground biomass (BG biomass, g), leaf %N, aerial N (g), chlorophyll a and b (Chl, mg m^{-2}), chlorophyll a and b: %N, porewater salinity (ppt), ORP (mV), and porewater ammonium (NH_4^+, uM) per treatment from the greenhouse experiment. Letters indicate significant differences between treatments. The degrees of freedom for all is 5.*

	F	p-value	Control	High Nutrient	Low Nutrient	High Salinity	Low Salinity	Flooded
AG Biomass	3.2	0.04	0.25 (0.1)^{ab}	0.23 (0.01)^{ab}	0.44 (0.01)^{ab}	0.03 (0.21)^{b}	0.97 (0.28)^{a}	0.46 (0.09)^{ab}
BG Biomass	0.64	0.67	3.31 (0.75)	3.71 (0.45)	3.3 (0.44)	2.81 (0.04)	4.15 (0.62)	3.57 (0.37)
Leaf %N	2.75	0.06	3.26 (0.55)	4.45 (0.95)	2.71 (0.38)	5.03 (0.64)	2.19 (0.59)	2.62 (0.36)
Aerial N	2.63	0.07	0.72 (0.17)	1.0 (0.18)	0.99 (0.36)	0.14 (0.01)	1.65 (0.36)	1.16 (0.18)
Chl	0.95	0.95	38 (11)	31 (7)	33 (4)	51 (19)	40 (6)	29 (3)
N:Chl	3.07	0.04	0.09 (0.02)^{ab}	0.15 (0.02)^{a}	0.09 (0.02)^{ab}	0.11 (0.03)^{ab}	0.06 (0.02)^{b}	0.09 (0.02)^{ab}
Salinity	6.23	0.003	47 (6)^{ab}	47 (4)^{ab}	45 (3)^{abc}	56 (1)^{a}	32 (1)^{c}	40 (2)^{bc}
ORP	2.57	0.08	-120 (45)	-79 (19)	-132 (6)	-154 (13)	-114 (10)	-126 (8)
NH_4^+	0.70	0.63	9.6 (5.3)	13.6 (2.8)	8.7 (2.2)	17.1 (10.8)	9.9 (2.3)	8.6 (1.7)

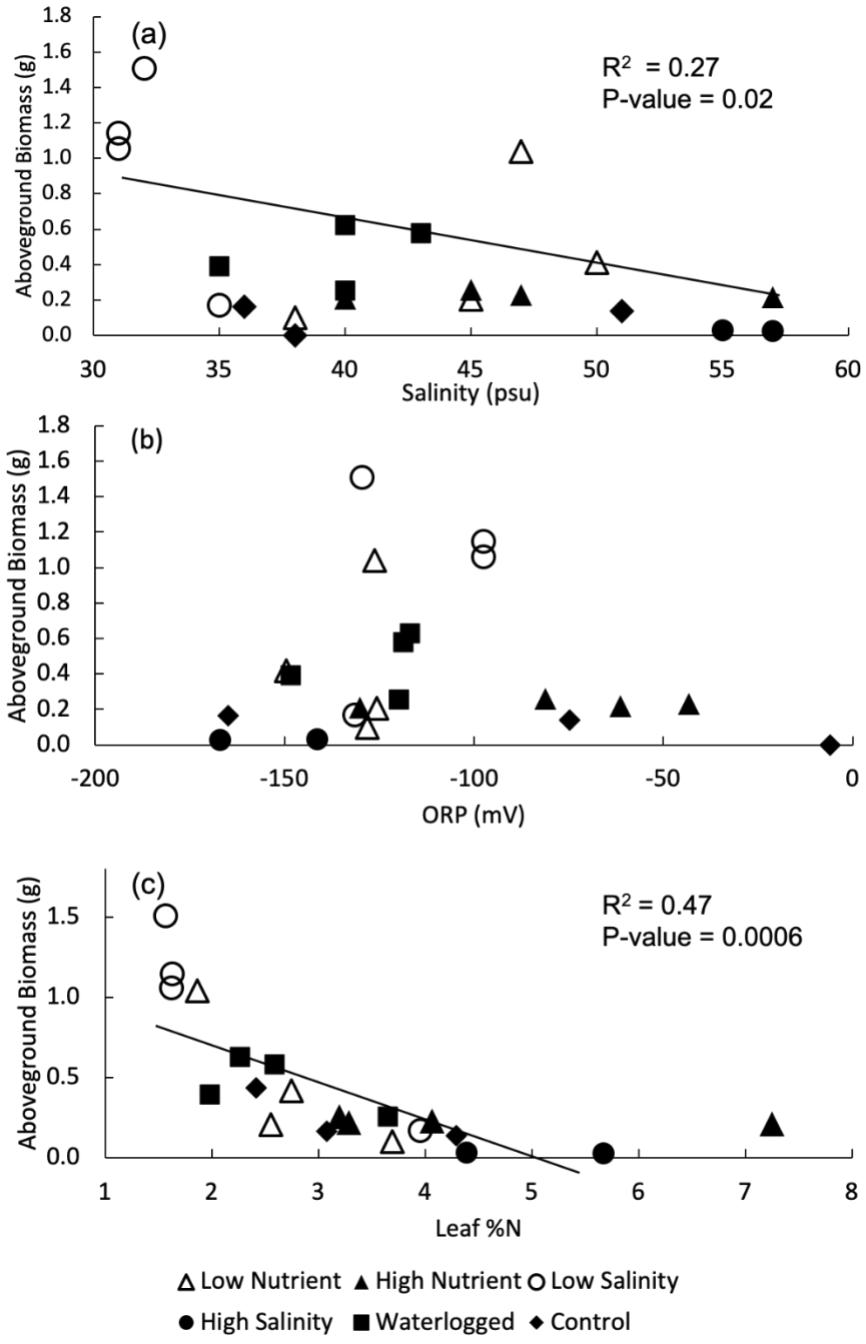

Figure 3.3: *Aboveground biomass versus (a) porewater salinity, (b) porewater ORP, (c) foliar %N. Trendline shows linear regression and statistics are noted on each panel when the relationship was significant.*

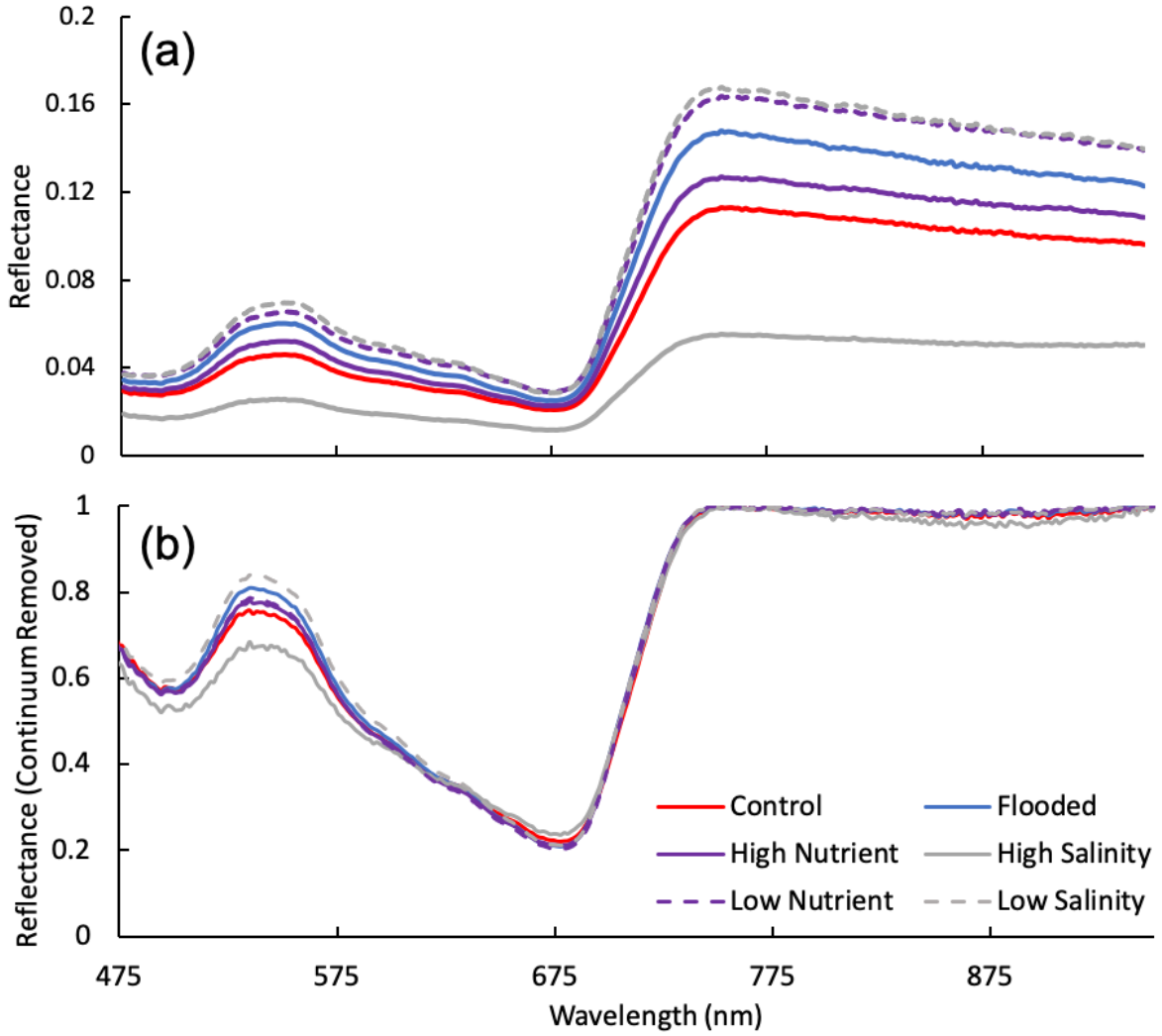

Figure 3.4: *(a) Average reflectance of selected leaves by treatment for the greenhouse experiment, (b) continuum removed average reflectance of selected leaves by treatment for the greenhouse experiment.*

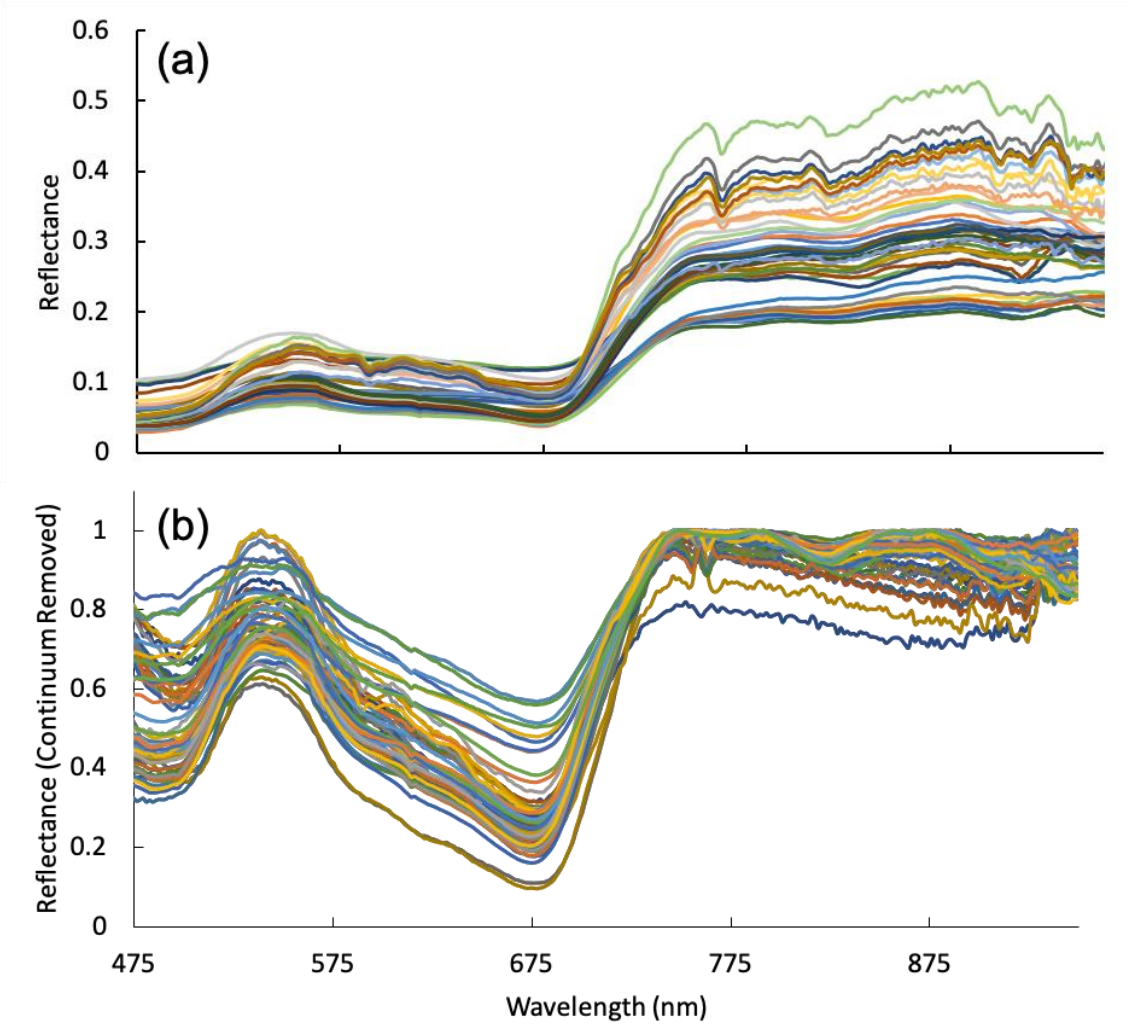

Figure 3.5: *(a) Spectra from field plots, (b) continuum removed spectra from field plots.*

Table 3.3: *Average ± standard deviation [minimum-maximum] for biomass. (g m-2), height (cm), density (culms m-2), leaf %N, ORP (mV), and salinity (ppt)*

Initiation date	Biomass	Height	Density	%N	ORP	Salinity
1989	135.4±21.8 [76.4-213.3]	33.6±2.4 [27.2-41.2]	40.3±7 [15-57]	n.d.	-19±32 [-104-69]	42±1 [40-45]
1974	104.1±29.4 [17.5-243.2]	28.2±2.9 [20.1-42.5]	157±20 [88-248]	1.61±0.03 [1.5-1.76]	-99±38 [-177-162]	42±1 [36-47]
1845	130.4±27.1 [7.8-569.9]	36±2.8 [14.9-68.7]	103±29 [5-484]	1.32±0.07 [0.91-2.05]	-192±6 [-222-131]	39±1 [33-58]

***Table 3.4**: Results of the elastic net regressions on reflectance and 1st (') and 2nd (") derivative and stepwise regression on vegetation indices for the greenhouse imagery. Validation data consists of greenhouse regressions applied to field imagery. * indicates significant predictor at p < 0.05, ** indicates significant predictor at p < 0.01. Factors are the significant spectral bands (nm) for the elastic net or vegetation indices for the stepwise regression.*

	Variable	BIC	AICc	RMSE training	R^2 training	RMSE validation	R^2 validation	Factors
Elastic Net	Leaf %N	54.5	55.8	0.5	0.85	3.7	0.39	651', 672'**, 775", 880", 948"
	Salinity	151.0	149.8	6.1	0.46	3.3	< 0.1	478', 622", 842"
	Redox	169.5	171.8	9.9	0.9	71.8	< 0.1	573", 755", 830', 909", 918"
Stepwise	Leaf %N	66.1	66.4	0.9	0.7	1.3	< 0.1	OSAVI2**, PRI*, RVI**, GRVI**
	Salinity	152.2	153.4	7.2	0.4	11.6	0.15	REP**, WI*, OSAVI2**
	Redox	197.9	199.4	29.8	0.23	16.2	< 0.1	WI*

***Table 3.5:** Results of the elastic net regressions on reflectance and 1st (') and 2nd (") derivative and stepwise regression on vegetation indices for the field imagery. Regressions were trained on a subset of field imagery points, with validation data consisting of the remainder of the plots from the field imagery. * indicates significant predictor at p < 0.05, ** indicates significant predictor at p < 0.01. Factors are the significant spectral bands (nm) for the elastic net or vegetation indices for the stepwise regression.*

	Variable	BIC	AICc	RMSE training	R^2 training	RMSE validation	R^2 validation	Factors
Elastic Net	Leaf %N	-27.5	-18.5	0.1	0.97	0.1	0.74	415", 449"**, 624", 803", 825"*, 869"**, 908', 907', 931'**
	Salinity	77.9	99.0	0.5	0.96	5.3	0.40	434"**, 464"**, 475"**, 598"**, 608" , 628", 699", 803"**, 843"**, 849", 916"
	Redox	232.3	253.4	13.0	0.97	120	0.22	463"*, 473"**, 795"**, 809"**, 830"**, 851", 857", 868", 884'*, 955", 961"**
Stepwise	Leaf %N	-5.3	-8.9	0.2	0.76	0.1	0.99	WI*, OSAVI*, GRVI*, MSAVI2*
	Salinity	159.4	155.5	3.3	0.6	1.9	0.61	NDVI*, WI, WDR-NDVI*
	Redox	337.6	334.6	87.2	0.2	39.5	< 0.1	PRI*

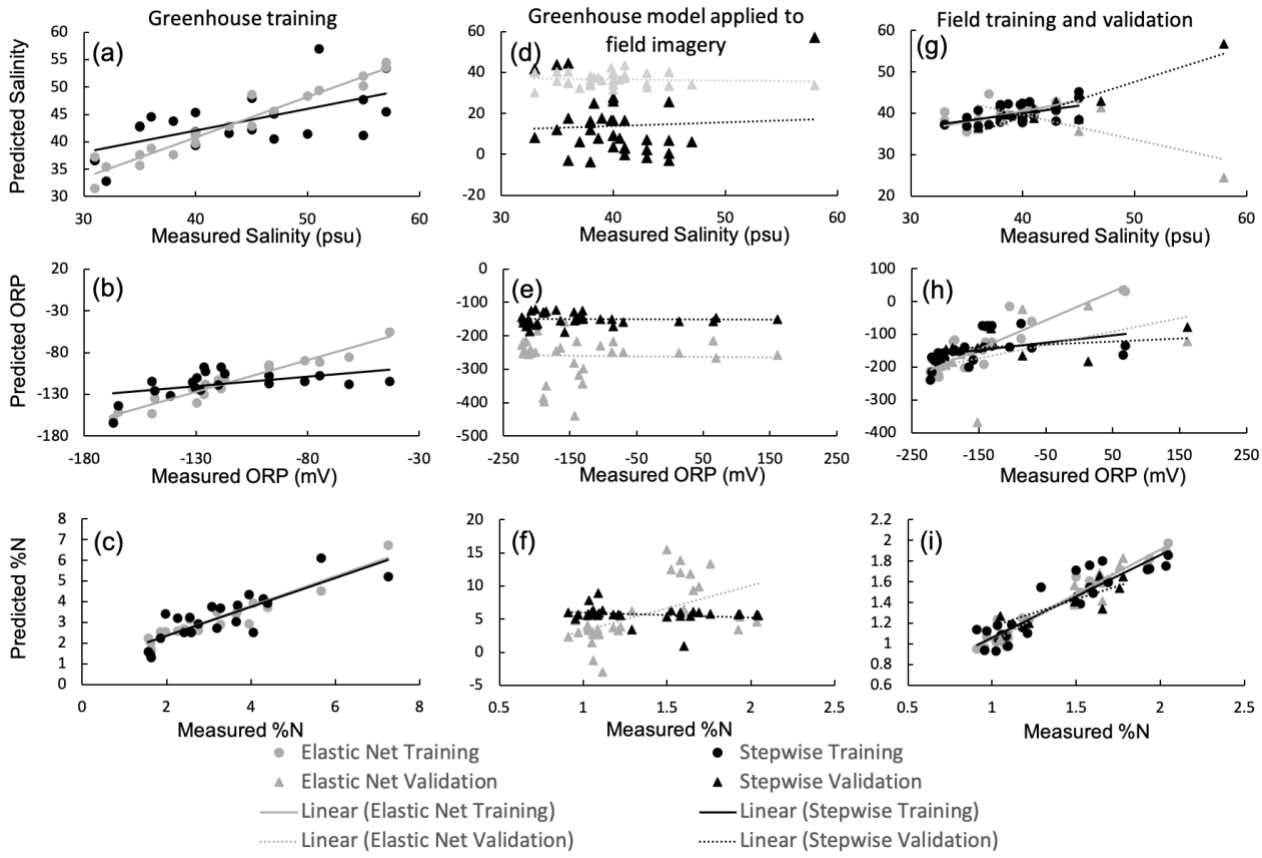

Figure 3.6: *Predicted versus measured for (a) greenhouse salinity model training set, (b) greenhouse salinity model applied to field imagery (validation), (c) field salinity model training and validation (subset of field imagery plots), (d) greenhouse ORP model training set, (e) greenhouse ORP model applied to field imagery, (f) field ORP model training and validation set (subset of field imagery plots), (g) greenhouse model leaf %N training set, (h) greenhouse leaf %N applied to field imagery, (i) field leaf %N training and validation set (subset of field imagery plots). Color indicates type of model (elastic net or stepwise), while shape indicates training or validation set. Solid lines indicate regression for the training set, while dashed lines indicate the regression for the validation set.*

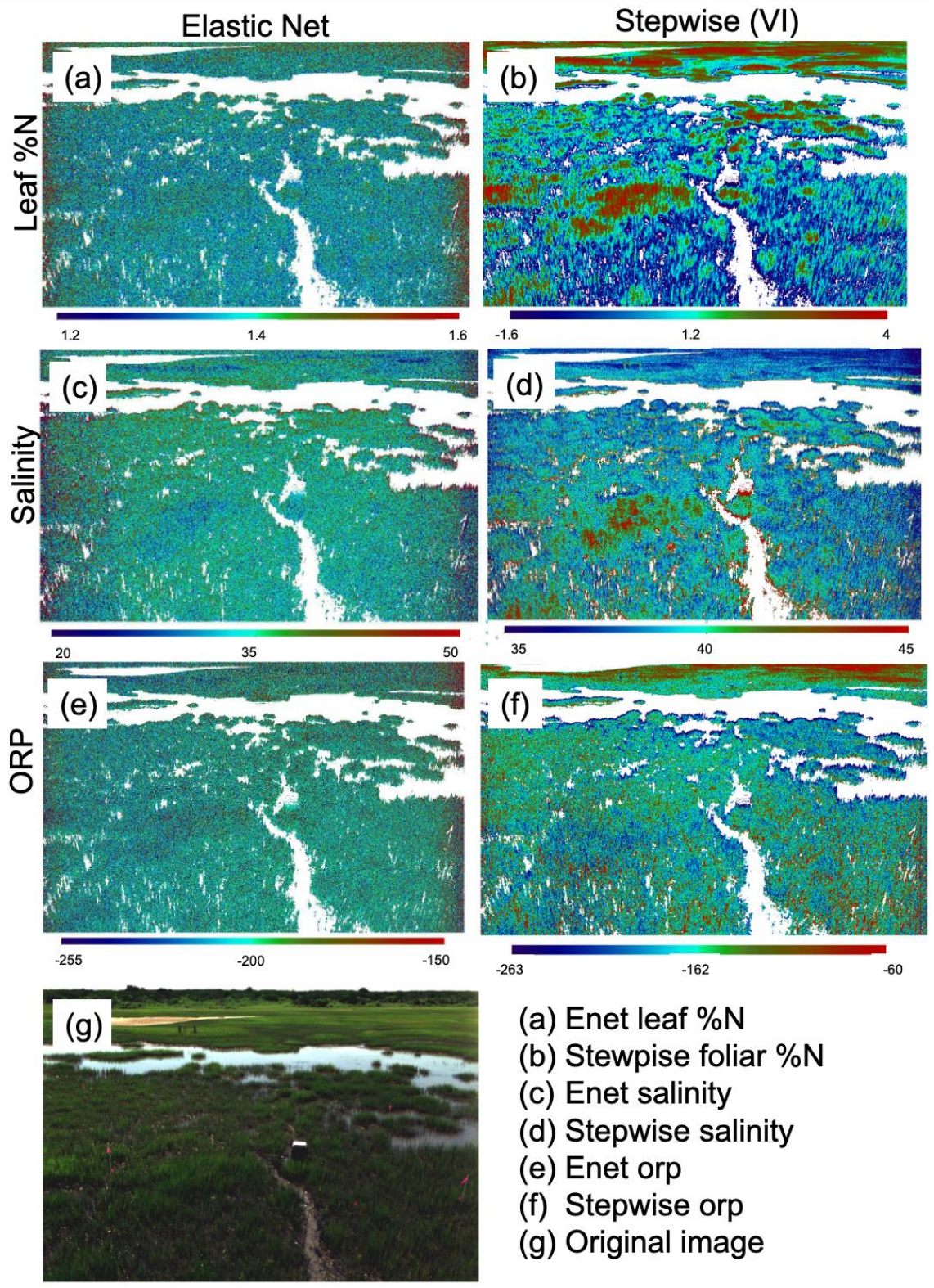

Figure 3.7*: Field prediction equations applied to field imagery: (a) elastic net regression for leaf %N, (b) stepwise VI regression for leaf %N, (c) elastic net regression for salinity, (d) stepwise VI regression for salinity, (e) elastic net regression for ORP, (f) stepwise regression for ORP, (g) original image*

3.4 Discussion

Models were developed successfully for a range of salinity and leaf N content using both vegetation indices and reflectance, but ORP was not well predicted with either method in laboratory or field validation. Models trained on the lab imagery were generally poor predictors when applied to field validation points, likely due to a variety of factors including differences in conditions between the field and laboratory experiment, mixed pixels, as well BRDF effects. However, models that were developed on the field imagery did successfully predict leaf %N and salinity in the field imagery validation points.

3.4.1 Spectral response to stress

Spectral detection of vegetation relies on several key absorption features that contribute to a distinctive 'vegetation curve' (as seen in Figures 3.4 and 3.5). Within the visible light range, reflectance is primarily dominated by leaf pigments in the palisade mesophyll such as chlorophyll *a* and *b,* carotenes, or anthocyanins. In the blue and red wavelengths (approximately 430-450 and 650-700 nm respectively) reflectance is low, while there is a distinctive peak in the green wavelengths (approximately 540 nm), as chlorophyll absorbs light at 430, 450, 660, and 650 nm. As the amount of chlorophyll decreases (from stress or senescence), other pigments in the leaves become visible and this region may be useful as a measure of vegetation stress (Knipling, 1970). The near infrared region (NIR, approximately 700-1200 nm) is characterized by high reflectance, as most of the energy in this region is transmitted or reflected by plants as an adaptation to prevent overheating (Jensen, 2006). The reflectance between the red and NIR (at approximately 700 nm) is characterized by a steep increase known as the 'red edge.'

Physiologically, the high reflectance in the NIR is due to a layer of spongy mesophyll, which consists of cells and intercellular air pockets that scatter incoming radiation (Jensen, 2006).

While vegetation indices are developed to minimize confounding factors and heighten useful variation within the spectra, they are also limited to a narrow range of bands which might not include wavelengths that could be better predictors of stress conditions. As such, two approaches were used in this study—the stepwise regression method to test existing indices, as well as the elastic net regression, which was used to extract other predictor wavelengths. For the models developed from the field imagery, stepwise regression proved a more significant predictor for N and salinity. Many vegetation indices have been developed to predict either leaf %N or leaf greenness, which tend to be closely connected, and the predictive indices included in this model reflect this. Salinity and redox potential have fewer developed indices and these indices were primarily developed for upland, salt-sensitive plants, so may not be as effective in this context.

3.4.2 Nitrogen

Field leaf %N (0.91 to 1.61%) was generally much lower than the %N content in the greenhouse-grown plants (5.8% to 7.0%), providing little overlap in values across datasets. It is likely that the potting mix enhanced N sufficiently that N did not vary substantially among treatments, and was only marginally higher in the high salinity and high nutrient treatments ($p = 0.06$, Table 3.2). In high salinity conditions, the minimum required tissue concentration of nitrogen increases, likely due to the production and accumulation of the nitrogen-based osmoregulatory compounds proline and glycinebetaine, which promote salt tolerance (Bradley & Morris, 1991; Naidoo et al., 1992). However, the opposite trend was observed in other studies,

where increased salinity resulted in lower foliar nutrient concentrations. In this study, there was a significant negative relationship between aboveground biomass and leaf %N in the laboratory experiment, with the low salinity treatment having both the highest biomass and the lowest salinity (Figure 3.3). Differences in leaf physiology, such as the accumulation of osmoregulatory compounds, may influence reflectance and be detectable as changes in reflectance spectra.

While detection of foliar nitrogen has been widely applied to agricultural and terrestrial systems, there are relatively few studies in wetlands. Leaf nitrogen is often correlated with chlorophyll content, and numerous studies have linked chlorophyll absorption features and the red edge region with foliar nitrogen content (LaCapra et al., 1996; Read et al., 2002; Siciliano et al., 2008). In this study, the nitrogen:chlorophyll ratio varied with treatment, with the lowest ratio found in the low salinity treatment, and the highest in the high nutrient treatment.

Siciliano et al. (2008) found that *Salicornia virginica* fertilized with nitrogen demonstrated lower reflectance at 555 nm and 680 nm and steeper red-edge slopes, and that this was detectable using vegetation indices including PRI. NDVI has previously been found to correlate with leaf N in wheat (Cabrera-Bosquet et al., 2011). In this study, models developed from both lab and field imagery for leaf %N consistently had the highest R^2 and lowest RMSE. In the greenhouse experiment, wavelengths selected through the elastic net leaf %N regression were near chlorophyll absorption or florescence features (the first derivatives at 651 nm and 672 nm), however, no wavelengths associated with the red edge were identified. In the regressions developed from the field imagery, the second derivative at 415 nm was a predictor of nitrogen content, which is similar to Read et al. (2002), where decreased reflectance at 410 nm was associated with nitrogen stress in cotton plants. However, contrary to other findings, most of the predictor wavelengths from the field imagery identified using the elastic net were located in the

NIR region. Whereas, in the stepwise regression model from the field imagery, vegetation indices commonly used to detect green biomass (NDVI, MSAVI2, GRVI and OSAVI (Haboudane et al., 2002; Gitelson, 2004; Motohka et al., 2010)) were significant predictors of leaf N, explaining 76% and 99% of variation in training and validation datasets, respectively.

For the field models, there were some selected vegetation indices that used wavelengths similar to those selected by the elastic net model. In the field leaf %N model, the vegetation indices included WI (using wavelengths 900 and 970 nm), OSAVI (using wavelengths 800 and 670 nm), and MSAVI2 (using wavelengths 800 and 680), while the wavelengths included in the elastic net model included 907, 908, and 803 nm, similar to the wavelengths used in the vegetation indices.

3.4.3 Salinity

The range of porewater salinity found in the field (33-58 ppt) were replicated in the lab (31-57 ppt), suggesting that any salinity-induced impacts to plants may be comparable. The negative relationship between salinity and biomass in the greenhouse experiment is consistent with prior work (Bradley & Morris, 1991; Brown et al., 2006; MacTavish & Cohen, 2017). High salinity can result in reduced stomatal conductance and CO_2 assimilation (Giurgevich & Dunn, 1979), increased leaf respiration (Levering & Thomson, 1971), and accumulation of osmoregulatory compounds in tissues (Naidoo et al., 1992). Longstreth & Strain (1977) found that increasing salinity resulted in higher leaf xylem pressure and higher specific leaf weight, potentially due to increases in mesophyll thickness developed as a mechanism for salt avoidance. Thicker mesophyll results in a greater internal leaf area were gaseous exchange takes place, and thus lowers resistance to CO_2 uptake, which may compensate for salinity-induced resistance to CO_2

uptake (Longstreth & Nobel, 1979). Scattering in the mesophyll contributes to NIR reflectance (Jensen, 2006), so changes in leaf structure could have resulted in the reduced reflectance in the NIR region in the high salinity treatment. Additionally, secreted salt crystalloids (e.g. Bradley & Morris, 1991a) were visible on leaves at higher salinity treatments and may have influenced the spectra. In *Avicennia germinans*, the reflectance in the blue (400-500 nm) and red (630-680 nm) regions was increased when leaves were covered in salt crystalloids (Esteban et al., 2013), however, the reverse was seen in this study.

In salt-sensitive plants, reflectance in the NIR region is lower with salinity stress, likely due to cell structure damage (Zhang et al., 2011). However, in halophytes, while NIR reflectance may also decrease at higher salinity due to cell structure damage, at moderate salinity reflectance in this region may increase (Zhang et al., 2011). Our results are contrary to this paradigm, where the average reflectance between low, control, and high salinities in the NIR region more closely resembled that of the salt sensitive plants, possibly because plants were subjected to much higher salinities than in the Zhang et al. (2011) study. In the greenhouse study, a combination of WI, NDVI, WDR NDVI were the best predictors of porewater salinity, explaining 60% and 61% of the variation in the field training and validation sets, respectively. The WI is sensitive to leaf water content (Penuelas et al, 1997), which responds to salt stress in *S. alterniflora* (Longstreth & Strain, 1977). NDVI and WDR NDVI are sensitive to leaf greenness and chlorophyll concentrations (Gitelson, 2004), which may decrease with salinity stress as plants shunt available N to organic compounds needed for osmoregulation.

Zhang et al. (2011) found that the regions of 395-410 nm, 483-507 nm, 632-697 nm, 731-762 nm, 812-868, 884-909 nm, and 918-930 nm were the wavelengths most sensitive to salt stress and suggests that photosynthetic pigments are highly affected by salt stress. In this study,

five out of the eleven wavelengths that were predictors of porewater salinity for the field equations were in the visible range, although they were not located in the ranges indicated above. This could be due to differences in species and biological responses to salinity stress; Zhang et al. (2011) found that the spectral response to salinity was species dependent, and did not investigate *S. alterniflora* specifically.

The stepwise field model for salinity used the vegetation indices NDVI (800 and 860 nm), WI (900 and 970 nm), and WDR NDVI (800 and 680 nm) while the elastic net model included the similar wavelengths 803, 699, and 916. These similarities highlight that these are important absorption features around these wavelengths.

3.4.4 Waterlogging

S. alterniflora can tolerate substantially lower redox potentials than what was achieved in the greenhouse experiment (-167 mV to -43 mV) and begins to show symptoms of oxygen deficiency at values below -200 mV (Mendelssohn et al., 1981). This likely explains the lack of relationship between biomass and redox that observed (Figure 3.3b). However, wider range of porewater redox potential in the field (-222 mV - +161.5 mV)_was likely sufficient to generate the hypoxic condition that limit essential plant functions. The leaf structure of *S. alterniflora* may change due to differences in redox potential, which could influence the spectra of the plant. Many wetland plants, adapted to the anaerobic conditions that occur in flooded soils, contain aerenchyma to transport oxygen from aerial parts to flooded roots where it supports aerobic root metabolism and oxidation of the rhizosphere (Pezeshki, 1997). In *S. alterniflora,* aerenchyma development may be induced by low oxygen conditions (Burdick, 1989; Naidoo et al., 1992; Maricle & Lee, 2002). However, in extremely waterlogged soils, aerenchyma transport is not

always sufficient to allow entirely aerobic metabolism to take place in the roots (Mendelssohn et al., 1981) and the metabolic pathway switches to fermentation where the enzyme alcohol dehydrogenase (ADH) is used to reduce pyruvate to ethanol and can be used as an indication of oxygen deficiency. *S. alterniflora* shows heightened ADH activity in low redox conditions (< -200 mV), indicating that it is susceptible to root oxygen deficiencies (Mendelssohn, et al., 1981; Burdick & Mendelssohn, 1987). Additionally, in low redox conditions, adenosine triphosphate (ATP) yield is increased at the expense of glucose consumption, resulting in higher respiration and decreased growth (Mendelssohn et al., 1981). Low redox conditions also reduce root elongation and a smaller root system that may be unable to support the shoot (Pezeshki, 1997). Uptake of NH_{4+} is reduced in anoxic conditions, influencing photosynthesis and potentially leaf N (Morris & Dacey, 1984; Pezeshki, 1997). Soil oxygen-deficiency may also induce stress symptoms such as stomatal closure, limiting gas exchange, photosynthesis and oxygen transport to roots (Pezeshki, 1997). These adaptions and changes to leaf structure and biochemistry may be visible as differences in spectral response.

There are relatively few studies attempting to remotely detect waterlogging stress in plants. A study on the spectral response of *Acer rubrum* to flooding found elevated reflectance at 550 nm and 770 nm and a good correlation between those wavelengths and redox potential (Anderson et al., 1996). In bean and barley plants, waterlogging resulted in increased reflectance in the visible region, with the most significant differences occurring between 508-654 nm and 692-742 nm (Smith et al., 2004). Smith et al. (2004) also found that while the red edge shifted towards longer wavelengths over time in control plants, in waterlogged plants this shift was reduced, possibly due to inhibition of maturation and lower chlorophyll content in the waterlogged plants. In the greenhouse experiment, the second derivative at 573 and 755 nm,

which are within or near these previously identified regions, predicted porewater redox along with the derivative at 830 nm and the second derivative at 918 and 909 nm. This model did not translate well to the field imagery, however (Table 3.4), potentially because of the lack of overlap in values between lab and field ORP, and that the relatively high lab values may not be sufficient to elicit stress symptoms. Additionally, the effects of hypoxia may be more evident in the root system of *S. alterniflora*, rather than in the aboveground biomass and therefore, less detectable using leaf imagery.

Models developed to detect ORP using field imagery did not include wavelengths that had been previously identified in the literature. The second derivatives at 830, 961, 473, 809, 795, and 463 nm as well as the first derivative at 884 nm were somewhat predictive of porewater redox in the field, but only explained 0.22% of the variation upon validation. Vegetation indices were also relatively poor predictors of ORP. PRI was developed as an indication of photosynthetic efficiency, which is often correlated with plant stress (Thenot, 2002) and while this index emerged as the best VI to predict ORP, it was not successfully validated (Table 3.4). Often, under stress conditions, photosynthetic capacity decreases and the amount of incoming radiation is greater than is required for photosynthesis; in this case, under stress, excess energy is dissipated through the xanthophyll cycle. PRI incorporates 531 nm, which is linked to the xanthophyll cycle, and is inversely related to photosynthetic light use efficiency (Gamon et al., 1992). While PRI has not been used previously to detect waterlogging stress, it has been used to detect salt stress in a coastal shrub (Naumann et al., 2008), and the plants in the greenhouse may be affected by a combination of salinity and waterlogging stress that is detected by PRI. Vegetation indices established to detect waterlogging stress have largely been developed on terrestrial plants and may not be as effective for wetland species. Additionally, redox stress in the

field is likely acting in tandem with other stressors such as salinity, temperature, and nutrient availability, which may confound these results. Future studies could focus on generating a wider range of redox potential in a greenhouse setting to elucidate this particular stress response.

For the greenhouse experiment, the wavelengths selected through the elastic net regression generally did not align with the wavelengths used in the indices selected in the stepwise regression. However, for the redox potential model derived from lab imagery, the WI, which uses wavelengths 900 and 970 nm, was the best predictor, while the wavelengths in the elastic net model included the second derivative at 909nm, which is in the water absorption region. However, this was not the case in the field-derived model.

3.4.5 Limitations of models

Neither type of model developed in the laboratory using the vegetation indices or the reflectance and first and second derivative resulted in good predictions of marsh state in the field. This is likely due to a combination of factors including differences in illumination and view angle, effects of canopy structure, differences in scale, and potentially mixed pixels in the field imagery. The reference white panels are not perfectly Lambertian, and since the illumination angle and viewing angle are different in the lab and the field, it likely influences the conversion to reflectance. However, a correction for this can be carried out for future studies. Additionally, view angle and canopy structure have strong influences on reflectance due to multiple light scattering, leaf layering, and shading (Jensen, 2006). Future models could make use of radiative transfer models in order to account for this geometry. Mixed pixels were minimized in the laboratory setting by hand-selecting areas of leaf, but in spite of the application of the NDVI filter to the field imagery to isolate vegetation, mixed pixels containing some sediment are likely

given the larger pixel size in the field. This suggests that future refinements of these models must include greater field-based measurements and must incorporate varying scales of imagery to assess the potential impact of mixed pixels.

3.5 Conclusions

This study was the first step in developing indicators of salt marsh health using remote sensing. Overall, models were successful for predicting a range of salinity and leaf nitrogen content in both the laboratory and the greenhouse individually. Generally, models developed from previously published vegetation indices were more successful at predicting salinity and leaf %N than models developed from an elastic net regression approach. The failure to develop adequate models for ORP suggests the need for additional study to better isolate this stressor and understand how the plant physiologic and structural responses translate to the spectral reflectance. Although models developed from a controlled greenhouse experiment did not translate well to field imagery, likely due to a combination of factors including differences in environmental conditions, potentially mixed pixels in the field imagery, and BRDF effects, future experiments could better correct for these factors. The development of these spectral models may provide an efficient way to evaluate marsh states and stressors in the field at a large scale, which can inform marsh management decisions. Likewise, such an approach will develop useful tools for estimating critical ecosystem services such as carbon sequestration and habitat provision, as stressed plants tend to produce less biomass and are poorer habitat.

Chapter 4 : Conclusions

Predictions of successional processes (Chapter 2) were generally similar to those predicted from the 1990s, particularly for physico-chemical processes. However, in some marshes, invertebrate communities, sediment grain size dynamics, and biomass changed in ways that were not predicted based on age-related drivers alone. This indicates that while the chronosequence approach does retain some rigor and that time drives the evolution of some physico-chemical components of the marsh, changing external factors also have strong influences on marsh processes. In particular, changes associated with additional sand deposition and drowning from increased SLR appear to have effects in this marsh, particularly in the short zone, which overall had lower developmental maturity in the contemporary series. The endpoint of succession may depend more on these external factors and hyper-local forcings than simply the push of time alone. The future exacerbation of climate change and other human pressures will likely result in the developmental trajectory of the marsh deviating even further from predictions made in the 1990s.

Many abiotic factors, such as porewater redox potential, sediment organic matter, and sediment nutrient content responded predictably with marsh age. However, at some sites, grain size appeared to be driven more by initial or hyper-local conditions than marsh age alone. There were also some sites that experienced trajectory reversals, likely due to additional overwash. Biotic factors generally appear to be more affected by external stressors than abiotic factors. Patterns in biomass and plant height were strongly influenced by external factors such as edge erosion and SLR and interactions between plant biomass and invertebrate populations and distribution were important. Invertebrate populations generally did not follow predicted trajectories, and populations and distributions were tied to changes in biomass, SLR, and changes in predation pressures. The loss of the tall zone for the 1850 and 1974 marshes due to edge

erosion resulted in significant decreases in *I. obsoleta* populations in the oldest marshes, where they were previously found in the highest densities, while increases in populations of *L. irrorota* in the 1850 short zone are likely tied to die-off patches and decreases in biomass due to SLR. Likewise, SLR may play an important role in regulating invertebrate populations such as *Uca* spp. and *G. demissa* as the marsh is flooded for longer periods of time and the opportunity for predation increases.

While marshes are subjected to the push of time, stressors such as sea level rise, marsh drowning and changing salinity also seem to be playing a strong role in determining marsh trajectories, particularly for biotic factors. The exacerbation of these extrinsic factors will likely lead to further deviations from predicted ecosystem development. As such, it is imperative that methods for assessing marsh health over large areas are developed. In the investigation of stressor impacts on *S. alterniflora* (Chapter 3), models of porewater salinity, redox, and leaf nitrogen were developed in both a laboratory and a field setting. Models created from the laboratory setting did not predict marsh states well in the field for any variable, due to differences in environmental conditions, mixed pixels, and BRDF effects, which could be controlled for in future studies. However, foliar nitrogen and salinity were reliably predicted in the field based on reflectance or vegetation indices developed from field imagery. Porewater redox was not well predicted using either reflectance or vegetation indices, which suggests the need for further study to isolate the spectral and physical response of this stressor.

This study was a first step in developing remote sensing models to detect regions of marsh stress. Future work is needed to scale up to airborne or satellite-based imagery, which would allow for a greater range of application, but introduces challenges as the pixel size increases and spatial detail is lost (Eon et al., 2019). Additionally, further work could be

conducted in order to isolate the spectral response of *S. alterniflora* to flooding by exposing plants to a greater range of ORP values that more closely resemble values observed in the field in a greenhouse experiment.

Understanding ecosystem trajectory is essential for developing restoration efforts, addressing management questions, and predicting and evaluating essential ecosystem services, such as blue carbon storage. Marsh development is influenced by more than just time, and stressors and external forcings that occur at a large scale require the use of technology such as remote sensing. The ability to predict marsh stressors may be an important tool for determining the vulnerability and resilience of marshes and could aid in conservation efforts by identifying the most essential locations for conservation and assist in evaluating how stressors impact critical ecosystem services such as carbon sequestration potential.

References

Akaike, H. (1998). Information Theory and an Extension of the Maximum Likelihood Principle. In E. Parzen, K. Tanabe, & G. Kitagawa (Eds.), *Selected Papers of Hirotugu Akaike* (pp. 199–213). Springer New York. https://doi.org/10.1007/978-1-4612-1694-0_15

Alber, M., Swenson, E. M., Adamowicz, S. C., & Mendelssohn, I. A. (2008). Salt Marsh Dieback: An overview of recent events in the US. *Estuarine, Coastal and Shelf Science*, *80*(1), 1–11. https://doi.org/10.1016/j.ecss.2008.08.009

Anderson, John E., & Perry, J. E. (1996). Characterization of wetland plant stress using leaf spectral reflectance: Implications for wetland remote sensing. *Wetlands*, *16*(4), 477–487.

Andrews, J. D., & Hewatt, W. G. (1957). Oyster Mortality Studies in Virginia. II. The Fungus Disease Caused by Dermocystidium marinum in Oysters of Chesapeake Bay. *Ecological Monographs*, *27*(1), 2–25. JSTOR. https://doi.org/10.2307/1948568

Argese, E., Cogoni, G., Zaggia, L., Zonta, R., & Pini, R. (1992). Study on redox state and grain size of sediments in a mud flat of the Venice Lagoon. *Environmental Geology and Water Sciences*, *20*(1), 35–42. https://doi.org/10.1007/BF01736108

Artigas, F. J., & Yang, J. (2006). Spectral discrimination of marsh vegetation types in the New Jersey Meadowlands, USA. *Wetlands*, *26*(1), 271–277. https://doi.org/10.1672/0277-5212(2006)26[271:SDOMVT]2.0.CO;2

Bachmann, Charles M., Eon, R. S., Lapszynski, C. S., Badura, G. P., Vodacek, A., Hoffman, M. J., McKeown, D., Kremens, R. L., Richardson, M., Bauch, T., & Foote, M. (2019). A Low-Rate Video Approach to Hyperspectral Imaging of Dynamic Scenes. *Journal of Imaging*, *5*(1), 6. https://doi.org/10.3390/jimaging5010006

Bachmann, C.M., Bettenhausen, M. H., Fusina, R. A., Donato, T. F., Russ, A. L., Burke, J. W., Lamela, G. M., Rhea, W. J., Truitt, B. R., & Porter, J. H. (2003). A credit assignment approach to fusing classifiers of multiseason hyperspectral imagery. *IEEE Transactions on Geoscience and Remote Sensing*, *41*(11), 2488–2499. https://doi.org/10.1109/TGRS.2003.818537

Bachmann, C.M., Donato, T. F., Lamela, G. M., Rhea, W. J., Bettenhausen, M. H., Fusina, R. A., Du Bois, K. R., Porter, J. H., & Truitt, B. R. (2002). Automatic classification of land cover on Smith Island, VA, using HyMAP imagery. *IEEE Transactions on Geoscience and Remote Sensing*, *40*(10), 2313–2330. https://doi.org/10.1109/TGRS.2002.804834

Badura, G. P., Bachmann, C. M., Tyler, A. C., Goldsmith, S., Eon, R. S., & Lapszynski, C. S. (2019). A Novel Approach for Deriving LAI of Salt Marsh Vegetation Using Structure From Motion and Multiangular Spectra. *IEEE Journal of Selected Topics in Applied Earth Observations and Remote Sensing*, *12*(2), 599–613. https://doi.org/10.1109/JSTARS.2018.2889476

Barbier, E. B., Hacker, S. D., Kennedy, C., Koch, E. W., Stier, A. C., & Silliman, B. R. (2011). The value of estuarine and coastal ecosystem services. *Ecological Monographs*, *81*(2), 169–193. https://doi.org/10.1890/10-1510.1

Barbier, E. B., Koch, E. W., Silliman, B. R., Hacker, S. D., Wolanski, E., Primavera, J., Granek, E. F., Polasky, S., Aswani, S., Cramer, L. A., Stoms, D. M., Kennedy, C. J., Bael, D., Kappel, C. V., Perillo, G. M. E., & Reed, D. J. (2008). Coastal ecosystem-based management with nonlinear ecological functions and values. *Science (New York, N.Y.)*, *319*(5861), 321–323. https://doi.org/10.1126/science.1150349

Berg, P., & McGlathery, K. J. (2001). A high-resolution pore water sampler for sandy sediments. *Limnology and Oceanography*, *46*(1), 203–210. https://doi.org/10.4319/lo.2001.46.1.0203

Bertness, M. D. (1984). Ribbed Mussels and Spartina Alterniflora Production in a New England Salt Marsh. *Ecology*, *65*(6), 1794–1807. https://doi.org/10.2307/1937776

Bertness, M. D., & Silliman, B. R. (2008). Consumer Control of Salt Marshes Driven by Human Disturbance. *Conservation Biology*, *22*(3), 618–623. https://doi.org/10.1111/j.1523-1739.2008.00962.x

Boesch, D., & Turner, R. (1984). Dependence of Fishery Species on Salt Marshes: The Role of Food and Refuge. *Estuaries*, *7*(4), 460–468.

Bradley, P. M., & Morris, J. T. (1991a). Relative importance of ion exclusion, secretion and accumulation in Spartina alterniflora Loisel. *Journal of Experimental Botany*, *42*(12), 1525–1532.

Bradley, P. M., & Morris, J. T. (1991b). The influence of salinity on the kinetics of NH4+ uptake in Spartina alterniflora. *Oecologia*, *85*, 375–380.

Brower, J. E., & Zar, J. H. (1977). *Field and Laboratory Methods for General Ecology* (2nd ed.). Wm. C. Brown Company Publishers.

Brown, C. E., Pezeshki, S. R., & DeLaune, R. D. (2006). The effects of salinity and soil drying on nutrient uptake and growth of Spartina alterniflora in a simulated tidal system. *Environmental and Experimental Botany*, *58*(1), 140–148. https://doi.org/10.1016/j.envexpbot.2005.07.006

Burdick, D. M., & Mendelssohn, I. A. (1987). Waterlogging responses in dune, swale and marsh populations of Spartina patens under field conditions. *Oecologia*, *74*(3), 321–329. https://doi.org/10.1007/BF00378924

Burdick, David M. (1989). Root Aerenchyma Development in Spartina Patens in Response to Flooding. *American Journal of Botany*, *76*(5), 777. https://doi.org/10.2307/2444425

Cabrera-Bosquet, L., Molero, G., Stellacci, A., Bort, J., Nogués, S., & Araus, J. (2011). NDVI as a potential tool for predicting biomass, plant nitrogen content and growth in wheat genotypes subjected to different water and nitrogen conditions. *Cereal Research Communications*, *39*(1), 147–159. https://doi.org/10.1556/CRC.39.2011.1.15

Cheng, W., Massimo, M., Stoll, M.-P., Belluco, E., & Marani, M. (2006). Mapping mixed vegetation communities in salt marshes using. *Remote Sensing of Environment*, *107*, 559–570.

Chmura, G. L. (2013). What do we need to assess the sustainability of the tidal salt marsh carbon sink? *Ocean & Coastal Management*, *83*, 25–31. https://doi.org/10.1016/j.ocecoaman.2011.09.006

Chmura, G. L., Anisfeld, S. C., Cahoon, D. R., & Lynch, J. C. (2003). Global carbon sequestration in tidal, saline wetland soils. *Global Biogeochemical Cycles*, *17*(4), 1111. https://doi.org/10.1029/2002GB001917

Clements, F. E. (1916). *Plant Succession: An Analysis of the Development of Vegetation*. Carnegie Institution of Washington.

Coleman, D. J., & Kirwan, M. L. (2019). The effect of a small vegetation dieback event on salt marsh sediment transport. *Earth Surface Processes and Landforms*, *44*(4), 944–952. https://doi.org/10.1002/esp.4547

Collins, S. L., & Adams, D. E. (1983). Succession in grasslands: Thirty-two years of change in a central Oklahoma tallgrass prairie. *Vegetatio*, *51*(3), 181–190. https://doi.org/10.1007/BF00129437

Cowles, H. C. (1899). The Ecological Relations of the Vegetation on the Sand Dunes of Lake Michigan. Part I.-Geographical Relations of the Dune Floras. *Botanical Gazette*, *27*(2), 95–117.

Craft, C. (2016). Measuring Success. In *Creating and Restoring Wetlands* (pp. 267–288). Elsevier. https://doi.org/10.1016/B978-0-12-407232-9.00010-5

Cranford, P. J. (1988). Behaviour and ecological importance of a mud snail (*Ilyanassa obsoleta*) population in a temperate macrotidal estuary. *Canadian Journal of Zoology*, *66*(2), 459–466. https://doi.org/10.1139/z88-065

Crosby, S. C., Angermeyer, A., Adler, J. M., Bertness, M. D., Deegan, L. A., Sibinga, N., & Leslie, H. M. (2017). Spartina alterniflora Biomass Allocation and Temperature: Implications for Salt Marsh Persistence with Sea-Level Rise. *Estuaries and Coasts*, *40*(1), 213–223. https://doi.org/10.1007/s12237-016-0142-9

Daughtry, C. (2000). Estimating Corn Leaf Chlorophyll Concentration from Leaf and Canopy Reflectance. *Remote Sensing of Environment*, *74*(2), 229–239. https://doi.org/10.1016/S0034-4257(00)00113-9

Davis, C. A. (1910). Salt-marsh formation near Boston and its geological significance. *Economic Geology*, *5*(7), 623–639. https://doi.org/10.2113/gsecongeo.5.7.623

Davis, R. A. (2012). Barrier Island Systems—A Geologic Overview. In *Geology of Holocene Barrier Island Systems*.

Day, F. P., Crawford, E. R., & Dilustro, J. J. (2001). Aboveground Plant Biomass Change along a Coastal Barrier Island Dune Chronosequence over a Six-Year Period. *Journal of the Torrey Botanical Society*, *128*(3), 197. https://doi.org/10.2307/3088711

Debussche, M., Escarre, J., Lepart, J., Houssard, C., & Lavorel, S. (1996). Changes in Mediterranean plant succession: Old-fields revisited. *Journal of Vegetation Science*, *7*(4), 519–526.

Deegan, L. A., Johnson, D. S., Warren, R. S., Peterson, B. J., Fleeger, J. W., Fagherazzi, S., & Wollheim, W. M. (2012). Coastal eutrophication as a driver of salt marsh loss. *Nature*, *490*(7420), 388–392. https://doi.org/10.1038/nature11533

Donnelly, J. P., & Bertness, M. D. (2001). Rapid shoreward encroachment of salt marsh cordgrass in response to accelerated sea-level rise. *Proceedings of the National Academy of Sciences*, *98*(25), 14218–14223. https://doi.org/10.1073/pnas.251209298

Drexler, J. Z., Davis, M. J., Woo, I., & De La Cruz, S. (2020). Carbon Sources in the Sediments of a Restoring vs. Historically Unaltered Salt Marsh. *Estuaries and Coasts*. https://doi.org/10.1007/s12237-020-00748-7

Eon, R. S., Goldsmith, Sarah, Bachmann, C. M., Tyler, A. C., Lapszynski, C. S., Badura, G. P., Osgood, D. T., & Brett, R. (2019). Retreival of salt marsh above-ground biomass from high-spatial resolution, multi-view hyperspectral imagery using PROSAIL. *Remote Sensing*, *11*.

Esteban, R., Fernández-marín, B., Hernandez, A., Jiménez, E. T., León, A., García-mauriño, S., Silva, C. D., Dolmus, J. R., Dolmus, C. M., Molina, M. J., Gutierrez, N. N., Loaisiga, M. I., Brito, P., & García-plazaola, J. I. (2013). Salt crystal deposition as a reversible mechanism to enhance photoprotection in black mangrove. *Trees; Heidelberg*, *27*(1), 229–237. http://dx.doi.org.ezproxy.rit.edu/10.1007/s00468-012-0790-8

Fahrig, L., Hayden, B., & Dolan, R. (1993). Distribution of barrier island plants in relation to overwash disturbance: A test of life history theory. *Journal of Coastal Research*, 403–412.

Foster, B. L., & Tilman, D. (2000). Dynamic and static views of succession: Testing the descriptive power of the chronosequence approach. *Plant Ecology*, *146*, 1–10.

Friedrichs, C. T., & Perry, J. E. (2001). Tidal Salt Marsh Morphodynamics: A Synthesis. *Journal of Coastal Research*, 7–37.

Gamon, J. A., Peñuelas, J., & Field, C. B. (1992). A narrow-waveband spectral index that tracks diurnal changes in photosynthetic efficiency. *Remote Sensing of Environment*, *41*(1), 35–44. https://doi.org/10.1016/0034-4257(92)90059-S

Gedan, K. Bromberg, Silliman, B. R., & Bertness, M. D. (2009). Centuries of Human-Driven Change in Salt Marsh Ecosystems. *Annual Review of Marine Science*, *1*, 117–141.

Gedan, Keryn B., & Bertness, M. D. (2010). How will warming affect the salt marsh foundation species Spartina patens and its ecological role? *Oecologia*, *164*(2), 479–487. https://doi.org/10.1007/s00442-010-1661-x

Gitelson, A. A. (2004). Wide Dynamic Range Vegetation Index for Remote Quantification of Biophysical Characteristics of Vegetation. *Journal of Plant Physiology*, *161*(2), 165–173. https://doi.org/10.1078/0176-1617-01176

Gittman, R. K., & Keller, D. A. (2013). Fiddler crabs facilitate Spartina alterniflora growth, mitigating periwinkle overgrazing of marsh habitat. *Ecology*, *94*(12), 2709–2718.

Giurgevich, J. R., & Dunn, E. L. (1979). Seasonal patterns of CO2 and water vapor exchange of the tall and short height forms of Spartina alterniflora Loisel in a Georgia salt marsh. *Oecologia*, *43*, 139–156.

Godfrey, P. J., & Godfrey, M. M. (1976). *Barrier Island Ecology of Cape Lookout National Seashore and Vicinity, North Carolina*. https://www.nps.gov/parkhistory/online_books/science/9/chap2.htm

Goodbred, S. L., & Hine, A. C. (1995). Coastal storm deposition: Salt-marsh response to a severe extratropical storm, March 1993, west-central Florida. *Geology*, *23*(8), 679–682. https://doi.org/10.1130/0091-7613(1995)023<0679:CSDSMR>2.3.CO;2

Haboudane, D. (2004). Hyperspectral vegetation indices and novel algorithms for predicting green LAI of crop canopies: Modeling and validation in the context of precision agriculture. *Remote Sensing of Environment*, *90*(3), 337–352. https://doi.org/10.1016/j.rse.2003.12.013

Haboudane, Driss, Miller, J. R., Tremblay, N., Zarco-Tejada, P. J., & Dextraze, L. (2002). Integrated narrow-band vegetation indices for prediction of crop chlorophyll content for application to precision agriculture. *Remote Sensing of Environment*, *81*(2–3), 416–426. https://doi.org/10.1016/S0034-4257(02)00018-4

Hayden, B., Dueser, J. T., & Shugart, H. H. (1991). Long Term Research at the Virginia Coast Reserve: Modeling a highly dynamic environment. *Bioscience*, *41*(5), 310–318.

He, L., Song, X., Feng, W., Guo, B.-B., Zhang, Y.-S., Wang, Y.-H., Wang, C.-Y., & Guo, T.-C. (2016). Improved remote sensing of leaf nitrogen concentration in winter wheat using multi-angular hyperspectral data. *Remote Sensing of Environment*, *174*, 122–133. https://doi.org/10.1016/j.rse.2015.12.007

Heiri, O., Lotter, A. F., & Lemcke, G. (2001). Loss on ignition as a method for estimating organic and carbonate content in sediments: Reproducibility and comparability of results. *Journal of Paleolimnology*, *25*, 101–110.

Herrnkind, W. F. (1968). Adaptive Visually-Directed Orientation in *Uca pugilator*. *American Zoologist*, *8*(3), 585–598. https://doi.org/10.1093/icb/8.3.585

Hester, M. W., Mendelssohn, I. A., & McKee, K. L. (1998). Intraspecific Variation in Salt Tolerance and Morphology in Panicum hemitomon and Spartina alterniflora (Poaceae). *International Journal of Plant Sciences*, *159*(1), 127–138.

Hladik, C., Schalles, J., & Alber, M. (2013). Salt marsh elevation and habitat mapping using hyperspectral and LIDAR data. *Remote Sensing of Environment*, *139*, 318–330. https://doi.org/10.1016/j.rse.2013.08.003

Hopkinson, C., Cai, W.-J., & Hu, X. (2012). *Carbon sequestration in wetland dominated coastal systems—A global sink of rapidly diminishing magnitude* (Vol. 4). https://doi.org/10.1016/j.cosust.2012.03.005

Howes, B. L., Dacey, J. W. H., & Goehringer, D. D. (1986). Factors Controlling the Growth Form of Spartina Alterniflora: Feedbacks Between Above-Ground Production, Sediment Oxidation, Nitrogen and Salinity. *Journal of Ecology*, *74*(3), 881–898. https://doi.org/10.2307/2260404

Hughes, A. L. H., Wilson, A. M., & Morris, J. T. (2012). Hydrologic variability in a salt marsh: Assessing the links between drought and acute marsh dieback. *Estuarine, Coastal and Shelf Science*, *111*, 95–106. https://doi.org/10.1016/j.ecss.2012.06.016

Jensen, J. R. (2006). *Remote Sensing of the Environment: An Earth Resource Perspective* (2 edition). Pearson.

Johnson, E. A., & Miyanishi, K. (2008). *Testing the assumptions of chronosequences in succession*. *11*. http://doi.wiley.com/10.1111/j.1461-0248.2008.01173.x

Jordan, C. F. (1969). Derivation of Leaf-Area Index from Quality of Light on the Forest Floor. *Ecology*, *50*(4), 663–666. https://doi.org/10.2307/1936256

Ju, C.-H., Tian, Y.-C., Yao, X., Cao, W.-X., Zhu, Y., & Hannaway. (2010). Estimating Leaf Chlorophyll Content Using Red Edge Parameters. *Pedosphere*, *20*(5), 633–644.

Kastler, J. A., & Wiberg, P. L. (1996). Sedimentation and Boundary Changes of Virginia Salt Marshes. *Estuarine, Coastal and Shelf Science*, *42*(6), 683–700. https://doi.org/10.1006/ecss.1996.0044

Kirwan, M. L., & Mudd, S. M. (2012). Response of salt-marsh carbon accumulation to climate change. *Nature*, *489*(7417), 550–553.

Klemas, V. V. (2011). *Remote Sensing of Wetlands: Case Studies Comparing Practical Techniques*. https://doi.org/10.2112/JCOASTRES-D-10-00174.1

Knipling, E. B. (1970). Physical and physiological basis for the reflectance of visible and near-infrared radiation from vegetation. *Remote Sensing of Environment*, *3*, 155–159. https://doi.org/10.1016/S0034-4257(70)80021-9

Koch, E. W., Barbier, E. B., Silliman, B. R., Reed, D. J., Perillo, G. M., Hacker, S. D., Granek, E. F., Primavera, J. H., Muthiga, N., Polasky, S., Halpern, B. S., Kennedy, C. J., Kappel, C. V., & Wolanski, E. (2009). Non-linearity in ecosystem services: Temporal and spatial variability in

coastal protection. *Frontiers in Ecology and the Environment*, *7*(1), 29–37. https://doi.org/10.1890/080126

LaCapra, V. C., Melack, J. M., Gastil, M., & Valeriano, D. (1996). Remote sensing of foliar chemistry of inundated rice with imaging spectrometry. *Remote Sensing of Environment*, *55*(1), 50–58. https://doi.org/10.1016/0034-4257(95)00185-9

Levering, C. A., & Thomson, W. W. (1971). The ultrastructure of the salt gland of Spartina foliosa. *Planta*, *97*, 183–196.

Lichtenhaler, H., & Wellburn, A. R. (1983). Determinations of total carotenoids and chlorophylls a and b of leaf extracts in different solvents. *Biochemical Society Transactions*, *11*.

Linthurst, R. A., & Seneca, E. D. (1981). Aeration, Nitrogen and Salinity as Determinants of Spartina alterniflora Loisel. Growth Response. *Estuaries*, *4*(1), 53. https://doi.org/10.2307/1351542

Longstreth, D. J., & Strain, B. R. (1977). Effects of salinity and illumination on photosynthesis and water balance of Spartina alterniflora Loisel. *Oecologia*, *31*(2), 191–199. https://doi.org/10.1007/BF00346920

Longstreth, David J., & Nobel, P. S. (1979). Salinity Effects on Leaf Anatomy: Consequences for Photosynthesis. *Plant Physiology*, *63*(4), 700–703. https://doi.org/10.1104/pp.63.4.700

Lorenzen, C. J. (1967). Determination of chlorophyll and pheo-pigments: Spectrophotometric equations. *Limnology and Oceanography*, *12*(2), 343–346.

MacTavish, R. M., & Cohen, R. A. (2014). A Simple, Inexpensive, and Field-Relevant Microcosm Tidal Simulator for Use in Marsh Macrophyte Studies. *Applications in Plant Sciences*, *2*(11), 1400058. https://doi.org/10.3732/apps.1400058

MacTavish, R. M., & Cohen, R. A. (2017). Water column ammonium concentration and salinity influence nitrogen uptake and growth of Spartina alterniflora. *Journal of Experimental Marine Biology and Ecology*, *488*, 52–59. https://doi.org/10.1016/j.jembe.2016.12.009

Main, R., Cho, M. A., Mathieu, R., O'Kennedy, M. M., Ramoelo, A., & Koch, S. (2011). An investigation into robust spectral indices for leaf chlorophyll estimation. *ISPRS Journal of*

Photogrammetry and Remote Sensing, *66*(6), 751–761. https://doi.org/10.1016/j.isprsjprs.2011.08.001

Marani, M., D'Alpaos, A., Lanzoni, S., & Santalucia, M. (2011). Understanding and predicting wave erosion of marsh edges: MARSH EDGE EROSION. *Geophysical Research Letters*, *38*(21), n/a-n/a. https://doi.org/10.1029/2011GL048995

Maricle, B. R., & Lee, R. W. (2002). Aerenchyma development and oxygen transport in the estuarine cordgrasses Spartina alterniflora and S. anglica. *Aquatic Botany*, *74*(2), 109–120. https://doi.org/10.1016/S0304-3770(02)00051-7

Marsh, A., Blum, L. K., Christian, R. R., Ramsey, E., & Rangoonwala, A. (2016). Response and resilience of Spartina alterniflora to sudden dieback. *Journal of Coastal Conservation*, *20*(4), 335–350. https://doi.org/10.1007/s11852-016-0445-9

McKee, K. L., Mendelssohn, I. A., & D. Materne, M. (2004). Acute salt marsh dieback in the Mississippi River deltaic plain: A drought-induced phenomenon? *Global Ecology and Biogeography*, *13*(1), 65–73. https://doi.org/10.1111/j.1466-882X.2004.00075.x

Mcleod, E., Chmura, G. L., Bouillon, S., Salm, R., Björk, M., Duarte, C. M., Lovelock, C. E., Schlesinger, W. H., & Silliman, B. R. (2011). A blueprint for blue carbon: Toward an improved understanding of the role of vegetated coastal habitats in sequestering CO2. *Frontiers in Ecology and the Environment*, *9*(10), 552–560. https://doi.org/10.1890/110004

McLoughlin, S. M., Wiberg, P. L., Safak, I., & McGlathery, K. J. (2015). Rates and Forcing of Marsh Edge Erosion in a Shallow Coastal Bay. *Estuaries and Coasts*, *38*(2), 620–638. https://doi.org/10.1007/s12237-014-9841-2

Mendelssohn, I. A., McKee, K. L., & Patrick, W. H. (1981). Oxygen Deficiency in Spartina alterniflora Roots: Metabolic Adaptation to Anoxia. *Science, New Series*, *214*(4519), 439–441.

Mendelssohn, I. A., Mckee, K. L., & Patrick, W. H. (1981). Oxygen Deficiency in Spartina alterniflora Roots: Metabolic Adaptation to Anoxia. *Science*, *214*(4519), 439–441. https://doi.org/10.1126/science.214.4519.439

Mendelssohn, Irving A., & Morris, J. T. (2002). Eco-Physiological Controls on the Productivity of Spartina Alterniflora Loisel. In M. P. Weinstein & D. A. Kreeger (Eds.), *Concepts and Controversies in Tidal Marsh Ecology* (pp. 59–80). Springer Netherlands. https://doi.org/10.1007/0-306-47534-0_5

Miller, G., Morris, J., & Wang, C. (2017). *Mapping salt marsh dieback and condition in South Carolina's North Inlet-Winyah Bay National Estuarine Research Reserve using remote sensing* (Vol. 4). https://doi.org/10.3934/environsci.2017.5.677

Morgan, P. A., Burdick, D. M., & Short, F. T. (2009). The Functions and Values of Fringing Salt Marshes in Northern New England, USA. *Estuaries and Coasts*, *32*(3), 483–495. https://doi.org/10.1007/s12237-009-9145-0

Morgan, P. A., & Short, F. T. (2002). Using Functional Trajectories to Track Constructed Salt Marsh Development in the Great Bay Estuary, Maine/New Hampshire, U.S.A. *Restoration Ecology*, *10*(3), 461–473. https://doi.org/10.1046/j.1526-100X.2002.01037.x

Morris, J. T. (2000). Effects of Sea-level Anomalies on Estuarine Processes. In *Estuarine Science: A Synthetic Approach to Research and Practice*. Island Press.

Morris, J. T., & Dacey, J. W. H. (1984). EFFECTS OF O2 ON AMMONIUM UPTAKE AND ROOT RESPIRATION BY SPARTINA ALTERNIFLORA. *American Journal of Botany*, *71*(7), 979–985. https://doi.org/10.1002/j.1537-2197.1984.tb14164.x

Morris, J. T., Sundareshwar, P. V., Nietch, C. T., Kjerfve, B., & Cahoon, D. R. (2002). Responses of Coastal Wetlands to Rising Sea Level. *Ecology*, *83*(10), 2869–2877. https://doi.org/10.1890/0012-9658(2002)083[2869:ROCWTR]2.0.CO;2

Motohka, T., Nasahara, K. N., Oguma, H., & Tsuchida, S. (2010). Applicability of Green-Red Vegetation Index for Remote Sensing of Vegetation Phenology. *Remote Sensing*, *2*(12), 2369–2387. https://doi.org/10.3390/rs2102369

Murphy, J., & Riley, J. P. (1962). A modified single solution method for the determination of phosphate in natural water and uses ascorbic acid instead of stannous chloride. *Anal. Chem.*, *27*, 31–36.

Naidoo, G., Mckee, K. L., & Mendelssohn, I. A. (1992). Anatomical and metabolic responses to waterlogging and salinity in Spartina alterniflora and S. patens (Poaceae). *American Journal of Botany*, *79*, 765–770.

Naumann, J. C., Anderson, J. E., & Young, D. R. (2008). Linking physiological responses, chlorophyll fluorescence and hyperspectral imagery to detect salinity stress using the physiological reflectance index in the coastal shrub, Myrica cerifera. *Remote Sensing of Environment*, *112*(10), 3865–3875. https://doi.org/10.1016/j.rse.2008.06.004

Nellemann, C. (Ed.). (2009). *Blue carbon: The role of healthy oceans in binding carbon: a rapid response assessment*. GRID-Arendal.

O'Connell, J. L., Mishra, D. R., Cotten, D. L., Wang, L., & Alber, M. (2017). The Tidal Marsh Inundation Index (TMII): An inundation filter to flag flooded pixels and improve MODIS tidal marsh vegetation time-series analysis. *Remote Sensing of Environment*, *201*, 34–46. https://doi.org/10.1016/j.rse.2017.08.008

Odum, E. P. (1969). The strategy of ecosystem development. *Science*, *164*(262.270).

Osgood, D. T., Santos, M., & Zieman, J. C. (1995). Sediment physico-chemistry associated with natural marsh development on a storm-deposited sand flat. *Marine Ecology Progress Series*, *120*(1), 271–283.

Osgood, D. T., & Zieman, J. C. (1993). Spatial and Temporal Patterns of Substrate Physiochemical Parameters in Different-aged Barrier Island Marshes. *Estuarine, Coastal and Shelf Science*, *37*.

Patrick, W. H., & Delaune, R. D. (1977). *Chemical and biological redox systems affecting nutrietnt availabiltiy in the coastal wetlands*. *18*, 8.

Penuelas, J., Pinol, J., Ogaya, R., & Filella, I. (1997). Estimation of plant water concentration by the reflectance Water Index WI (R900/R970). *International Journal of Remote Sensing*, *18*(13), 2869–2875. https://doi.org/10.1080/014311697217396

Pezeshki, S. R. (1997). Photosynthesis and root growth in Spartina alterniflora in relation to root zone aeration. *Photosynthetica*, *34*(1), 107–114.

Pickett, S. T. A. (Ed.). (1989). Space-for-time substitution as an alternative to long-term studies. In *Long-term studies in ecology: Approaches and alternatives* (pp. 110–135). Springer-Verlag.

Priestas, A., Mariotti, G., Leonardi, N., & Fagherazzi, S. (2015). Coupled Wave Energy and Erosion Dynamics along a Salt Marsh Boundary, Hog Island Bay, Virginia, USA. *Journal of Marine Science and Engineering*, *3*(3), 1041–1065. https://doi.org/10.3390/jmse3031041

Ramsey, E., & Rangoonwala, A. (2008). Characterizing the marsh dieback spectral response at the plant and canopy level with hyperspectral and temporal remote sensing data. *US/EU-Baltic International Symposium, 2008 IEEE/OES*, 1–8.

Ramsey III, E., & Rangoonwala, A. (2005). Leaf Optical Property Changes Associated with the Occurrence of Spartina alterniflora Dieback in Coastal Louisiana Related to Remote Sensing Mapping. *Photogrammetric Engineering & Remote Sensing*, *71*(3), 299–311. https://doi.org/10.14358/PERS.71.3.299

Ramsey III, E., & Rangoonwala, A. (2006). Canopy reflectance related to marsh dieback onset and progression in coastal Louisiana. *Photogrammetric Engineering & Remote Sensing*, *22*(6), 641–652.

Raposa, K. B., McKinney, R. A., Wigand, C., Hollister, J. W., Lovall, C., Szura, K., Gurak, Jr., J. A., McNamee, J., Raithel, C., & Watson, E. B. (2018). Top-down and bottom-up controls on southern New England salt marsh crab populations. *PeerJ*, *6*, e4876. https://doi.org/10.7717/peerj.4876

Read, J. J., Tarpley, L., McKinion, J. M., & Reddy, K. R. (2002). Narrow-Waveband Reflectance Ratios for Remote Estimation of Nitrogen Status in Cotton. *Journal of Environment Quality*, *31*(5), 1442. https://doi.org/10.2134/jeq2002.1442

Redfield, A. C. (1972). Development of a New England Salt Marsh. *Ecological Monographs*, *42*(2), 201–237. https://doi.org/10.2307/1942263

Reed, D. J. (1995). The response of coastal marshes to sea-level rise: Survival or submergence? *Earth Surface Processes and Landforms*, *20*(1), 39–48. https://doi.org/10.1002/esp.3290200105

Rothschild, B., Ault, J., Goulletquer, P., & Héral, M. (1994). Decline of the Chesapeake Bay oyster population: A century of habitat destruction and overfishing. *Marine Ecology Progress Series*, *111*, 29–39. https://doi.org/10.3354/meps111029

Rozan, T. F., Taillefert, M., Trouwborst, R. E., Glazer, B. T., Ma, S., Herszage, J., Valdes, L. M., Price, K. S., & Luther III, G. W. (2002). Iron-sulfur-phosphorus cycling in the sediments of a shallow coastal bay: Implications for sediment nutrient release and benthic macroalgal blooms. *Limnology and Oceanography*, *47*(5), 1346–1354. https://doi.org/10.4319/lo.2002.47.5.1346

Seed, R., & Hughes, R. N. (1997). Chelal Characteristics and Foraging Behaviour of the Blue CrabCallinectes sapidusRathbun. *Estuarine, Coastal and Shelf Science*, *44*(2), 221–229. https://doi.org/10.1006/ecss.1996.0214

Siciliano, D., Wasson, K., Potts, D. C., & Olsen, R. C. (2008). Evaluating hyperspectral imaging of wetland vegetation as a tool for detecting estuarine nutrient enrichment. *Remote Sensing of Environment*, *112*(11), 4020–4033. https://doi.org/10.1016/j.rse.2008.05.019

Silliman, Brian R. (2014). Salt marshes. *Current Biology*, *24*(9), R348–R350.

Silliman, Brian R., & Newell, S. Y. (2003). Fungal farming in a snail. *Proceedings of the National Academy of Sciences*, *100*(26), 15643–15648. https://doi.org/10.1073/pnas.2535227100

Silliman, Brian R., van de Koppel, J., Bertness, M. D., Stanton, L. E., & Mendelssohn, I. A. (2005). Drought, Snails, and Large-Scale Die-Off of Southern U.S. Salt Marshes. *Science; Washington*, *310*(5755), 1803–1806.

Silliman, Brian Reed, & Bertness, M. D. (2002a). A trophic cascade regulates salt marsh primary production. *Proceedings of the National Academy of Sciences*, *99*(16), 10500–10505.

Silliman, Brian Reed, & Bertness, M. D. (2002b). A trophic cascade regulates salt marsh primary production. *Proceedings of the National Academy of Sciences*, *99*(16), 10500–10505.

Smith, K. L., Steven, M. D., & Colls, J. J. (2004). Spectral responses of pot-grown plants to displacement of soil oxygen. *International Journal of Remote Sensing*, *25*(20), 4395–4410. https://doi.org/10.1080/01431160410001729172

Smith, S. M., & Lee, K. D. (2015). The influence of prolonged flooding on the growth of Spartina alterniflora in Cape Cod (Massachusetts, USA). *Aquatic Botany*, *127*, 53–56. https://doi.org/10.1016/j.aquabot.2015.08.002

Solórzano, L. (1969). Determination of ammonia in natural waters by the phenolhypochlorite method. *Limnology and Oceanography*, *14*(5), 799–801. https://doi.org/10.4319/lo.1969.14.5.0799

Starr, G., Jarnigan, J. R., Staudhammer, C. L., & Cherry, J. A. (2018). Variation in ecosystem carbon dynamics of saltwater marshes in the northern Gulf of Mexico. *Wetlands Ecology and Management*. https://doi.org/10.1007/s11273-018-9593-z

Tansley, A. G. (1935). The Use and Abuse of Vegetational Concepts and Terms. *Ecology*, *16*(3), 284–307. https://doi.org/10.2307/1930070

Thenot, F., Méthy, M., & Winkel, T. (2002). The Photochemical Reflectance Index (PRI) as a water-stress index. *International Journal of Remote Sensing*, *23*(23), 5135–5139. https://doi.org/10.1080/01431160210163100

Tian, Y., Yao, X., Yang, J., Cao, W., & Zhu, Y. (2011). Extracting Red Edge Position Parameters from Ground- and Space-Based Hyperspectral Data for Estimation of Canopy Leaf Nitrogen Concentration in Rice. *Plant Production Science*, *14*(3), 270–281. https://doi.org/10.1626/pps.14.270

Turner, R. E., Howes, B. L., Teal, J. M., Milan, C. S., Swenson, E. M., & Tonerb, D. D. G.-. (2009). Salt marshes and eutrophication: An unsustainable outcome. *Limnology and Oceanography*, *54*(5), 1634–1642. https://doi.org/10.4319/lo.2009.54.5.1634

Turner, R. E., Swenson, E. M., Milan, C. S., Lee, J. M., & Oswald, T. A. (2004). Below-ground biomass in healthy and impaired salt marshes. *Ecological Research*, *19*(1), 29–35.

Tyler, A. C., Mastronicola, T. A., & McGlathery, K. J. (2003). Nitrogen fixation and nitrogen limitation of primary production along a natural marsh chronosequence. *Oecologia*, *136*(3), 431–438. https://doi.org/10.1007/s00442-003-1277-5

Tyler, A. C., & Zieman, J. C. (1999). Patterns of development in the creekbank region of a barrier island Spartina alterniflora marsh. *Marine Ecology Progress Series*, *180*, 161–177. https://doi.org/10.3354/meps180161

Walsh, J. P. (1998). *Low marsh succession along an over-wash salt marsh chronosequence* [Doctoral Dissertation]. University of Virginia.

Wu, C., Niu, Z., Tang, Q., & Huang, W. (2008). Estimating chlorophyll content from hyperspectral vegetation indices: Modeling and validation. *Agricultural and Forest Meteorology*, *148*(8–9), 1230–1241. https://doi.org/10.1016/j.agrformet.2008.03.005

Zhang, M., Ustin, S. L., Rejmankova, E., & Sanderson, E. W. (1997). Monitoring Pacific Coast Salt Marshes Using Remote Sensing. *Ecological Applications*, *7*(3), 1039–1053. https://doi.org/10.1890/1051-0761(1997)007[1039:MPCSMU]2.0.CO;2

Zhang, T.-T., Zeng, S.-L., Gao, Y., Ouyang, Z.-T., Li, B., Fang, C.-M., & Zhao, B. (2011). Using hyperspectral vegetation indices as a proxy to monitor soil salinity. *Ecological Indicators*, *11*(6), 1552–1562. https://doi.org/10.1016/j.ecolind.2011.03.025

Zou, H., & Hastie, T. (2005). Regularization and variable selection via the elastic net. *Journal of the Royal Statistical Society: Series B (Statistical Methodology)*, *67*(2), 301–320. https://doi.org/10.1111/j.1467-9868.2005.00503.x

Appendix

Table A.1: *Mean [SE] for all parameters collected during the contemporary sampling date in the short zone.*

Zone	Short					
Initiation Year	**1850**	**1974**	**1982**	**1989**	**1994**	**2012**
Salinity (ppt)	40.5 [3.31]	40.47 [0.96]	36.5 [0.57]	32.25 [4.71]	43.25 [1.31]	38.75 [2.17]
ORP (mV)	-170.69 [18.29]	-110.75 [17.37]	-149.64 [6.69]	-91.65 [18.51]	-27.28 [44.88]	-108.5 [42.57]
OM (0-10cm)	7.87 [0.87]	4.9 [0.73]	2.5 [0.28]	2.35 [0.29]	2.77 [0.3]	2.44 [0.86]
OM (10-20cm)	7.2 [1.15]	2.48 [0.26]	1.31 [0.12]	2.47 [0.21]	2.12 [0.48]	1.84 [0.26]
OM (20-30cm)	7.34 [1.17]	1.94 [0.23]	1.63 [0.41]	1.69 [0.17]	1.1 [0.09]	4.2 [1.76]
% Clay (0-10cm)	21.94 [2.95]	10.51 [1.14]	11.55 [1.45]	13.59 [1.26]	4.87 [1.96]	9.45 [2.42]
% Silt (0-10cm)	39.06 [6.46]	7.56 [1.99]	5.52 [1.06]	9.33 [1.2]	2.97 [1.06]	2.3 [1.33]
% Sand (0-10cm)	39 [9.05]	81.92 [3.03]	82.93 [2.43]	77.08 [1.52]	92.16 [1.02]	88.25 [2.8]
Chlorophyll a (mg/m2)	25.69 [4.77]	107.75 [11.2]	108.63 [10.95]	151.48 [16.56]	151.48 [20.5]	65.74 [22.97]
Phaeopigment (mg/m2)	58.65 [5.22]	46.01 [9.65]	47.34 [7.81]	21.63 [11.08]	29.65 [4.54]	16.56 [10.52]
Sediment %C (0-3cm)	1.99 [0.29]	1.91 [0.55]	0.76 [0.08]	0.8 [0.14]	1.53 [0.43]	0.26 [0.08]
Sediment %N (0-3cm)	0.16 [0.02]	0.1 [0.02]	0.05 [0]	0.06 [0.01]	0.07 [0.01]	0.07 [0.02]
Sediment C:N (0-3cm)	21.92 [8.97]	20.91 [2.35]	16.65 [0.95]	18.82 [1.33]	23.99 [4.79]	17.11 [6.03]
Sediment %C (0-10 cm)	20.65 [1.98]	17.91 [1.63]	14.7 [2.7]	17.08 [2.31]	15.84 [0.75]	19.54 [6.59]
Sediment %N (0-10 cm)	0.92 [0.07]	0.73 [0.09]	0.98 [0.46]	0.66 [0.11]	0.74 [0.05]	0.9 [0.23]
Sediment C:N (0-10 cm)	30.2 [1.91]	30.28 [1.95]	29.61 [2.62]	39.48 [9.46]	29.47 [2.23]	22.82 [7.15]
Sediment %C (10-20 cm)	14.86 [2.41]	15.86 [2.38]	11.57 [2.29]	16.46 [2.3]	7.75 [1.63]	17.96 [5.77]
Sediment %N (10-20 cm)	0.75 [0.1]	0.71 [0.13]	0.4 [0.09]	0.6 [0.09]	0.41 [0.05]	0.61 [0.15]
Sediment C:N (10-20 cm)	21.18 [2.22]	24.59 [1.89]	58.91 [18.56]	45.72 [9.14]	26.9 [9.6]	28.16 [6.07]
Sediment %C (20-30 cm)	14.69 [3.41]	15.2 [3.37]	11.7 [1.57]	14.44 [1.08]	9.38 [1.87]	18.37 [6.01]
Sediment %N (20-30 cm)	0.78 [0.13]	0.69 [0.14]	0.43 [0.09]	0.47 [0.04]	0.44 [0.11]	0.69 [0.18]

Sediment C/N (20-30 cm)	18.59 [2.11]	22.69 [2.44]	44.89 [6.48]	68.43 [13.99]	28.47 [6.55]	25.3 [6.84]
Sediment %P (0-10 cm)	0.0841 [0.0074]	0.0362 [0.0047]	0.0226 [0.0017]	0.0264 [0.0024]	0.0222 [0.0031]	0.0273 [0.0057]
Sediment %P (10-20cm)	0.0804 [0.0049]	0.0234 [0.0024]	0.0152 [0.0012]	0.0284 [0.0026]	0.0177 [0.0042]	0.02 [0.0039]
Sediment %P (20-30cm)	0.0772 [0.0078]	0.019 [0.0038]	0.0209 [0.0026]	0.0262 [0.0046]	0.0163 [0.0011]	0.025 [0.0057]
June Biomass (g/m^2)	--	74.82 [11.34]	117.49 [32.04]	181.08 [30.96]	--	282.18 [58.82]
June Plant density (plants/m^2)	--	363.43 [23.61]	220.57 [50.58]	190 [24.46]	--	472 [44.06]
June Height (cm)	--	0.21 [0.03]	26.71 [2.31]	37.35 [2.93]	--	28.35 [2.95]
July Biomass (g/m^2)	235.18 [41.62]	198.02 [41.22]	239.36 [43.56]	468.23 [69.18]	344.79 [83.5]	435.39 [152.39]
July Density (plants/m^2)	274.52 [19.28]	165.91 [10.44]	187.14 [44.88]	112 [9.17]	65 [19.49]	183 [28.72]
July % flowering	0 [0]	0 [0]	0 [0]	0 [0]	0 [0]	0 [0]
July Height (cm)	33.15 [2.54]	31.63 [2.35]	36.81 [2.46]	50.6 [3.65]	36.25 [3.96]	44.05 [4.53]
Sept. Biomass (g/m^2)	451.59 [124.5]	266.82 [101.86]	287.62 [99.83]	334.08 [58.37]	260.87 [181.2]	1118.6 [304.59]
Sept. Density (plants/m^2)	400 [71.89]	329.14 [50.58]	370 [71.26]	304 [35.13]	212 [130.54]	664 [69.59]
Sept. % flowering	4.29 [2.02]	12.86 [5.65]	6.25 [2.63]	7.5 [3.13]	18.33 [7.99]	20 [4.08]
Sept. Height (cm)	29.59 [1.2]	26.46 [3.86]	28 [4.63]	37 [2.05]	24.12 [8.37]	37.23 [1.97]
Foliar %C	36.41 [1.27]	33.01 [0.56]	32.19 [0.27]	29.22 [2.03]	32.29 [0.12]	32.26 [0.37]
Foliar %N	1.68 [0.06]	1.61 [0.03]	1.99 [0.11]	1.27 [0.07]	1.57 [0.03]	1.78 [0.06]
Foliar C:N	26.34 [1.93]	24.1 [0.61]	19.25 [0.95]	26.6 [2.5]	24.07 [0.44]	21.22 [0.59]
Belowground Root Wt (g, 0-10 cm)	6.48 [0.96]	6.08 [1.62]	3.29 [0.82]	1.45 [0.35]	4.6 [1.14]	3.1 [1.53]
Belowground Rhizome Wt (g, 0-10 cm)	1.65 [0.41]	1.48 [0.43]	0.86 [0.21]	0.34 [0.14]	1 [0.38]	1.23 [0.69]
Uca spp. (burrows/m2)	15.97 [2.96]	17.39 [2.98]	38.13 [15.38]	23.25 [5.14]	29.25 [10.55]	35.25 [24.92]
L. irrorota (individuals/ m2)	29.83 [6.86]	48.22 [7.95]	53.5 [11.98]	88.63 [8.13]	68.75 [21.99]	20.75 [12.31]

I. obsoleta (individuals/ m2)	3.34 [2.69]	14.7 [5.33]	4.75 [2.54]	11.63 [3.64]	0 [0]	20.75 [20.42]
G. demissa (individuals/ m2)	6.28 [2.39]	9.09 [2.55]	6.5 [3.41]	3.13 [0.97]	0 [0]	0 [0]
C. virginica (individuals/ m2)	0.07 [0.05]	0.48 [0.33]	0 [0]	0.38 [0.18]	0 [0]	0 [0]
G. demissa (% cover)	5 [2.57]	6.09 [2.18]	1.88 [1.32]	0.63 [0.63]	0 [0]	0 [0]
C. virginica (% cover)	0.21 [0.17]	0.48 [0.43]	0 [0]	0 [0]	0 [0]	0 [0]
% Algae cover	1.03 [0.52]	1.96 [1.96]	0 [0]	0 [0]	0 [0]	20 [20]

Table A.2: Mean [SE] for all parameters collected during the contemporary sampling date in the tall zone.

Zone	**Tall**					
Initiation Year	1850	1982	1989	1990	1994	2012
Salinity (ppt)	340.38]	36.25 [1.31]	35.08 [0.71]	32.25 [2.14]	35.13 [1.03]	33 [0.22]
ORP (mV)	-195.69 [4.51]	-89.43 [35.62]	-91.24 [20.79]	-97.33 [35.69]	-126 [10.61]	-56.13 [106.86]
OM (0-10cm)	8.79 [0.57]	2.11 [0.14]	4.06 [0.65]	3.97 [0.39]	2.69 [0.19]	2.25 [0.59]
OM (10-20cm)	7.78 [0.48]	1.03 [0.2]	3.06 [0.66]	1.62 [0.27]	2.4 [0.66]	3.01 [1.13]
OM (20-30cm)	7.53 [0.26]	0.93 [0.08]	1.86 [0.21]	1.63 [0.32]	1.95 [0.37]	3.62 [0.9]
% Clay (0-10cm)	20.74 [2.77]	14.43 [1.45]	10.06 [0.84]	7.46 [1.72]	5.05 [1.25]	11.7 [2.29]
% Silt (0-10cm)	51.36 [9.55]	8.92 [1.16]	10.79 [2.43]	3.33 [0.93]	5.39 [2.23]	6.91 [1.3]
% Sand (0-10cm)	27.91 [12.25]	76.65 [2.47]	79.15 [2.74]	89.2 [2.32]	89.55 [3.39]	81.39 [2.73]
Chlorophyll a (mg/m2)	32.02 [4.26]	113.23 [15.42]	121.35 [11.9]	117.13 [16.04]	171.98 [17.45]	124.86 [15.32]
Phaeopigment (mg/m2)	69.61 [6.59]	47.99 [4.03]	51.36 [9.5]	53.85 [11.7]	47.55 [9.4]	30.81 [10.27]
Sediment %C (0-3cm)	1 [0.21]	0.52 [0.02]	1.28 [0.28]	1.71 [0.47]	1.25 [0.34]	0.41 [0.02]
Sediment %N (0-3cm)	0.11 [0.02]	0.04 [0]	0.09 [0.02]	0.12 [0.03]	0.08 [0.02]	0.02 [0]
Sediment C:N (0-3cm)	32.08 [24.62]	16.3 [1.94]	15.81 [0.62]	15.77 [1.07]	17.11 [1.27]	21.39 [0.03]
Sediment %C (0-10 cm)	25.79 [7.95]	14.15 [1.53]	19.9 [4.65]	28.06 [5.78]	22.13 [4.71]	15.02 [4.53]

Sediment %N (0-10 cm)	0.71 [0.2]	0.51 [0.07]	0.75 [0.2]	0.95 [0.23]	0.73 [0.15]	0.65 [0.15]
Sediment C:N (0-10 cm)	41.81 [2.6]	30.01 [3.97]	30.83 [3.72]	35.15 [1.97]	35.73 [2.02]	22.5 [4.32]
Sediment %C (10-20 cm)	16.42 [1.22]	17.02 [0.59]	20.49 [4.37]	30.74 [6.26]	27.09 [4.81]	15.97 [2.76]
Sediment %N (10-20 cm)	0.6 [0.08]	0.67 [0.07]	0.72 [0.14]	0.95 [0.15]	1.06 [0.26]	0.55 [0.09]
Sediment C:N (10-20 cm)	26.93 [3.94]	31.14 [2.92]	32.52 [2.69]	38.17 [2.65]	32.27 [4.94]	28.46 [4.85]
Sediment %C (20-30 cm)	26.38 [5.85]	13.88 [0.62]	18.28 [4.17]	22.23 [7.75]	30.34 [5.29]	13.56 [5.19]
Sediment %N (20-30 cm)	0.77 [0.12]	0.43 [0.03]	0.65 [0.12]	0.71 [0.23]	0.92 [0.07]	0.6 [0.14]
Sediment C/N (20-30 cm)	35.96 [6.15]	41.09 [4.03]	33.87 [2.69]	38.87 [3.69]	37.59 [4.21]	19.4 [6.14]
Sediment %P (0-10 cm)	0.0664 [0.0043]	0.0319 [0.0026]	0.0308 [0.0038]	0.0261 [0.0025]	0.0211 [0.0022]	0.0209 [0.0035]
Sediment %P (10-20cm)	0.0622 [0.0052]	0.0274 [0.0162]	0.03 [0.0075]	0.027 [0.0052]	0.0156 [0.0007]	0.0223 [0.0024]
Sediment %P (20-30cm)	0.0556 [0.0008]	0.0316 [0.0116]	0.0158 [0.0021]	0.0176 [0.0035]	0.0217 [0.0064]	0.0239 [0.0029]
June Biomass (g/m^2)	581.25 [76.44]	45.41 [20.44]	251.35 [20.4]	368.75 [177.38]	275.88 [29.28]	639.01 [88.62]
June Plant density (plants/m^2)	294 [36.53]	66 [28.4]	225.33 [21.16]	172 [30.8]	228 [25.61]	336 [42.83]
June Height (cm)	35.64 [1.25]	30.07 [2.2]	42.11 [3.55]	54.41 [7.16]	37.61 [1.59]	54.35 [5.18]
July Biomass (g/m^2)	839.45 [91.91]	329.54 [136.49]	497.62 [53.97]	565.33 [219.28]	946.11 [72]	1004.63 [137.65]
July Density (plants/m^2)	172.67 [33.88]	60.25 [19.82]	192.36 [15.47]	30 [5.61]	100 [10.33]	150.46 [19.92]
July % flowering	0 [0]	0 [0]	0 [0]	0 [0]	0 [0]	0 [0]
July Height (cm)	57.05 [3.17]	37.03 [10.79]	49.68 [2.43]	48.32 [5.89]	58.31 [2.26]	61.3 [5.66]
Sept. Biomass (g/m^2)	541.51 [121.25]	154.05 [56.65]	777.41 [116.53]	415.12 [147.1]	843.25 [131.81]	1628.18 [368.65]
Sept. Density (plants/m^2)	460 [66.92]	188 [62.78]	465.33 [30.92]	248 [50.78]	516 [54.07]	684 [64.46]
Sept. % flowering	7.5 [2.5]	0 [0]	7.5 [2.5]	8.75 [3.98]	25.42 [2.08]	17.5 [4.79]
Sept. Height (cm)	28.39 [2.32]	23.8 [8.12]	42.39 [3.27]	31.4 [4.53]	35.48 [2.86]	40.48 [4.58]

Foliar %C	33.17 [0.35]	31.51 [0.5]	32.84 [1.35]	31.29 [1.41]	34 [1.34]	33.58 [0.89]
Foliar %N	1.88 [0.05]	2.36 [0.19]	1.78 [0.06]	1.52 [0.11]	1.65 [0.06]	1.8 [0.07]
Foliar C:N	20.68 [0.57]	15.66 [0.99]	21.63 [0.53]	24.46 [1.17]	24 [0.43]	22.13 [1.41]
Belowground Root Wt (g, 0-10 cm)	5.8 [1.42]	3.38 [0.8]	4.96 [1.28]	11.55 [1.31]	6.28 [0.75]	4.25 [3.22]
Belowground Rhizome Wt (g, 0-10 cm)	1.85 [0.09]	1.43 [0.46]	2.31 [0.64]	4.03 [0.72]	2.31 [0.39]	0.73 [0.39]
Uca spp. (burrows/m2)	4.38 [1.31]	69 [25.02]	7.33 [1.92]	53.38 [2.81]	27.88 [11.72]	13.14 [5.65]
L. irrorota (individuals/ m2)	1.13 [0.4]	71 [33.4]	84.67 [15.07]	89 [17.25]	84 [18.77]	4.64 [2.1]
I. obsoleta (individuals/ m2)	0 [0]	1.25 [1.25]	73.83 [25.98]	17.38 [17.38]	18.88 [8.78]	0.07 [0.07]
G. demissa (individuals/ m2)	0 [0]	4.5 [2.87]	6.5 [4.82]	0.5 [0.5]	20.75 [5.24]	11.57 [4.53]
C. virginica (individuals/ m2)	0.13 [0.13]	0 [0]	0 [0]	0 [0]	0.13 [0.13]	1.21 [0.66]
G. demissa (% cover)	0 [0]	2.5 [1.44]	2.58 [2.08]	0.63 [0.63]	9.38 [1.48]	6.07 [2.78]
C. virginica (% cover)	0 [0]	0 [0]	0 [0]	0 [0]	0 [0]	0.36 [0.36]
% Algae cover	0 [0]	0 [0]	0 [0]	0 [0]	0 [0]	2.14 [1.55]

Table A.3*: Regression equations used to estimate aboveground biomass for 1995/1996. X stands for height of S. alterniflora stem.*

Marsh initiation date	Equation	R^2
1991, 1994	$0.0004x^2 + 0.009x$	0.92
1989 and 1982	$0.0004x^2 + 0.01x$	0.86
1974	$0.0002x^2 + 0.232x$	0.73
1850	$0.0002x^2 + 0.218x$	0.83

***Table A.4**: Regression equations used to estimate aboveground biomass for 2017. X stands for height of S. alterniflora stem.*

Marsh initiation date	Equation	R^2
2011, 1994, 1991	$0.0009x^2 - 0.0042x$	0.92
1989 and 1982	$0.0006x^2 + 0.0033x$	0.95
1974	$0.0009x^2 - 0.0085x$	0.89
1850	$0.0007x^2 - 0.005x$	0.91

***Table A.5**: Results from t-test or Kruskal-Wallis (KW) comparing contemporary and historic means*

		Short Zone			Tall Zone		
	Initiation Date	**df**	**t**	**p-value**	**df**	**t**	**p-value**
Salinity	1850	6.69	4.58	0.0029**	16.96	-0.64	0.53
	1974	9.84	1.52	0.16	--	--	--
	1982	8.29	2.25	0.05	15.03	0.98	0.34
	1989	8.56	1.59	0.045*	4.99	0.64	0.55
	1991	--	--	--	11.73	-0.62	0.55
	1994	3	0.62	0.58	15.33	0.63	0.54
ORP	1850	10.2	6.4	<0.0001**	10.18	-1.63	0.13
	1974	12	0.06	0.95	--	--	--
	1982	5.25	2.39	0.06	15.42	-1.95	0.070*
	1989	7.44	0.22	0.83	4.27	-2.98	0.038*
	1991	--	--	--	8.15	1.96	0.08
	1994	3.05	1.35	0.27	13.56	1.26	0.23
%OM	1850	11.16	0.77	0.46	11.05	-7.21	<0.0001**
	1974	9.34	1.57	0.15	--	--	--
	1982	9.01	1.63	0.14	13.42	-4.98	0.0002**
	1989	8.67	-2.34	0.045*	3.60	-0.78	0.48
	1991	--	--	--	13.56	-9.45	<0.0001**
	1994	3.08	-5.06	0.01*	13.51	-13.95	<0.0001**
Sed. %P	1850	9.50	1.18	0.27	7.25	-3.05	0.012*
	1974	5.77	-1.53	0.18	--	--	--
	1982	6.07	-4.90	0.0026**	12.45	-14.36	<0.0001**
	1989	4.36	0.15	0.88	2.30	-2.17	0.15
	1991	--	--	--	--	--	--

	1994	3.74	-3.32	0.032*	11.95	-4.00	0.0018**
Sed. %N	1850	7.15	0.23	0.83	10.69	0.86	0.41
	1974	7.2	-1.03	0.34	--	--	--
	1982	7.95	-1.80	0.11	19.78	-1.45	0.16
	1989	11.66	-1.96	0.07	3.18	0.53	0.63
	1991	--	--	--	9.47	-4.8	0.0008**
	1994	2.96	-7.61	0.005**	8.54	-9.41	<0.0001**
%Clay	1850	11.99	1.86	0.09	7.4	1.49	0.18
	1974	11.31	8.58	<0.0001**	--	--	--
	1982	9.84	2.86	0.017*	20.99	3.42	0.0026**
	1989	8.06	-0.02	0.99	2.84	0.66	0.56
	1991	--	--	--	7.56	1.22	0.26
	1994	3.88	0.92	0.41	8.77	3.09	0.013**
%Sand (KW)	1850	1	0.27	0.60	1	0.59	0.44
	1974	1	8.82	0.003**	--	--	--
	1982	1	2.41	0.12	1	0.64	0.42
	1989	1	2.67	0.12	1	1.23	0.27
	1991	--	--	--	1	0.86	0.35
	1994	1	0.00	1	1	3.01	0.08
%Silt (KW)	1850	1	2.02	0.16	1	2.24	0.13
	1974	1	1.35	0.25	--	--	--
	1982	1	0.42	0.52	1	5.76	0.016*
	1989	1	3.50	0.06	1	0.05	0.83
	1991	--	--	--	1	0.86	0.35
	1994	1	1.15	0.28	1	6.17	0.013*
Chl *a*	1850	--	--	--	21.76	-0.83	0.42
	1974	--	--	--	--	--	--
	1982	--	--	--	24.34	-5.33	<0.0001**
	1989	--	--	--	--	--	--
	1991	--	--	--	14.78	-4.85	0.0002**
	1994	--	--	--	20.32	-8.38	<0.0001**
Density	1850	10.97	0.45	0.66	7.77	-1.72	0.12
	1974	9.28	2.21	0.05*	--	--	--
	1982	11.28	0.22	0.83	10.69	4.05	0.002**
	1989	5.96	0.67	0.53	2.15	0.93	0.44
	1991	--	--	--	7.86	2.23	0.06
	1994	4.8	-0.4	0.71	15.41	-0.15	0.89
Height	1850	5.35	5.73	0.0018**	10.67	2.81	0.017*
	1974	9.52	3.72	0.0043**	--	--	--

	1982	7.15	5.17	0.0012**	12.86	1.38	0.19
	1989	5.81	3.18	0.020*	4.68	3.49	0.020*
	1991	--	--	--	7.34	-3.14	0.016*
	1994	3.04	0.51	0.6472	14.32	0.59	0.57
Biomass	1850	8.09	0.33	0.75	15.53	3.07	0.0076**
	1974	8.51	2.33	0.046*	--	--	--
	1982	11.85	1.87	0.043*	17.72	2.64	0.017**
	1989	8.06	0.19	0.86	3.56	0.01	0.99
	1991	--	--	--	13.96	1.36	0.20
	1994	4.47	-0.07	0.95	14.95	-2.18	0.046*
***G. demissa* (KW)**	1850	1	3.85	0.050*	1	0.0000	1
	1974	1	0.37	0.55	--	--	--
	1982	1	0.0022	0.96	1	1.5060	0.22
	1989	1	2.52	0.11	1	2.5103	0.11
	1991	--	--	--	--	--	--
	1994	1	2.6250	0.11	1	11.6325	0.0006**
***I. obsoleta* (KW)**	1850	1.00	6.56	0.0105*	1.00	11.77	0.0006**
	1974	1.00	1.49	0.22	--	--	--
	1982	1.00	4.35	0.037*	1.00	5.50	0.019*
	1989	1.00	6.07	0.014*	1.00	0.29	0.59
	1991	--	--	--	--	--	--
	1994	1.00	1	0.39	1.00	5.31	0.021
***L. irrorata* (KW)**	1850	1	0.63	0.43	1	3.24	0.072
	1974	1	15.27	<0.0001**	--	--	--
	1982	1	3.20	0.074	1	5.57	0.0183*
	1989	1	19.06	<0.0001**	1	9.64	0.0019**
	1991	--	--	--	--	--	--
	1994	1	10	0.0013**	1	7.90	0.0049**
***Uca* spp. (KW)**	1850	1	1.82	0.18	1	0.039	0.84
	1974	1	19.95	<0.0001**	--	--	--
	1982	1	12.14	0.0005**	1	11.53	0.0007**
	1989	1	19.90	<0.0001**	1	6.03	0.014*
	1991	--	--	--	--	--	--
	1994	1	3.27	0.071	1	7.91	0.0049*
PC1	1850	10.05	-0.85	0.41	15.39	-0.00006	0.5
	1974	10.61	2.75	0.02*	--	--	--
	1982	8.45	-0.21	0.84	20.95	-0.99	0.3
	1989	7.94	-1.4	0.20	3.61	1.11	0.3
	1991	--	--	--	8.32	-2.45	0.04*

	1994	3.87	-3.74	0.02*	13.19	-3.36	0.005**
PC2	1850	11.96	6.01	<0.0001**	15.2	1.53	0.15
	1974	10.83	10.03	<0.0001**	--	--	--
	1982	8.68	6.45	0.0001**	11.81	1.88	0.084
	1989	9.34	3.91	0.0033**	3.59	2.71	0.060
	1991	--	--	--	8.49	0.08	0.94
	1994	3.3	0.91	0.42	16.56	0.66	0.52

Table A.6*: Regression equations used to estimate aboveground biomass for 2018. X stands for height of S. alterniflora stem.*

Marsh initiation date	Equation	R^2
2011, 1994, 1991	$0.0004x^2 + 0.013x$	0.63
1989 and 1982	$0.0011x^2 - 0.0151x$	0.88
1974	$0.008x^2 - 0.0016x$	0.94
1850	$0.0009x^2 - 0.0124x$	0.91

***Table A.7**: Parameter estimates and confidence intervals for the greenhouse elastic net regression.*

		Estimate	Wald ChiSquare	p-value	Lower 95% CI	Upper 95% CI
Leaf %N	Intercept	5.01	6.91	0.0086*	4.70	6.33
	652'	1125.58	0.11	0.74	-284.41	4367.15
	673'	17681.80	20.63	<.0001*	10419.50	22654.70
	775"	-3767.078	0.84	0.36	-8587.8	-843.03
	881"	-1224.627	0.59	0.44	-2912.7	-1.1981
	949"	207.29	0.01	0.93	-249.16	2243.57
Salinity	Intercept	39.55	31.49	<.0001*	27.39	52.29
	478'	-9256.04	0.43	0.51	-36141	12790.70
	622"	-19782.16	0.19	0.66	-94885	12498.10
	842"	-22090.16	1.32	0.25	-58222	-14960
ORP	Intercept	-139.259	11.51	0.0007*	-263.36	-132.17
	788"	90009.02	0.30	0.58	-69886	459347.00
	884"	-75089.63	0.70	0.40	-407330	-61290

***Table A.8**: Parameter estimates and confidence intervals for the greenhouse stepwise regression.*

	Term	Estimate	t Ratio	p-value	Lower 95% CI	Upper 95% CI
Leaf %N	Intercept	35.82	3.39	0.0037*	15.82	54.86
	OSAVI2	-22.45	-3.03	0.0079*	-37.31	-8.30
	PRI	60.86	2.54	0.0218*	20.01	142.15
	RVI	1.42	3.14	0.0063*	0.77	2.63
	GRVI	-33.75	-3.85	0.0014*	-57.54	-23.439
Salinity	Intercept	-4037.09	-3.15	0.0059	-7455.70	-2000.6
	REP	5.84	3.22	0.0051	3.00	10.63
	WI	297.72	2.20	0.0423	36.13	581.75
	OSAVI2	-295.07	-2.52	0.022	-580.32	-101.98
	Intercept	-528.64	-2.95	0.0086	-808.29	-185.03
ORP	WI	396.71	2.29	0.0341	74.43	681.04

***Table A.9**: Parameter estimates included in the elastic net regression models developed from the field plots.*

Model	Term	Estimate	Wald ChiSquare	p-value	Lower 95% CI	Upper 95% CI
Leaf %N	Intercept	1.47	180.84	<.0001*	1.37	1.98
	448.691 "	3924.16	23.91	<.0001*	396.31	6244.14
	930.999'	-69.68	16.53	<.0001*	-142.38	-21.266
	869.289"	976.74	8.60	0.0034*	180.81	2107.55
	825.443"	769.28	5.36	0.0207*	-1006.4	1758.22
	624.076"	-749.54	1.41	0.23	-2701	3135.85
	802.708"	482.70	1.02	0.31	-171.37	2845.56
	908.264'	-102.68	0.34	0.56	-654.85	306.20
	414.589"	-186.05	0.18	0.67	-6440.5	847.71
	906.64'	-12.94	0.02	0.90	-475.46	527.32
Salinity	Intercept	38.97	3653.35	<.0001*	38.31	42.03
	474.674"	65786.96	52.11	<.0001*	38780.80	124047.00
	802.708"	-15871.62	32.21	<.0001*	-41059	-11272.00
	843.306"	-13913.96	32.03	<.0001*	-41833	-3943.50
	434.076"	20277.00	17.38	<.0001*	7764.61	40614.50
	464.931"	-42458.85	16.18	<.0001*	-69800	54835.50
	598.093"	-15228.37	7.12	0.0076*	-13402	16151.00
	849.802"	2526.70	3.67	0.06	-94892	5786.76
	698.777"	-3666.25	2.07	0.15	-13402	16151.00
	628.948"	11556.70	1.80	0.18	-103302	33510.60
	916.383"	758.20	0.49	0.48	-22312	4082.31
	607.836"	3122.85	0.35	0.56	-10864	67110.10
	Intercept	-200.84	884.29	<.0001*	-223.09	849.12
ORP	830.315"	325765.90	52.34	<.0001*	-486245	462125.00
	961.853"	-76765.24	40.88	<.0001*	-212502	-34411
	473.05"	1063163.00	19.87	<.0001*	-9987.9	3028879.00
	809.204"	-182613.6	11.16	0.0008*	-3.7e+6	-110516
	794.588"	219443.60	7.22	0.0072*	-276264	725618.00
	883.905"	30716.75	5.42	0.0199*	-33860	110778.00
	463.307"	-656804.8	4.15	0.0416*	-2.2e+6	614063.00
	851.426"	-94781.92	3.77	0.05	-528534	-25875
	867.665"	-51418.93	0.40	0.53	-538338	135719.00
	955.357"	5311.25	0.14	0.71	-209894	59833.20
	857.922"	12511.06	0.13	0.72	-286222	231113.00

Table A.10: *Parameter estimates and confidence intervals for models developed from field vegetation indices.*

	Term	Estimate	t Ratio	p-value	Lower 95% CI	Upper 95% CI
Leaf %N	Intercept	-8.0	2.39	0.0029*	-12.98	4.98
	WI	3.88	0.98	0.0007*	-1.41	5.94
	OSAVI	4.52	1.59	0.0095*	-1.68	8.34
	GRVI	-3.29	0.59	<.0001*	-4.72	-1.31
	MSAVI2	-2.39	1.01	0.0267*	-4.53	2.19
Salinity	Intercept	154.59	5.96	<.0001*	70.48	228.87
	NDVI	-130.66	-4.47	0.0002*	-283.08	-22.49
	WI	-30.31	-1.80	0.08	-63.43	2.72
	WDR_NDVI	65.06	3.66	0.0012*	19.12	179.92
ORP	Intercept	-199.84	-7.25	<.0001*	-236.40	-148.69
	PRI	-2785.24	-2.58	0.0161*	-5888.10	-1191.40